AD-A039 659 CARNEGIE-MELLON UNIV PITTSBURGH PA DEPT OF ELECTRICA--ETC F/G 9/5
THIN-FILM ACOUSTO-OPTIC SURFACE WAVE INTERACTIONS AND DEVICES.(U)
AUG 76 C S TSAI N00014-75-C-0948

UNCLASSIFIED NL

1 OF 2
AD A039659

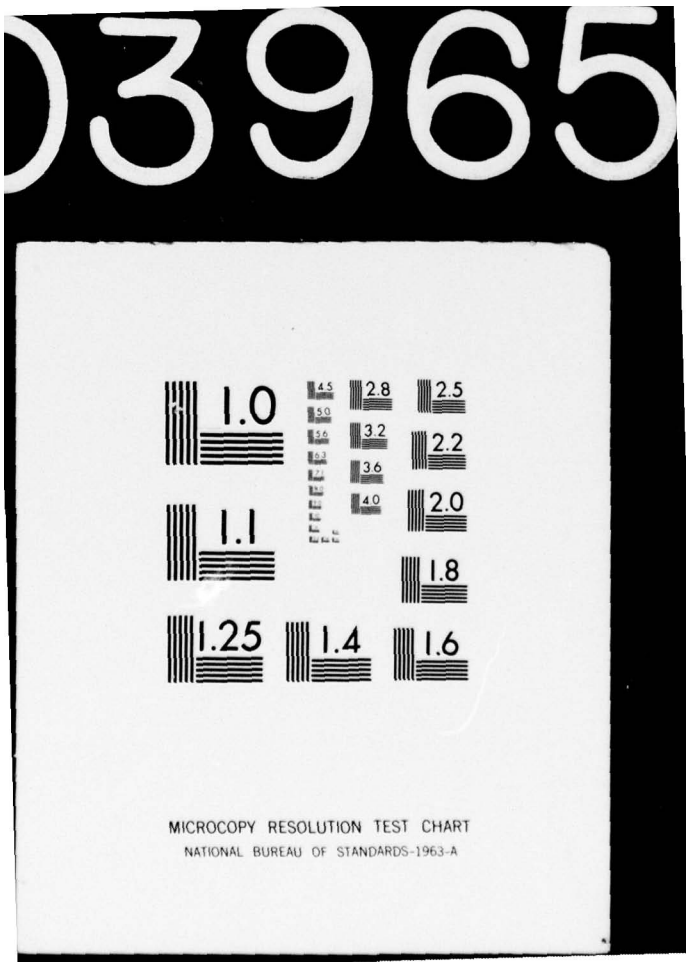
03965
1.0
1.1
1.25
1.4
1.6
1.8
2.0
2.2
2.5
2.8
3.2
3.6
4.0
4.5
5.0
5.6
6.3
7.1
8.0
9.0
MICROCOPY RESOLUTION TEST CHART
NATIONAL BUREAU OF STANDARDS-1963-A

See 1473 in back

Carnegie-Mellon University

PITTSBURGH, PENNSYLVANIA

THIN-FILM ACOUSTOOPTIC SURFACE WAVE INTERACTIONS AND DEVICES

FINAL REPORT

FOR

OFFICE OF NAVAL RESEARCH

Contract No. N00014-75-C-0948

NR384-411

For the Period

1 May 1973 - 30 June 1976

Prepared by

Dr. Chen S. Tsai, Professor

Department of Electrical Engineering

Carnegie-Mellon University

Pittsburgh, Pennsylvania 15213

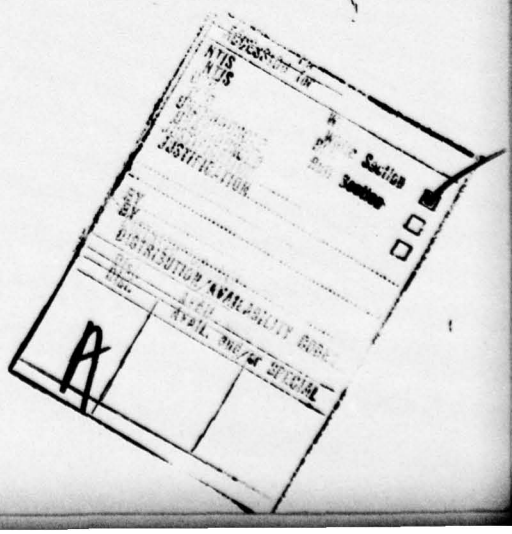

TABLE OF CONTENTS

LIST OF FIGURE CAPTIONS FOR PART I

Fig. 1 Interference Pattern of the Surface Acoustic Waves from a Two-Element Phased-Array Transducer (Frequency = 5.5 MHz, a_s = 3.14 Wavelength, d_s = 6.28 Wavelength, the phase shift between the excitations to the Two Transducers is 180^o for the Upper Plot.)

Fig. 2 Phase-scanning of Surface Acoustic Array (Frequency = 7.1 MHz, Aperture of Element Transducer = 1.5 Wavelength, Separation of Adjacent Element Transducers = 3.0 Wavelength) Number of Element Transducers = 6, ϕ = Phase Shift Between Adjacent Elements.

Fig. 3 Reconstruction of the Beam Pattern of a Linear Electromagnetic Phased-Array Antenna Using a Surface Acoustic Wave Plane Array Transducer.

Fig. 4 Four-Element Stepped Array Transducer.

Fig. 5 Diffraction Patterns of Element Transducer #1 or #4 at f = 68 MHz:
(a) Open-Circuited Configurations
(b) Short-Circuited Configurations
(Horizontal Scale: 1.0 mm per major division)

Fig. 6 Diffraction Patterns of Element Transducers #2 or #3 at f = 68 MHz:
(a) Open-Circuited Configurations
(b) Short-Circuited Configurations
(Horizontal Scale: 1.0 mm per major division)

Fig. 7 Comparison of the Measured and Calculated Diffraction Patterns for the Four-Element Stepped Array at f = 68 MHz.
(Horizontal Scale: 1.0 mm per major division)

Fig. 8 Frequency Scanning of the SAW from a Four-Element Stepped Array. Beam Patterns Were Taken at One Inch from the Array Transducer.
(Horizontal Scale: 1.0 mm per major scale, corresponding to an angular scan of 2.3^o)

LIST OF FIGURE CAPTIONS FOR PART II

Fig. 1 Guided-Wave Acousto-optic Bragg-Diffraction From A Single Surface Acoustic Wave.

Fig. 2 Guided-Wave Acousto-optic Bragg-Diffraction From Multiple Tilted Surface Acoustic Waves.

Fig. 3 a) Depth Dependence of the Strain Fields for the SAW Propagating Along the Z-axis of Y-cut $LiNbO_3$ substrate,

b) Depth Dependence of the Accompanying Piezoelectric Fields to (a),

c) Profiles of the TE Optical Waveguide Modes in Y-cut $LiNbO_3$ Out-Diffused Layers (Y_t is the Turning Point).

Fig. 4 Depth Dependence of the Relative Elasto-optic and Electro-optic Contributions to Bragg Diffraction: (a) For Z-Propagating SAW, (b) For 21.8^o - Propagating SAW.

Fig. 5 Relative Bragg Diffraction Efficiency vs the Acoustic Frequency in Y-cut $LiNbO_3$ Out-Diffused Waveguides: (a) Penetration Depth of the TE_o Mode = 13.5μm, (b) Penetration Depth of the TE_o Mode = 7.0μm.

Fig. 6 Frequency Response of the Guided-Wave Acousto-optic Bragg-Diffraction From A Single SAW:

(a) L_1 = 2.5 mm, L_2 = 1.66 mm and L_3 = 1.11 mm

(b) L_1 = 5.0 mm, L_2 = 3.32 mm and L_3 = 2.22 mm

Fig. 7 Guided-Wave Acousto-optic Bragg-Diffraction From Two Tilted Surface Acoustic Waves.

Fig. 8 Effect of the Phase Shift Between Two Tilted SAWs on the Resultant Frequency Response (Theoretical).

Fig. 9 Guided-Wave Acousto-optic Bragg-Diffraction From Two Tilting Surface Acoustic Waves.

Fig. 10 (a) Frequency Repsonses of the Bragg-Diffracted Light Power for the Individual Acoustic Waves,

(b) Frequency Response of the Bragg-Diffracted Light Power for the Combined Acoustic Waves.

THIN-FILM ACOUSTO-OPTIC SURFACE WAVE INTERACTIONS AND DEVICES

Prof. Chen S. Tsai, Principal Investigator
Department of Electrical Engineering
Carnegie-Mellon University
Pittsburgh, Pa. 15213

I. INTRODUCTION

In this final report major research progress and findings which have been made on the contract entitled, "Thin-Film Acousto-Optic Surface Wave Interactions and Devices", (N00014-67-A-0314-0020 and N00014-75-C-0948) are described. The overall objectives of this investigation are: (1) to study the diffraction phenomena of multiple surface acoustic waves in both isotropic and anisotropic substrates and the thin-film (guided-wave) acousto-optic interactions, and the related new devices, (2) to establish the design constraints and criteria of the related devices, and (3) to explore the potential applications of the related devices. The specific topics which have been investigated include:

(1) surface acoustic waves (SAW) from plane array transducer,
(2) surface acoustic waves from stepped array transducer,
(3) guided-wave acousto-optic bragg-diffraction from a single SAW,
(5) guided-wave acousto-optic bragg-diffraction from two - tilted SAWs,
(5) guided-wave acousto-optic bragg-diffraction by an N-SAW array-general case,
(6) guided-wave acousto-optic bragg-diffraction from multiple tilted SAWs-experimental results,
(7) guided-wave acousto-optic bragg-diffraction from phased SAWs,
(8) wideband applications using guided-wave acousto-optic bragg devices.

The objectives of this contract have been achieved.

PART I
MULTIPLE SURFACE ACOUSTIC WAVE DIFFRACTION PHENOMENA AND DEVICES

Most of the Surface Acoustic Wave (SAW) applications for radar signal processing involve interdigital array transducers of the type in which variable pitches are implemented along the acoustic propagation path (1). Although several possible applications have been suggested for a second type of array transducers in which a number of interdigital transducers are placed side by side in a direction perpendicular to the acoustic propagation path, relatively little experimental work involving this type of array transducer (henceforth called the transverse array transducers) has been reported (2). We have fabricated transverse array transducers in which the aperture of the element transducer and the separation between adjacent element transducers are only a few acoustic wavelengths on PZT and Y-cut $LiNbO_3$ substrates. This transverse array transducer has two versions, namely, the plane array and the stepped array. We have studied the diffraction pattern and its electronic scanning of the resultant acoustic beam from such array transducers. Two types of electronic scanning, namely, the phase and frequency scanning have been investigated. Phase and frequency scanning of the acoustic beam were achieved by varying the phase slope and the frequency, respectively, of the rf excitations to the appropriate array transducers.

The results show that for a limited angular scan as the one considered in this study the diffraction patterns and their phase and frequency scanning may be described, to a large degree, in terms of the phased-and frequency-scanning array antenna theory with some modifications. Some applications with both types of array transducers are described. In particular, the stepped array transducer is shown to have several immediate applications in connection with wideband guided-light beam deflection.

II. SURFACE ACOUSTIC WAVES FROM PLANE ARRAY TRANSDUCER

A. Phase Scanning of the SAW Array on Isotropic Substrate

Experiments have been carried out using multi-element array transducer configurations such as the one shown in the insert in Figure 2. The array transducers were fabricated on the isotropic piezoelectric substrate of PZT ceramics and consist of two to eight elements operating at 5.5-7 MHz, but only the results for the two- and six-element arrays are presented in this report. For the 5.5 MHz two-element array the element transducer aperture and the separation between them are, respectively, 1.2 and 2.4 mm, corresponding to three and six acoustic wavelengths. For the 7 MHz six-element array they are, respectively, 0.47 and 0.94 mm, corresponding to one and a half and three acoustic wavelengths. Individual transducer elements were rf excited with a variable phase shifter between adjacent elements. The interference patterns and their electronic phase scanning were probed by measuring the piezoelectric field accompanying the acoustic field using a tungsten probe (6). The results are shown in Figures 1 and 2. The interference pattern as shown in Fig. 1 agrees very well with that of a one-dimensional double-slit in optics (7). A slight irregularity in the experimental data is believed to be due to the nonideal surface condition of the PZT in which an aggregate of pits up to 30μm size was observed. In Fig. 2 the calculated diffraction patterns for an isotropic linear microwave phased-array antenna using the well known formula (8) are also shown. This formula is given in Equation (1)

$$I(\theta) = \left[\frac{\sin\left(\frac{\pi a}{\Lambda} \sin(\theta)\right)}{\frac{\pi a}{\Lambda} \sin(\theta)} \right]^2 \cdot \left[\frac{\sin\left\{ \pi N \left(\frac{d}{\Lambda}\right)(\sin(\theta) - \sin(\theta_o)) \right\}}{\sin\left\{ \pi \left(\frac{d}{\Lambda}\right)(\sin(\theta) - \sin(\theta_o)) \right\}} \right]^2 , \quad (1)$$

TABLE I. Comparison between experimental and theoretical results.

PHASED-ARRAY PARAMETERS	THEORETICAL RESULTS	DEGREE OF AGREEMENT
Rayleigh Beam Width of the Main-Lobe	Λ/Nd	Very Good
Phase-Shift Required Per Scanned Beam Width Position φ	2π/N	Very Good
Scannable Beam Width Positions	N	Very Good
Side-Lobe Strength	(6)	Fair

Λ = wavelength; N = number of array elements; and d = separation between elements.

where:

$I(\Theta)$ = far-field diffraction pattern

a = aperture of element transducer

Λ = wavelength of the surface acoustic wave

Θ = angle of the far-field point measured from the boreside direction of the linear array

N = number of array elements

d = separation between adjacent elements

ϕ_o = phase shift between adjacent elements

$$\sin \Theta_o = \left(\frac{\phi_o}{2\pi}\right)\left(\frac{\Lambda}{d}\right)$$

The degree of agreement between the experimental and the calculated results is indicated in Table I. It is seen that the experimental results agree well with the calculated values with regard to the beam width and the positions of the main and side lobes. However, it is noted that the measured side lobe strength for the six-element array is substantially larger than that of the calculated value. This disagreement is believed to be due to the unequal acoustic waves, both in amplitude and phase, being generated in each element transducer resulting from the coupling among the element transducers. A detailed measurement of this coupling effect in conjunction with the stepped array transducer will be given in Section III.A.

Finally, it should be noted that as a result of their excessive acoustic losses PZT ceramics are not the best materials for phase scanning devices operating at frequencies much higher than 7 MHz. Phase scanning experiments at higher frequencies may utilize materials such as ZnO and CdS in their basal plane for a large angular scan and materials such as $LiNbO_3$ and Y-cut quartz for a limited angular scan.

B. Processing of Phased-Array Antenna Signals Using a Plane SAW Array Transducer

The experimental results have indicated that the diffraction phenomena and the phase scanning properties of surface acoustic waves on an isotropic substrate from a plane array transducer closely resemble that of an isotropic linear electromagnetic phased array. Consequently, such an array transducer may be employed to create a replica of the diffraction pattern of a linear receiving phased-array antenna, in addition to its obvious application as an acoustic beam scanner. The receiving antenna diffraction pattern

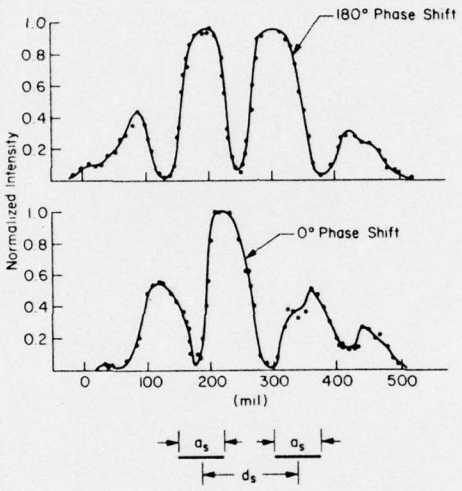

Fig. 1 Interference Pattern of the Surface Acoustic Waves from a Two-Element Phased-Array Transducer (Frequency = 5.5 MHz, a_s = 3.14 Wavelength, d_s = 6.28 Wavelength, the phase shift between the excitations to the Two Transducers is 180^o for the Upper Plot.)

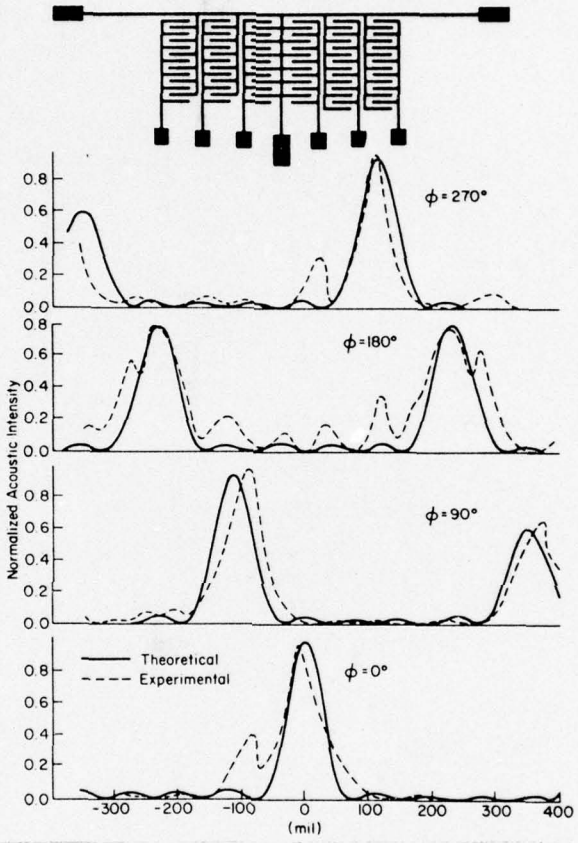

Fig. 2 Phase-scanning of Surface Acoustic Array (Frequency = 7.1 MHz, Aperture of Element Transducer = 1.5 Wavelength, Separation of Adjacent Element Transducers = 3.0 Wavelength) Number of Element Transducers = 6, ϕ = Phase Shift Between Adjacent Elements.

can be reconstructed by simply applying, one to one, the outputs of the antenna elements to the transducer elements. It follows that such an array transducer can be used as a signal processor for a linear receiving phased-array antenna requiring no phase shifters or delay lines the way conventional signal processors do. First, the basic relations which indicate the acoustic reconstruction of the beam pattern of the electromagnetic array antenna are derived, to be followed by a description of a possible configuration for the proposed signal processor and its distinct advantages.

1. Acoustic Reconstruction of the Beam Pattern of a Linear Electromagnetic Receiving Array Antenna

Consider a linear electromagnetic receiving array antenna and a plane SAW array transducer each having N identical elements. The outputs of the antenna elements are applied to the transducer elements in the manner just described (see Fig. 3).

Rewriting Eq. (1), the far-field beam patterns of the electromagnetic wave and surface acoustic wave arrays are given as follows

$$I(\Theta_i) = \left[\frac{\sin\left(\frac{\pi a_i}{\Lambda_i}\sin(\Theta_i)\right)}{\left(\frac{\pi a_i}{\Lambda_i}\sin(\Theta_i)\right)}\right]^2 \left[\frac{\sin\left\{\pi N\left(\frac{d_i}{\Lambda_i}\right)(\sin(\Theta_i) - \sin(\Theta_{oi}))\right\}}{\sin\left\{\pi\left(\frac{d_i}{\Lambda_i}\right)(\sin(\Theta_i) - \sin(\Theta_{oi}))\right\}}\right]^2 \quad (2)$$

where the first factor is called the element factor and the second factor is the array factor. The subscript i designates e for the electromagnetic wave array and s for the SAW array, e.g., a_e and a_s designate, respectively, the aperture of the element of the electromagnetic wave array and the SAW array.

When a target signal from a direction Θ_e is received by the electromagnetic wave array the phase shift between adjacent elements ϕ_{oe} is given by

$$\phi_{oe} = 2\pi\left(\frac{d_e}{\Lambda_e}\right)\sin(\Theta_e) \quad (3)$$

Since this same phase shift is carried over to the SAW array we have $\phi_{os} = \phi_{oe}$. The far-field beam pattern of the SAW array is obtained by substituting ϕ_{os} into Eq. (2). Thus we have

$$I(\Theta_s) = \left[\frac{\sin\left(\frac{\pi a_s}{\Lambda_s}\sin(\Theta_s)\right)}{\left(\frac{\pi a_s}{\Lambda_s}\sin(\Theta_s)\right)}\right]^2 \left[\frac{\sin\left\{N\pi\left(\frac{d_s}{\Lambda_s}\right)\sin(\Theta_s) - N\pi\left(\frac{d_e}{\Lambda_e}\right)\sin(\Theta_e)\right\}}{\sin\left\{\pi\frac{d_s}{\Lambda_s}\sin(\Theta_s) - \pi\frac{d_e}{\Lambda_e}\sin(\Theta_e)\right\}}\right]^2, \quad (4)$$

It is immediately clear that for a phase shift $\Theta_{os} = \Theta_{oe}$ corresponding to a target direction Θ_e the main lobe of the resulting SAW beam pattern is scanned by an angle Θ_s given by the following relation

$$\sin(\Theta_s) = \frac{\left(d_e/\Lambda_e\right)}{\left(d_s/\Lambda_s\right)}\sin(\Theta_e) \quad (5)$$

From Eq. (5) we see that $\Theta_s = \Theta_e$ when $d_s/\Lambda_s = d_e/\Lambda_e$, namely, the angular scan of the SAW beam is identical to that of the electromagnetic wave when the separation between adjacent element transducers in acoustic wavelength is identical to that between adjacent antenna elements in electromagnetic wavelength. Also, $\Theta_s > \Theta_e$ when $d_s/\Lambda_s < d_s/\Lambda_e$ and $\Theta_s < \Theta_e$ when $d_s/\Lambda_s > d_e/\Lambda_e$.

Just as in many scanning devices it is the number of resolvable beam widths (not the scanning angle) which is of real importance. We recall from the basic relations of the phased-array antenna given in Table I that the total number of scannable beam width positions between adjacent grating lobes is identical to the number of array elements N, independent of the separation of adjacent array elements. Thus, d_s/Λ_s for the SAW array need not be in the order of unity or smaller as the electromagnetic array does. This is a very important consideration for the design of a SAW array because the wavelength of the acoustic wave is smaller than that of the electromagnetic wave by a factor of approximately 10^5 and also because many SAW materials are acoustically anisotropic and, therefore, only a relatively small angular range along certain directions may be considered isotropic or approximately isotropic.

From Equation (4) the angular scan of the $\pm$ mth grating lobes may be determined by the equation $\pi(d_s/\Lambda_s)\sin(\Theta_s) - \pi(d_e/\Lambda_e)\sin(\Theta_e) = \pm m\pi$, where m is an integer. In the proposed SAW signal processor to be described in the following subsection only the main lobe will be utilized. For this purpose the aperture of the element transducer a_s must be properly chosen so that the strengths of the grating lobes are substantially smaller than that of the main lobe.

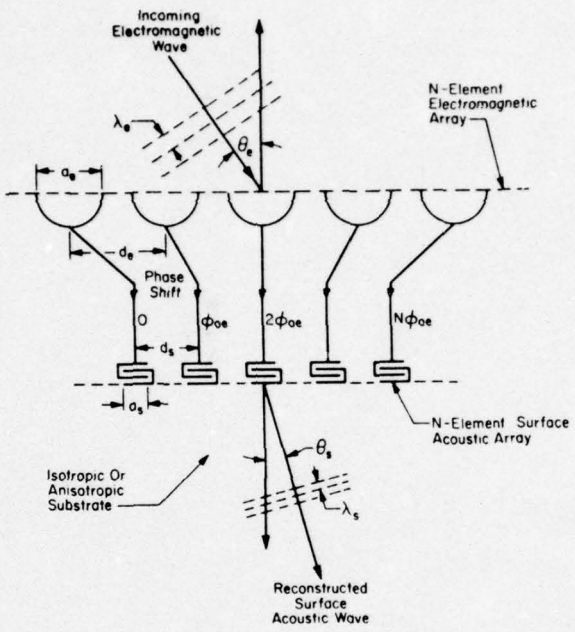

Fig. 3 Reconstruction of the Beam Pattern of a Linear Electromagnetic Phased-Array Antenna Using a Surface Acoustic Wave Plane Array Transducer.

2. Surface Acoustic Wave Signal Processor with No Phase Shifters

In one form of such a signal processor, a number of output transducers (equal to N for an array antenna and the corresponding array transducer of N elements) are placed along a certain circumference at a far-field location of the acoustic beam. The aperture size of each output transducer is determined by the beam width of the diffraction pattern. An acoustic lens may also be incorporated to bring the far-field diffraction pattern to a more convenient location. Such a signal processor is capable of forming N resolvable target signals simultaneously without requiring any phase-shifter or delay line. It should be noted that for a conventional signal processor N phase shifters or delay lines are required to form N target signals sequentially in an N-element linear phased-array antenna, and for simultaneous processing N^2 phase shifters or delay lines are required (9). As a result, the conventional signal processing technique is complicated and expensive when N is large. Thus, in addition to its obvious application for acoustic beam scanning, the array transducer described above is useful as a signal processor, requiring no phase shifter or delay lines, for sonars and electromagnetic phased-array antenna applications. The distinct advantages of the proposed acoustic surface wave signal processor over the conventional signal processor are its low cost in addition to its compactness, small size, and light weight. It should be noted that in order to alleviate the limitation of acoustic losses the proposed processor may process the target signals at a convenient intermediate frequency by down-conversion and heterodynning as conventional processors do.

III. SURFACE ACOUSTIC WAVES FROM STEPPED ARRAY TRANSDUCER

Multi-element array transducer configurations such as the one shown in Figure 4 were fabricated on the isotropic substrate of PZT ceramics and the anisotropic substrate of Y-cut $\pm$ 21.8° propagating $LiNbO_3$ but only the results for the latter are given here. For the 68 MHz four-element array the aperture of the element transducer and the separation between adjacent element transducers are, respectively, three and four acoustic wavelengths, corresponding to 150 and 200 μ. Each element transducer has five finger pairs and thus has a bandwidth of approximately 20%. To demonstrate the frequency scanning of this array transducer the conducting pads were connected in such a way that the four-element transducers were driven in parallel and adjacent element transducers were driven opposite phase. The diffraction pattern of individual element transducers and the interference pattern of the array transducer and its electronic scanning were obtained by measuring the intensity of the first-order diffracted light using a scannable laser light probe (10).

A. Near- and Far-Field Diffraction Patterns of Element Transducer and the Coupling Between Element Transducers

Diffraction and beam steering of surface acoustic waves generated by a single interdigital transducer of relatively large aperture, on an anisotropic substrate, has been rather extensively studied in recent years (11-15). One of the conclusions of the studies is that as a result of the acoustic anisotropy the diffraction spreading of an acoustic beam in an anisotropic substrate is $(1 + \gamma)$ times the diffraction spreading in an isotropic substrate. Here γ designates an anisotropy parameter and is equal to the slope of the power flow. Thus, depending on the sign of γ diffraction spreading of a surface acoustic beam on an anisotropic substrate can be either accentuated or reduced in comparison to that on an isotropic substrate. For the substrate of a Y-cut $LiNbO_3$ plate γ is, respectively, -0.901 and 0.393 for a surface acoustic beam propagating along the z-axis and in the $\pm$ 21.8° direction from the z-axis (15). Thus the far-field interference patterns of multi-element SAW arrays can be generated and studied at a much shorter distance from the array transducer with propagation along the $\pm$ 21.8° direction than along the z-axis. For this reason stepped array transducers were fabricated along the $\pm$ 21.8° direction.

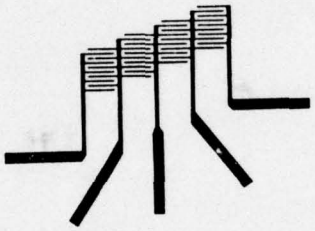

Fig. 4 Four-Element Stepped Array Transducer.

Since one of the purposes of this study is to determine the maximum angular scan achievable, the aperture of each element transducer, namely three acoustic wavelengths, was chosen considerably smaller than that being employed by other investigators so that the beam width of the element factor in Eq. (2) could be sufficiently large. Consequently, it was also of interest to determine if the diffraction spreading of such a small aperture could still be described by a single γ of 0.393. Also, in order to study the coupling strength among the element transducers, the gap (inactive region) between adjacent element transducers was chosen as small as one wavelength. Coupling can arise from either electrical coupling by radiation and capacitive effects or acoustic coupling.

In order to measure the near- and far-field diffraction patterns of element transducers and the coupling strength between element transducers the conducting pads of the element transducers were connected in the open- and short-circuited configurations shown in the insert of Figures 5 and 6. The spot size of the laser light probe, defined between the half-power points, was about 30μm. The results are shown in Figures 5 and 6. From the plots we find that the measured beam width of the far-field diffraction pattern agrees with the calculated value, using $\gamma = 0.393$, within 5% and that the diffraction pattern carries no side lobes. Also, from the near-field acoustic intensity distributions it was found that in both open- and short-circuit configurations the coupling associated with the middle two element transducers was considerably stronger than that with the end element transducers. It was also found that the acoustic field from the four-element transducers were not of equal strength, the #3 element transducer being the weakest. The reason for this large irregularity was traced down to a degraded conducting pad for this particular element transducer.

From the experimental data on the coupling strengths and an examination of the interdigital electrode configuration, we tentatively conclude that the reason for the excessive coupling with the middle two transducers but not the two end transducers is the usage of the common-electrode configuration (see Fig. 4) for the former. Further study on this important coupling problems is in progress.

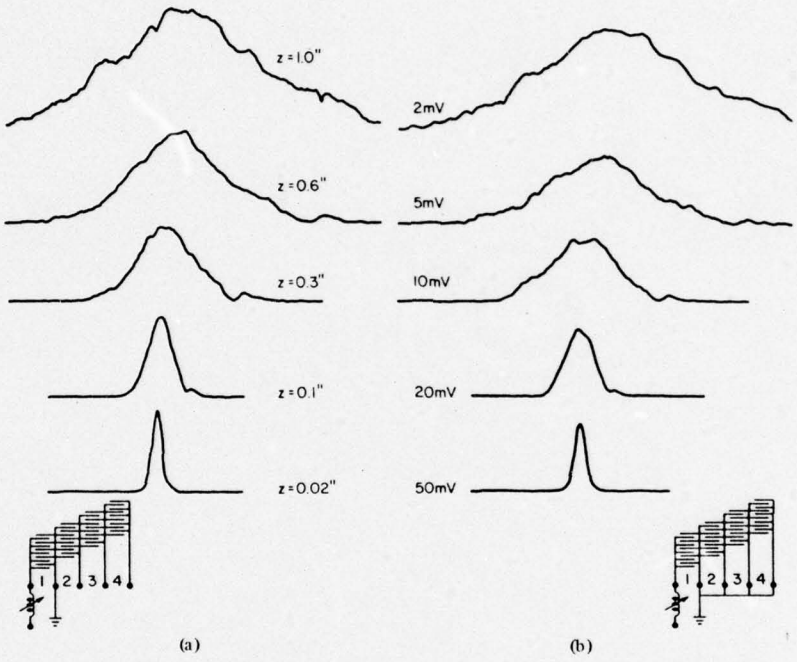

Fig. 5 Diffraction Patterns of Element Transducer #1 or #4 at f = 68 MHz:

(a) Open-Circuited Configurations

(b) Short-Circuited Configurations

(Horizontal Scale: 1.0 mm per major division)

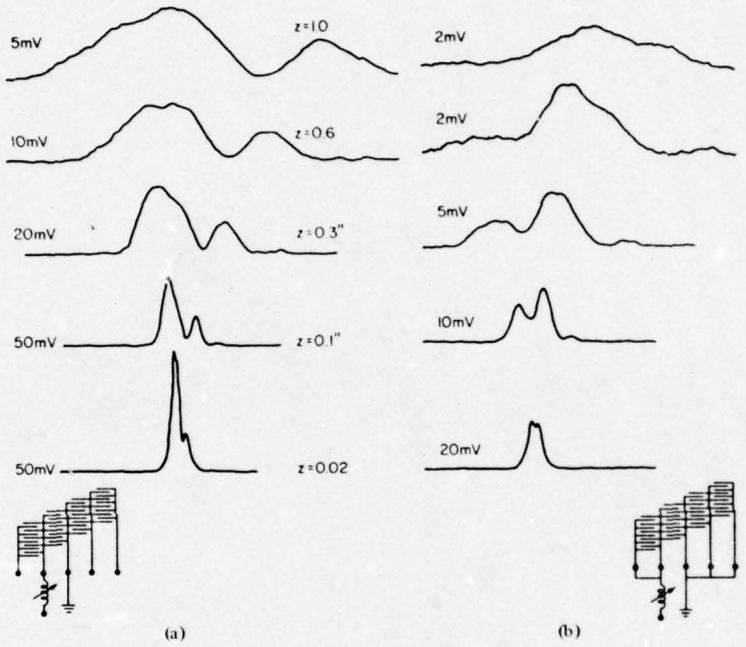

Fig. 6 Diffraction Patterns of Element Transducers #2 or #3 at f = 68 MHz:

(a) Open-Circuited Configurations

(b) Short-Circuited Configurations

(Horizontal Scale: 1.0 mm per major division)

B. Interference Patterns of the Four-Element Stepped Array

As mentioned previously, in order to demonstrate frequency scanning, the element transducers were driven in parallel and the adjacent element transducers were driven in opposite phase. Each element transducer has five interdigital finger pairs and has, therefore, a theoretical acoustic bandwidth of approximately 20%. The measured bandwidth is 18%. The step height between adjacent element transducers is three half acoustic wavelengths at the center frequency of 68 MHz.

The far-field diffraction patterns which were taken at a distance of one inch from the array transducer are shown in Figure 7. Note that the measured beam width agrees within 5% of the calculated value for an array with equal amplitude and exactly opposite phase between adjacent element transducers but the side lobe strength is considerably larger than the calculated value (not shown). This discrepancy is believed to be mainly due to the unequal acoustic amplitude for each element transducer and a phase shift other than 180° (henceforth called the phase deviation) between adjacent element transducers--a result of coupling among element transducers. Based on symmetry considerations, element transducers #2 and #3 should have identical phase deviation. The same is true for element transducers #1 and #4.

To verify the explanation given above, computer plots for the diffraction pattern using the amplitudes of the element transducers (as determined from the measured near-field acoustic intensity profile) and a series of assumed phase deviations $\Delta\phi$ for the two middle transducers in comparison to the two end transducers have been obtained. Figure 7 shows the degree of agreement between the experimental plot and the computer plot with an assumed phase deviation of 30° at the center frequency of 68 MHz. The relative amplitudes for the element transducers #1, 2, 3, and 4 are, respectively, 1.0, 0.6, 0.3, and 0.9.

C. Frequency Scanning of the SAW from the Four-Element Stepped Array

The derivation given below follows the approach commonly employed for frequency-scanning linear array antennas (16). We observe that the step height in the SAW stepped array corresponds to the incremental transmission line in frequency-scanning array antennas. Since adjacent element transducers of the stepped array studied are excited in opposite phase the phase shift between adjacent element transducers on an isotropic substrate ϕ is

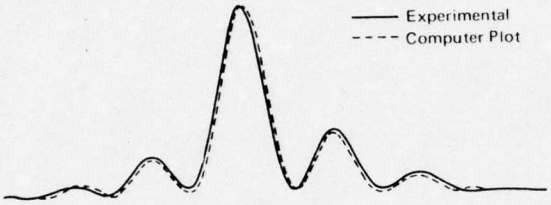

Fig. 7 Comparison of the Measured and Calculated Diffraction Patterns for the Four-Element Stepped Array at f = 68 MHz. (Horizontal Scale: 1.0 mm per major division)

$$\phi = 2\pi \frac{d_s}{\Lambda_s} \sin(\theta_s) + \frac{2\pi}{\Lambda_s} S + \pi \qquad (6)$$

or

$$\phi = 2\pi \left\{ \frac{f}{f_o} \left(\frac{d_s}{\Lambda_{so}} \sin(\theta_s) + \frac{P}{2} \right) + \frac{1}{2} \right\}$$

where:

d_s = separation between adjacent element transducers

S = step height between adjacent element transducers

$= P(\Lambda_{so}/2)$

P = integer

Λ_{so} = acoustic wavelength at the center frequency f_o

Λ_s = acoustic wavelength at the frequency f

θ_s = angle of the far-field point measured from the boreside direction of the linear array.

Using Equation (6) the maxima of the m^{th} grating lobes of a stepped array on an anisotropic substrate (characterized by the anisotropic parameter γ) are given by the following expression,

$$\sin(\theta_{sm}) = (1 + \gamma) \frac{\gamma_{so}}{d_s} \left\{ (m - 1) \frac{f_o}{f} - \frac{P}{2} \right\} \qquad (7)$$

Note that for the stepped array transducer being studied p = 3 (the step height S is equal to three half acoustic wavelengths at the center frequency) and therefore $\theta_{so} = 0$ for $m = 2$ at $f = f_o$. In other words, the second grating lobe is peaked at the forward direction at the center frequency. This particular grating lobe was studied in the frequency scanning experiment to be described later.

For an array of N elements the Rayleigh beam width of the beam pattern, $\delta\theta_{diff}$ is given by $(1 + \gamma)\gamma_s/Nd_s$. Using Eq. (7) the number of resolvable beam width positions R for a frequency tuning of $\Delta f = f - f_o$ can be easily obtained. For the case in which θ_{sm} is sufficiently small so that $\sin(\theta_{sm}) = \theta_{sm}$ the following simplified expression for R is obtained

$$R \approx (1+\gamma)\left(m-\frac{1}{2}\right)\left(\frac{f_o}{f}-1\right)\frac{\lambda_{so}}{d_s}\Bigg/\left\{(1+\gamma)\lambda_s/Nd_s\right\} = -N\left(m-\frac{1}{2}\right)\frac{\Delta f}{f_o} \qquad (8)$$

Thus the fractional frequency tuning required for the scanning of one Rayleigh beam width position is

$$\frac{\Delta f}{f_o} = -\frac{2}{N(2m-1)} \qquad (9)$$

For the stepped array transducer being studied N = 4 and m = 2 as described previously. Thus, $(\Delta f/f_o)$ required for the scanning of one resolvable beam width position is 16.6%, namely Δf = 11.3 MHz with f_o = 68 MHz.

Frequency scanning of the diffraction pattern is illustrated in a series of plots shown in Figure 8. Fron the plots the frequency tuning for one Rayleigh beam width position is found to be about 8 MHz which compares fairly with the calculated value of 11.3 MHz.

D. Possible Applications of the Frequency Scanning Transducer Array

In this subsection only a few immediate applications will be discussed.

1. Electro-Acousto-Optic Signal Processor for Phased-Array Antenna

This processor consists of a plane array transducer for the generation of a multi-channel SAWs and a laser reflection and projection system (17). The laser beam is reflected from the substrate in which the multi-channel SAW propagates. The phased signals from the antenna array elements are applied, one to one, to the array transducer elements. From the deflection angle of the first-order diffracted light in the direction of the SAW propagation and in the direction orthogonal to it the frequency and angle of arrival of the target signal can be determined. It should be noted that the aperture in acoustic wavelength of the element transducers of the array transducer studied in (17) was at least 10 times larger than that of the array transducers studied here. As a result, each individual acoustic beam remained collimated at the acousto-optic interaction region and no measurement of the far-field diffraction pattern such as the ones presented in this report (Section III.B) was made.

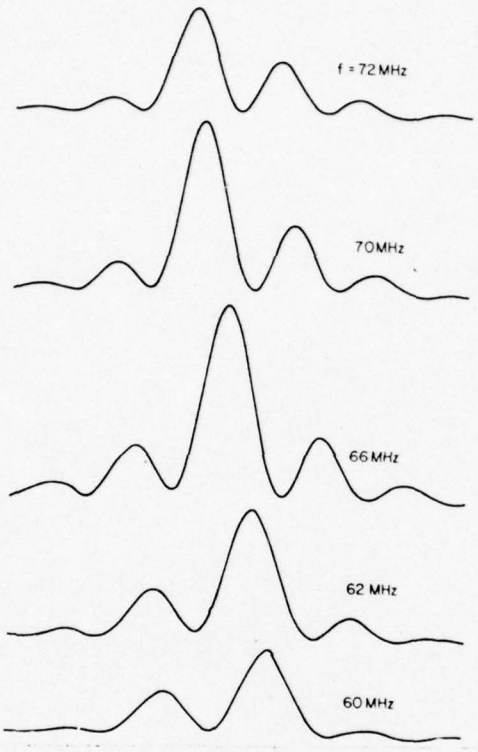

Fig. 8 Frequency Scanning of the SAW from a Four-Element Stepped Array. Beam Patterns Were Taken at One Inch from the Array Transducer. (Horizontal Scale: 1.0 mm per major scale, corresponding to an angular scan of 2.3^{o})

2. Acoustic Spectrum Analyzer

The frequency scanning array transducer may be utilized for spectrum analysis for the target signals without employing a light beam as the first application does. One version of this acoustic spectrum analyzer may take the same form as that of the signal processor described in Section II.B. Since N frequency channels are resolvable with an array transducer of N elements a number of N output transducers are placed along a circumference at a far-field location of the acoustic beam. The aperture size of each output transducer is determined by the beam width of the diffraction pattern. Finally, the frequency resolution is inversely proportional to N (see Equation (9)).

3. Wideband Guided-Light Beam Deflector and Acousto-optic Spectrum Analyzer

In addition to its use as an acoustic beam scanner the frequency scanning array transducer can also be employed to achieve wideband light beam deflection in thin film integrated optics systems. This is possible because scanning of the acoustic beam enables the acoustic beam to track the Bragg condition and, therefore, make efficient diffraction possible for a wide frequency band (18, 19). It has been pointed out that the control of the acoustic beam spread in thin-film acousto-optic beam deflection is very important in order to reduce competing Bragg processes which cause unwanted effects such as the reduction in the resolvable spots and the unwanted modes switching (20). Thus, the shaping and steering of the acoustic beam using the stepped array will certainly provide a very useful means for such a desirable control. By employing the beam steering technique we expect to achieve a large number of resolvable spots at a sufficiently small acoustic beam spread to minimize the unwanted effects mentioned above. Based on the same argument it follows that the efficiency and channel capacity of a thin-film acousto-optic spectrum analyzer may be improved considerably when a frequency scanning array transducer is employed instead of a single transducer. A thin-film acousto-optic spectrum analyzer using a single transducer has been suggested (21). We have demonstrated experimentally that a wider bandwidth is achievable with a thin-film acousto-optic beam deflector which employs a two-element array transducer fabricated on the out-diffused optical waveguide of a Y-cut $LiNbO_3$, substrate (22). The results of this study and other related studies are described in Part II of this report.

REFERENCES FOR PART I

(1) See for example, the special issue on Microwave Acoustics, IEEE Trans. Microwave Theory Techniques, MTT-17 (Nov. 1969); in particular, E. Stern, "Microsound Components, Circuits, and Applications", and the special issue on Microwave Acoustic Signal Processing, IEEE Trans. Sonics/Ultrasonics, SU-20 (Apr. 1973).

(2) It came to the attention of the authors at the Conference referred to in (3) that J. B. Harrington, et al., of Hughes Aircraft Company and A. A. Oliner of Polytechnic Institute of New York had also considered such a transducer array but involving techniques other than the ones discussed in this report. See J. B. Harrington, M. E. Pedinoff, and A. E. Clough, Program Summary Status, "Intercept Techniques Time Frequency Coded Communications Study", RADC Contract F30602-71-C-0128 (Jun. 1972).

(3) C. S. Tsai, "Acoustic Surface Wave Phased-Array", Midwinter Solid State Research Conference-The Science and Technology of Optical/Acoustical Surface and Guided Waves, University of California at Irvine, Irvine, CA (Jan. 21-26, 1973).

(4) P. Hartemann, "Frequency Selective Scanning of Acoustic Surface Waves", Electron. Lett., 9, 246-247 (May 31, 1973); R. M. DeLaRue, C. Stewart, C. D. W. Wilkinson, and I. R. Williamson, "Frequency-Controlled Beam Steering of Surface Acoustic Waves Using a Stepped Transducer Array", Electron. Lett., 9, 326-327 (Jul. 26, 1973).

(5) K. L. Davis and V. L. Newhouse, "Steering of Acoustic Surface Waves by Nonlinear Mixing", Appl. Phys. Lett., 21, 323-325 (1972).

(6) D. A. Richardson and G. S. Kino, "Probing of Elastic Surface Waves in Piezoelectric Media", Appl. Phys. Lett., 16, 83-84 (Jan. 1970).

(7) J. M. Stone, Radiation and Optics (New York: McGraw-Hill, 1963).

(8) See for example, M. I. Skolnik, Introduction to Radar Systems (New York: McGraw-Hill, 1962); J. L. Allen, "Array Antennas: New Applications for an Old Technique", IEEE Spectrum, 115-130 (Nov. 1964); and "Phased Array Antennas", Proceedings of the 1970 Phased Array Antenna Symposium, A. A. Oliner and G. H. Knittle, Eds. (Airtech House, 1972); Microwave Scanning Antennas Series, R. C. Hansen, Ed. (New York: Academic Press, 1966).

(9) L. B. Lambert, M. Arm and A. Aimette, "Electro-optical Signal Processors for Phased Array Antennas", Optical and Electro-Optical Information Processing (Massachusetts: MIT Press, 1965).

(10) See for example, A. J. Slobodnik and P. H. Carr, "Microwave Frequency Acoustic Surface Waves", 1968 IEEE Symposium on Sonics and Ultrasonics, Paper C-7, New York, NY (Sep. 1968); A. J. Slobodnik, Jr., "Microwave Frequency Acoustic Surface Wave Propagation Losses in $LiNbO_3$", Appl. Phys. Lett., 14, 94-96 (Feb. 1969); E. G. H. Lean, C. C. Tseng, and C. G. Powell, "Optical Probing of Surface Acoustic Wave Harmonic Generation", Appl. Phys. Lett., 16, 32-35 (Jan. 1970); and G. Cambon, M. Rouzeyre, and G. Simon, "Optical Probing of Surface Rayleigh Waves", Appl. Phys. Lett., 18, 295-298 (Apr. 1971).

(11) See for example, M. S. Kharusi and G. W. Farnell, "Diffraction and Beam Steering for Surface-Wave Comb Structures on Anisotropic Substrates", IEEE Trans. Sonics/Ultrasonics, SU-18, 35-42 (1971).

(12) I. M. Mason and E. A. Ash, "Acoustic Surface-Wave Beam Diffraction on Anisotropic Substrates", J. Appl. Phys. 42, 5343-5351 (1971).

(13) F. V. Cho, R. L. Lawson, and B. J. Hunsinger, "A Note on the Determination of the Diffraction Pattern of Interdigital Surface-Wave Devices", IEEE Trans. Sonics/Ultrasonics, SU-17, 199-200 (1970).

(14) R. D. Weglein, M. E. Pedinoff, and H. Winston, "Diffraction Spreading of Surface Waves on $LiNbO_3$", Electron. Lett., 6, 654-656 (1970).

(15) T. L. Szabo and A. J. Slobodnik, Jr., "The Effect of Diffraction on the Design of Acoustic Surface Wave Devices", IEEE Trans. Sonics/Ultrasonics, SU-20, 240-251 (1973).

(16) M. I. Skolnik, Radar Handbook (New York: McGraw-Hill, 1970).

(17) J. B. Harrington, M. E. Pedinoff, and A. E. Clough, Program Summary Status, "Intercept Techniques Time Frequency Coded Communications Study", RADC Contract F-30602-71-C-0128 (Jun. 1972).

(18) See for example, A. Korpel, R. Adler, P. Desmares, and W. Watson, "A Television Display Using Acoustic Deflection and Modification of Coherent Light", Proc. IEEE, 54, 1429-1439 (1966); G. A. Coquin, J. P. Griffin and L. K. Anderson, "Wideband Acousto-optic Deflectors Using Acoustic Beam Steering", IEEE Trans. Sonics/Ultrasonics, SU-17, 34-40 (1970); D. A. Pinnow, "Acousto-Optic Light Deflection: Design Considerations for First-Order Beam-Steering Transducers", IEEE Trans. Sonics/Ultrasonics, SU-18, 209-214 (1971).

(19) C. S. Tsai, "Thin-Film Acousto-Optic Surface Wave Interactions", ONR-ARPA Electro-Optic Program Review, Paper V-3, Arlington, VA (Oct. 2-4, 1973).

(20) J. F. Weller, T. G. Giallorenzi, and A. F. Milton, "Light Deflection in Single and Multimode Waveguides Using the Acousto-Optic Interaction", Topical Meeting on Integrated Optics, Paper WA9-1, New Orleans, LA (Jan. 21-24, 1974).

(21) M. C. Hamilton and D. A. Wille, "Acousto-Optic Diffraction in Optical Waveguides", Topical Meeting on Integrated Optics, Paper WA8-1, New Orleans, LA (Jan. 21-24, 1974); C. S. Tsai, "Wideband Guided-Wave Acousto-Optic Devices and Their Applications", Proceedings of the 1974 Electro-Optical Systems Design Conference/International Laser Exposition, pp. 192-200, Nov. 5-7, San Francisco, CA.

(22) C. S. Tsai, S. K. Yao, and M. A. Alhaider, "A High Performance Acousto-Optic Guided-Light Beam Device Using Intersecting Surface Acoustic Beams", Integrated Optics and Fiber Optics Communication Conference, Post Deadline Paper D.12, Naval Electronics Laboratory Center, San Diego, CA, May 15-17, 1974 (Unpublished).

PART II

GUIDED - WAVE ACOUSTO-OPTIC INTERACTIONS AND DEVICES

Noncollinear, coplanar acousto-optic Bragg interaction, involving surface acoustic waves (SAW) and guided-optical waves (Fig. 1), has been a subject of considerable interest in recent years (1-17). Some of the more obvious advantages of the related guided-wave A-O Bragg devices over their bulk-type counterparts are: (1) since the energies of both the guided-optical waves and the SAWs are concentrated in a thin layer and also since both waves spread (by diffraction) only in one dimension, less RF drive power is required to achieve a high diffraction efficiency with the guided-wave devices, (2) the dispersion properties of both the guided-light waves and the SAWs enable the phase matching conditions to be fulfilled for a wider range of acoustic frequency and, therefore, a wider device bandwidth is inherent with guided-wave devices, (3) guided-wave devices have smaller size and lighter weight, and have less critical isolation and alignment problems, (4) there exists a good possibility for batch fabrication of the guided-wave devices and thus for a great reduction in cost, and (5) as a result of their planar configuration the guided-wave devices are easier to fabricate and are more compatible with future fiber/integrated optic systems. Indeed, very efficient diffraction has been demonstrated in recent experiments using Y-cut $LiNbO_3$ waveguiding layers (5, 11-14). For example, a diffraction efficiency of 85% and a -3db bandwidth of 100 MHz, requiring only 190-mw electric drive power, have been demonstrated using a single SAW of 180-MHz center frequency (14). This efficient interaction results, not only from the fact that the frequency range of the SAW may be chosen to achieve a good matching between optical confinement and the SAW penetration depth, but also from the fact that the electro-optic effect arising from the intense piezoelectric field, which accompanies the SAW, can enhance the interaction in the Y-cut $LiNbO_3$ substrate (18).

However, for many potential applications involving guided-wave A-O devices bandwidth is the most important device characteristic, particularly for a number of anticipated wideband applications to be discussed later in this report. For example, in beam deflection and switching applications the wider the device bandwidth, the larger will be the number of scannable spot diameters and the faster will be the switching speed of the deflected light beam. Bandwidth of a guided-wave acousto-optic Bragg device is limited by both the acoustic bandwidth of the SAW transducer and the Bragg bandwidth.

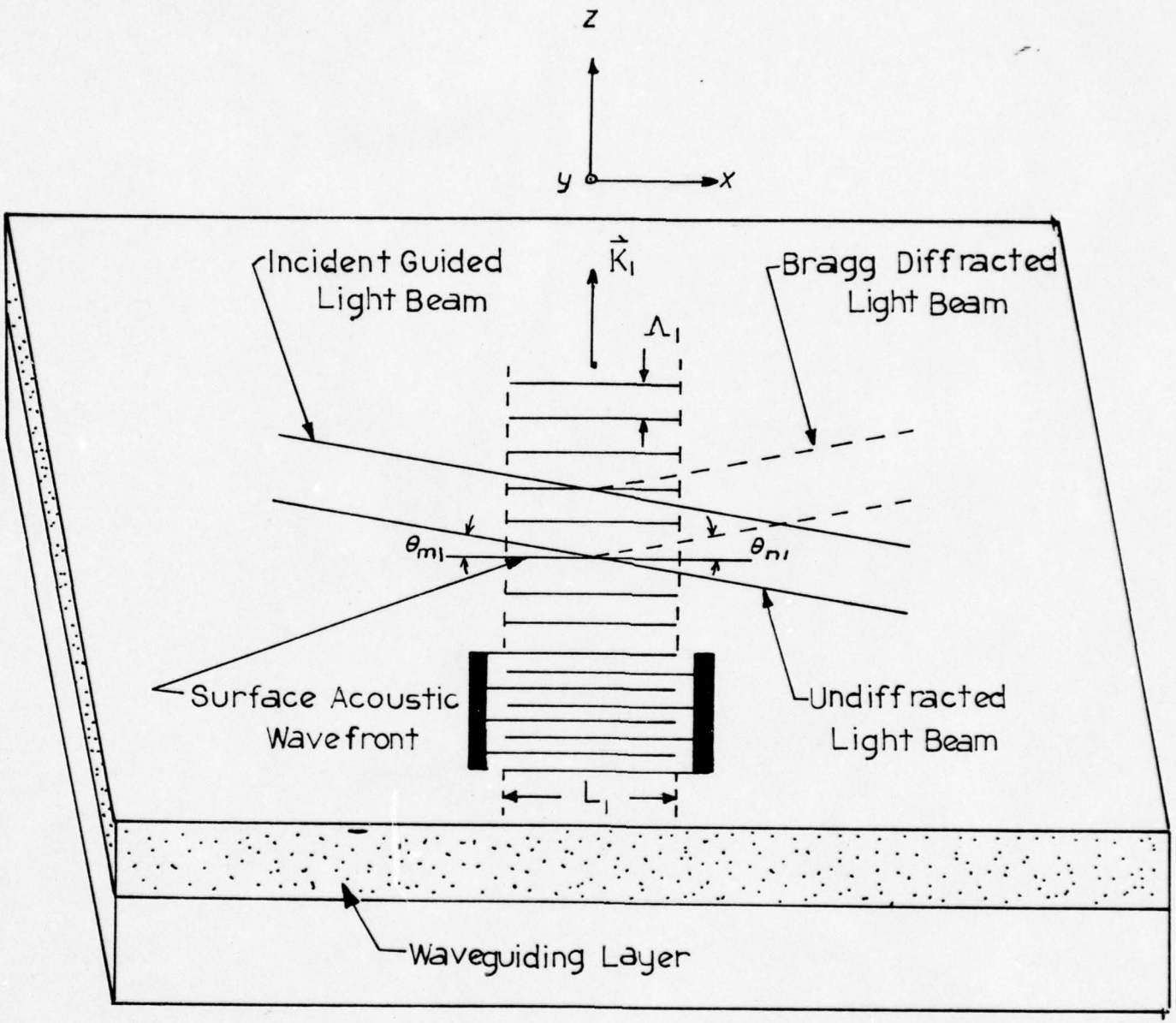

Fig. 1 Guided-Wave Acousto-optic Bragg-Diffraction From A Single Surface Acoustic Wave.

The first inherent limitation of guided-wave A-O devices which employ a single interdigital transducer and, thus, a single SAW is their relatively small acoustic bandwidth. This limitation results from the fact that the fractional acoustic bandwidth is inversely proportional to the number of finger electrode pairs while the electric-acoustic conversion efficiency is proportional to the number of finger electrode pairs squared (19). It follows that a balance between the fractional acoustic bandwidth and the electric-acoustic conversion efficiency will automatically limit the former to a relatively small value.

With regard to the second inherent limitation on the device bandwidth, it is observed that unlike bulk-type devices (20), the Bragg bandwidth of guided-wave devices is not only limited by the acoustic center frequency, the acoustic bandwidth, and the aperture of the SAW, but also depends on the diffraction efficiency of the device and the optical modes involved (14). While this dependence for the devices which employ Y-cut $LiNbO_3$ substrate is presented in this report, it suffices to point out here that in order to realize a large Bragg bandwidth (assuming an acoustic bandwidth sufficiently larger than the Bragg bandwidth) the aperture of the single SAW must be chosen very small. This requirement in turn results in a drastic decrease in diffraction efficiency. Under such an unfavorable condition a device with both large diffraction efficiency and large bandwidth requires a large rf drive power which may easily result in the failure of the interdigital transducer. Thus, it can be concluded that diffraction efficiency-bandwidth product of a guided-wave A-O device using a single SAW is rather limited.

In this study, we have experimented with two device configurations utilizing multiple SAWs, mainly, tilted (11-14) and phased SAWs (6, 10, 11), in order to determine their bandwidth capability. The first device configuration employs multiple interdigital SAW transducers which are characterized by staggered center frequencies and propagation axes tilted with respect to each other. It is clear that the multiple tilted SAWs generated by such a transducer array can be made to satisfy the Bragg condition in each frequency band and thus enable a broad composite frequency response to be realized. The second device configuration is characterized by multiple interdigital SAW transducers of identical center frequency and propagation axis, but arranged

in a stepped configuration. As a result of the step height a phase shift is introduced between adjacent SAWs, and the resultant wavefront can be scanned by varying the acoustic frequency, as described in Section III. Scanning of the wavefront enables a composite acoustic beam of large aperture to track the Bragg condition and, therefore, makes efficient diffraction possible for a relatively wide frequency band. Preliminary experimental results have borne out the above observations. For example, by employing just two tilted SAWs on a Y-cut $LiNbO_3$ out-diffused waveguide, a -3db bandwidth of 200 MHz with 50% diffraction efficiency was obtained, requiring a total electric drive power of only 200 mw (13). Also, by employing six-element phased SAWs, a -3db bandwidth of 110 MHz with 50% diffraction efficiency was obtained, requiring a total electric drive power of only 68 mw (21). These performance figures greatly exceed that obtained in previous devices which employ only a single SAW.

In this report theoretical and experimental results relating the two wideband device configuration referred to above are described. First, the diffraction efficiency and the bandwidth of the acousto-optic Bragg diffraction using a single SAW in a Y-cut $LiNbO_3$ out-diffused optical guiding layer are analyzed in detail. The methodology for numerical computation has been established to calculate the diffraction efficiency and the bandwidth as a function of the optical and acoustic parameters such as the penetration depth of the guiding layer, waveguide modes, direction of propagation, center frequency and aperture of the SAW. The same analytical approach and numerical computation methodology are then applied to the case of two tilted SAWs and finally to the case of N-tilted and phased SAWs. The resultant diffraction efficiency and the bandwidth, as a function of various device parameters such as the center frequency and the beam aperture of the individual SAWs, the tilt angle and the step height as well as the phase shift between adjacent SAWs, and the optical waveguide modes involved are calculated. Experiments using two to four tilted SAWs and two to six-element phased SAWs in single-mode Y-cut $LiNbO_3$ out-diffused waveguides (22) were carried out to verify the theoretical predictions. In one of the wideband units being studied, a device bandwidth of 358 MHz has been realized. A bandwidth of 358 MHz enables the device to deflect a light beam of 1-cm aperture into 1000 resolvable spot diameters at a random-access switching time of 2.8 μs. The development of this wideband technique has paved the way for using such guided-wave acousto-optic devices for a number of wideband applications. Experimental demonstration of four applications is described together with preliminary performance figures.

IV. GUIDED-WAVE ACOUSTO-OPTIC BRAGG DIFFRACTION FROM A SINGLE SURFACE ACOUSTIC WAVE

A. Coupled-Mode Analysis

We have employed the coupled-mode approach similar to that employed by Ohmachi (3) for the analysis of noncollinear, coplanar Bragg diffraction from multiple-tilted SAWs (see Figure 2). It should be noted, however, that while a step-index optical wave-guide is considered in Reference 3, a gradient-index optical waveguide is considered in this study as Y-cut $LiNbO_3$ out-diffused waveguiding layers (22) were utilized in the devices being studied. As a result, the numerical computations involved are considerably more complicated. It is also to be noted that in this study the contribution to the interaction from the electro-optic effect which accompanies the SAW is taken into account because this contribution is important in $LiNbO_3$ substrates. However, the contribution from the surface ripple is neglected as it is small compared to the elasto-optic and the electro-optic contributions.

Although our main concern is with the interaction configuration involving multiple-tilted SAWs, we shall first consider the one involving only a single SAW or, equivalently, the interaction configuration involving the first SAW of multiple-tilted SAWs as the results obtained will reveal the key device parameters as well as the limitations of the devices using a single SAW. The methodology for numerical computation which is developed for the case involving a single SAW can be conveniently extended to the case involving two or more tilted SAWs. Only an outline of the analysis and some of the most relevant results will be presented in this report. The complete analysis and results for the general case involving any number of tilted SAWs will be published elsewhere.

Since a Y-cut $LiNbO_3$ out-diffused waveguide can support only TE modes (22), we assume that the coplanar Bragg diffraction involves the interactions among the incident light of the m^{th} TE mode, the diffracted light of the n^{th} TE mode and a piezoelectric SAW propagating in the z-direction (see Figure 1). In the following analysis the subscript 1 designates the quantities relating the first SAW. The corresponding angles of incidence and diffraction, θ_{m1} and θ_{n1}, measured from the normal to the acoustic wave vector K_1, are determined not only by the optical and acoustic wavelengths but also by the refractive indices, n_{m1} and n_{n1}, for the m_1^{th} and n_1^{th} modes,

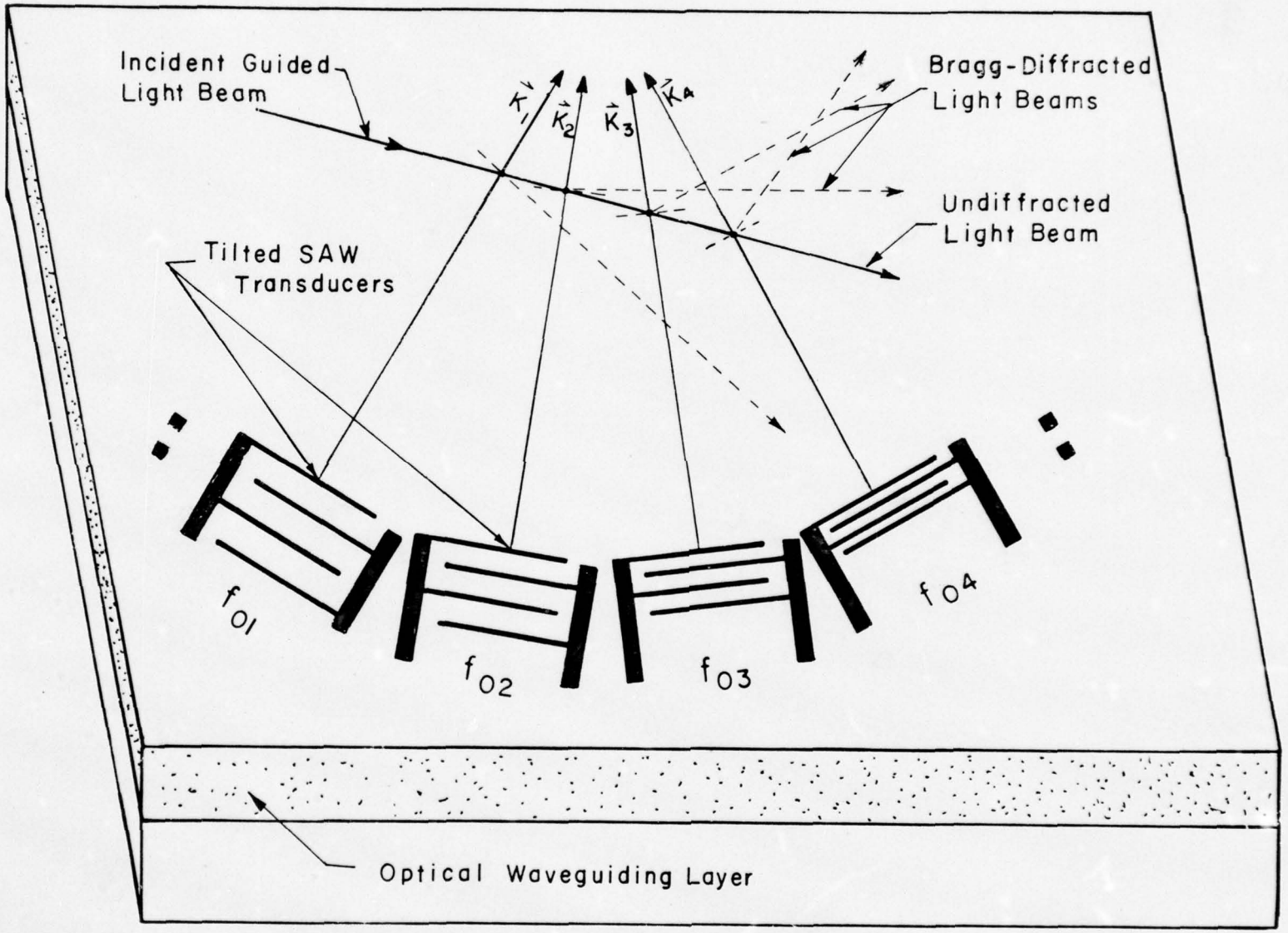

Fig. 2 Guided-Wave Acousto-optic Bragg-Diffraction From Multiple Tilted Surface Acoustic Waves.

respectively (3, 23). Note that when there is no mode conversion between the diffracted and undiffracted light waves, $n_1 \equiv m_1$ and $n_{n1} \equiv n_{m1}$, and thus the Bragg condition reduces to the well known one in an isotropic medium (20).

Assuming that the medium is lossless both optically and acoustically, the corresponding electric fields $\hat{E}_{m1}$ and $\hat{E}_{n1}$ of the undiffracted and diffracted light waves, the strain field $\hat{S}_1$ of the SAW and its accompanying piezoelectric field $\hat{E}_{p1}$ can be written as follows:

$$\hat{E}_{m1}(x,y,z,t)=1/2E_{m1}(x)U_{m1}(y)\exp j(\omega_{m1}t-k_{m1x}x-k_{m1z}z) + C.C \quad (1a)$$

$$\hat{E}_{n1}(x,y,z,t)=1/2E_{n1}(x)U_{n1}(y)\exp j(\omega_{n1}t-k_{n1x}x-k_{n1z}z) + C.C \quad (1b)$$

$$\hat{S}_1(y,z,t)=1/2S_{I1}U_{aI1}(y)\exp j(\Omega_1 t-K_1 z + \phi_1) + C.C, \ (I=1,2,3,4,5,6) \quad (1c)$$

$$\hat{E}_{p1}(y,z,t)=1/2E_{pi1}U_{pi1}(y)\exp j(\Omega_1 t-K_1 z + \phi_1) + C.C, \ (i = 1,2,3) \quad (1d)$$

where $E_{m1}(x)$ and $E_{n1}(x)$ are the spatial distribution of the undiffracted and diffracted light waves to be determined; S_{I1} and E_{pi1} are the components of the strain field and its accompanying piezoelectric field, respectively, $U_{m1}(y)$, $U_{n1}(y)$, $U_{aI1}(y)$ and U_{pi1} are, respectively, the normalized field distribution (along the waveguide thickness) of the light waves, the acoustic wave and the piezoelectric field. It is to be noted that for simplicity the subscripts I and i will be dropped henceforth. The frequencies of the light waves and the acoustic wave are designated by ω_{m1}, ω_{n1}, and Ω_1, respectively, Similarly, k_{m1}, k_{n1} and K_1 designate the corresponding wave numbers and the suffixes x and z represent the x and z components. Finally, ϕ_1 designates the phase of the SAW.

When Equations (1a), (1b), (1c) and (1d) are substituted into the wave equation for the electric field of the optical waves a set of coupled wave equations for $E_{m1}(x)$ and $E_{n1}(x)$ are obtained. These coupled wave equations are then readily reduced to the following decoupled form:

$$\frac{\partial^2 E_{m1}(x)}{\partial x^2} - jK_1\Delta\theta_1 \frac{\partial E_{m1}(x)}{\partial x} + A_1B_1E_{m1}(x) = 0 \quad (2a)$$

$$\frac{\partial^2 E_{n1}(x)}{\partial x^2} + jK_1\Delta\theta_1 \frac{\partial E_{n1}(x)}{\partial x} + A_1B_1E_{n1}(x) = 0 \quad (2b)$$

From Equations (2a) and (2b) general solutions for $E_{m1}(x)$ and $E_{n1}(x)$ are easily found. By matching the boundary conditions $E_{m1}(0) \equiv 1$ and $E_{n1}(0) \equiv 0$ to these general solutions, the electric field of the undiffracted and diffracted light waves at the output of the interaction region ($x = L_1$) are given as follows:

$$E_{m1}(L_1) = \left\{ \cos(q_1 L_1) - j(K_1 \Delta\theta_1 / 2q_1)\sin(q_1 L_1) \right\} \exp j(K_1 \Delta\theta_1 L_1/2) \qquad (2c)$$

$$E_{n1}(L_1) = j(B_1/q_1)\sin(q_1 L_1)\exp j \left\{ -(K_1 \Delta\theta_1 L_1/2) + \phi_1 \right\} \qquad (2d)$$

where

$$q_1^2 \equiv (K_1 \Delta\theta_1/2)^2 + A_1 B_1 \qquad (2e)$$

$$A_1 \equiv \frac{\omega_{n1}^2 n_{m1}^2 n_{n1}^2}{4c^2 k_{m1} \cos\theta_{m1}} \left\{ p_1 S_1 \int_0^\infty U_{m1} U_{n1} U_{a1}\, dy + r_1 E_{p1} \int_0^\infty U_{m1} U_{n1} U_{p1}\, dy \right\} \Big/ \int_{-\infty}^{\infty} U_{m1}^2\, dy \qquad (2f)$$

$$B_1 \equiv \frac{\omega_{m1}^2 n_{m1}^2 n_{n1}^2}{4c^2 k_{n1} \cos\theta_{n1}} \left\{ p_1 S_1 \int_0^\infty U_{m1} U_{n1} U_{a1}\, dy + r_1 E_{p1} \int_0^\infty U_{m1} U_{n1} U_{p1}\, dy \right\} \Big/ \int_{-\infty}^{\infty} U_{n1}^2\, dy \qquad (2g)$$

p_1 = relevant photoelastic constant or constants

r_1 = relevant electro-optic coefficient or coefficients

c = velocity of light in free space

$\Delta\theta_1$ = deviation of the incident angle from the Bragg angle

It is to be noted that the input boundary values to an adjacent SAW in the case with multiple-tilted SAWs are simply those given by Equations (2c) and (2d) with appropriate phase factors added to account for the propagation delay between the two SAWs.

B. Diffraction Efficiency

From Equations (2c)-(2g), the diffraction efficiency which is the ratio of the diffracted light power at the output ($x = L_1$) and the incident light power at the input of the interaction region ($x = 0$) can be found:

$$\zeta_1 = g_1^2 \left\{ \frac{\sin\left[g_1^2 + (K_1\Delta\theta_1 L_1/2)^2\right]^{1/2}}{\left[g_1^2 + (K_1\Delta\theta_1 L_1/2)^2\right]^{1/2}} \right\}^2 \tag{3a}$$

where

$$g_1^2 \equiv A_1 B_1 L_1^2 = \left(\frac{\pi^2}{4\lambda_o^2}\right)(n_{m1}^3 n_{n1}^3 \Gamma_{m1n1}^2 L_1^2/\cos\theta_{m1}\theta_{n1}) \tag{3b}$$

$$\Gamma_{m1n1}^2 = \left\{\int_o^\infty U_{m1}U_{n1}(p_1S_1U_{a1}+r_1E_{p1}U_{p1})dy\right\}^2 \Big/ \left\{\int_{-\infty}^\infty U_{m1}^2 dy \int_{-\infty}^\infty U_{n1}^2 dy\right\} \tag{3c}$$

λ_o = wavelength of the incident light wave in free space

L_1 = aperture of the SAW

From Equation (3a) it is seen that the diffraction efficiency is a sensitive function of Γ_{m1n1}^2, the so-called overlap integral (1) and also that dependence on the material parameters differs drastically from that in bulk-type acousto-optic interactions (20). An efficient diffraction can occur only when the confinement of the undiffracted and diffracted light waves matches the penetration depth of the SAW.

Finally, the relationship between the parameter g_1^2 and the total acoustic power P_{A1} are shown to be given as follows:

$$P_{A1} \cong -1/2L_1 \int_o^\infty \mathrm{Re}\left\{(V_x+V_y+V_z)^* (-e_1E_{p1}U_{p1}+c_1S_1U_{a1})\right\} dy \tag{3d}$$

$$g_1^2 \cong -\left(\frac{\pi^2}{2\lambda_o^2}\right)\left(\frac{n_{m1}^3 n_{n1}^3 L_1}{\cos\theta_{m1}\cos\theta_{n1}}\right)\left(\frac{1}{\int_o^\infty \mathrm{Re}\left\{(F_x+V_y+V_z)^* (-e_1E_{p1}U_{p1}+c_1S_1U_{a1})\right\}dy}\right)\Gamma_{m1n1}^2 P_{A1} \tag{3e}$$

where Re designates the fact that only the real part is to be taken; e_1 and c_1 are, respectively, the relevant piezoelectric and stiffness constants; V_x, V_y, and V_z designate the relevant displacement velocities. It is to be noted that in Equation (3d) the piezoelectric contribution to the acoustic power is neglected as it is small compared with the strain contribution.

For the case with the SAW propagating in either the Z-direction or the 21.8° from the Z-axis of a Y-cut $LiNbO_3$ substrate with which experiments have been carried out (Section IV) all relevant parameters are known (24,25). Thus, the relative contributions to the diffraction due to the elasto-optic and electro-optic effects (Eq. (3c)) as well as the relationship between P_{A1} and g_1^2 (Eq. (3e)) can be calculated numerically.

Numerical calculation of the relative elasto-optic and electro-optic contributions to the diffraction has been carried out for the case of He-Ne laser light (0.6328 μm) propagating in a Y-cut $LiNbO_3$ out-diffused optical guiding layer. The relevant SAW propagation parameters are taken from Ref. 25. For example, the depth dependence of the strains of the Z-propagating SAW and the accompanying piezoelectric field have been calculated using these parameters and are given in Figs. 3(a) and 3(b), respectively. Note that the penetration depth of the SAW is inversely proportional to the acoustic frequency. It is assumed in this calculation that both the diffracted and the undiffracted light waves belong to the same TE mode, namely, $n_{m1}=n_{n1}$. This assumption is based on the fact that no mode conversion has been observed in the experiments to be described later. The normalized optical field distribution $U_{m1}(y)$ or $U_{n1}(y)$ for the three lowest order modes are regenerated from the formulation given in Ref. 26 and are shown in Fig. 3(c).

Finally, the relevant photoelastic constants and electro-optic coefficients are needed for the numerical calculation of Eq. 3(c). For the SAW propagating along or approximately along the Z(c)-axis of the Y-cut $LiNbO_3$ substrate the dominant strain components responsible for the interaction are S_2 and S_3 with the corresponding photoelastic constants $P_{31}=P_{32}=0.178$ and $P_{33}=.088$ (27). The corresponding electro-optic coefficients are $r_{33}=31\times10^{-10}$ volt/cm and $r_{31}=r_{32}=0$. It can be shown that for the SAW propagating along or approximately along $\pm$ 21.8° from the Z(c)-axis five components of the strain fields and two components of the associated electric field contribute to the diffraction. The two dominant strain components are S_5 and S_6 with the corresponding photoelastic constants $(-0.38P_{14})= -0.06$ and $(-0.048P_{11} -0.297P_{31}+0.048P_{13}+0.297_{33}) = 0.024$. The dominant electric field component is E_1 with the corresponding electro-optic coefficient $(0.128r_{13} + 0.8r_{33} + 0.256r_{42}) = 32.9\times10^{-10}$ volt/cm.

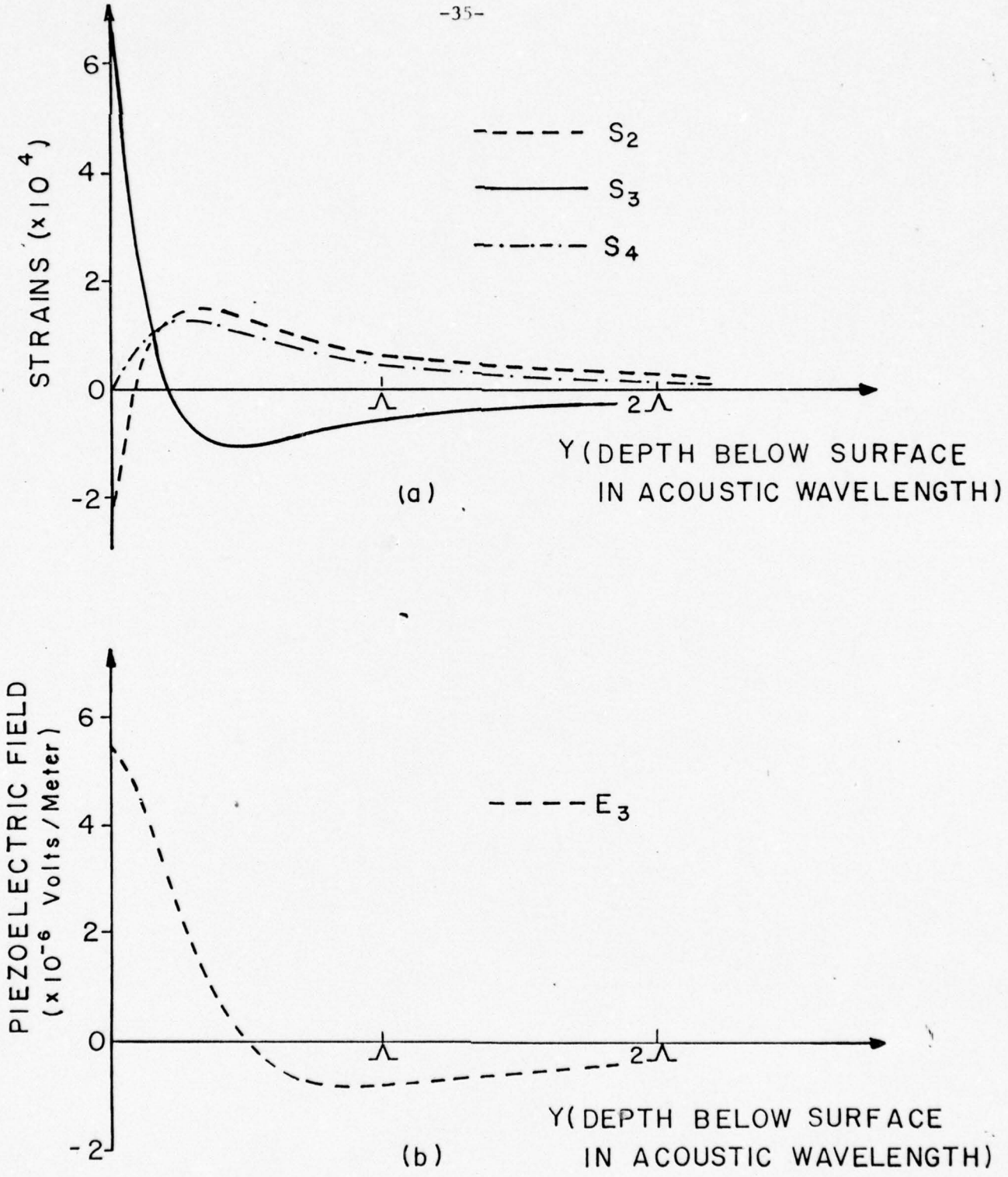

Fig. 3 a) Depth Dependence of the Strain Fields for the SAW Propagating Along the Z-axis of Y-cut $LiNbO_3$ substrate,

b) Depth Dependence of the Accompanying Piezoelectric Fields to (a).

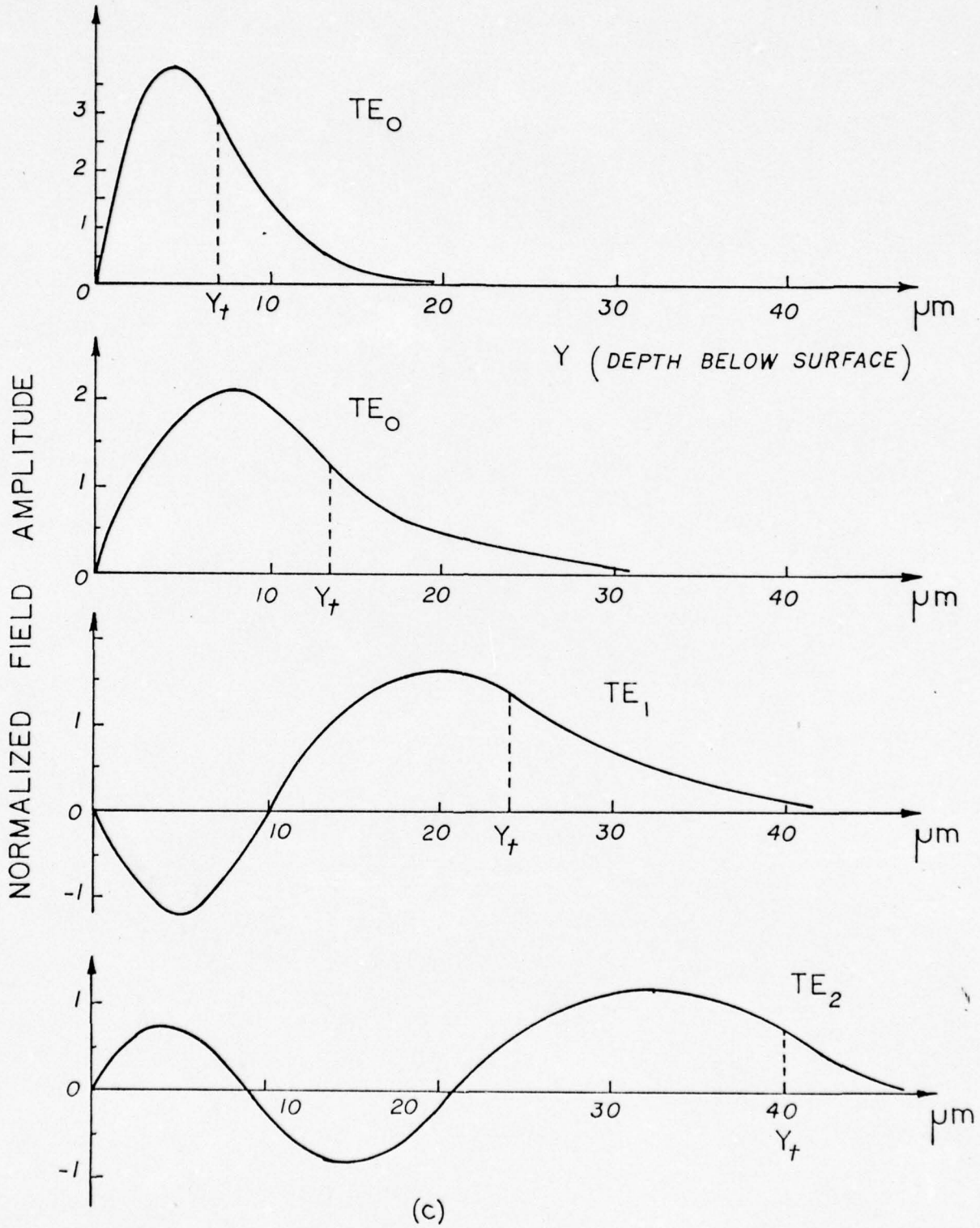

Fig. 3 c) Profiles of the TE Optical Waveguide Modes in Y-cut $LiNbO_3$ Out-Diffused Layers (Y_t is the Turning Point).

Using the acoustic and optical field distributions and the elasto-optic and electro-optic parameters as described above, spatial variations of the relative elasto-optic and electro-optic contributions to the Bragg diffraction have been calculated. The results are shown in Fig. 4. From Figs. 4(a) and 4(b) it is seen that while the electro-optic effect is the dominant cause of the diffraction in the case of the Z-propagating SAW, both the electro-optic and the elasto-optic effects contribute nearly equally to the diffraction for the case of the 21.8° -propagating SAW. Similarly, the relative Bragg diffraction efficiency as a function of the acoustic frequency, with the penetration depth of the waveguide mode as a parameter, can also be calculated. Fig. 5 shows the calculated results for the two directions of propagation using a SAW of 1.74mm aperture and an optical TE_o mode of two penetration depths. These plots clearly show that the Z-propagating SAW can provide more efficient Bragg diffraction at relatively low acoustic frequency. In contrast, the 21.8° -propagating SAW provides more efficient Bragg diffraction at higher acoustic frequency. Furthermore, the smaller the penetration depth of the optical guiding layer the higher will be the diffraction efficiency and the operating frequency.

C. Bandwidth Limitations

From Equation (3a) it can also be seen that the interaction bandwidth assuming a sufficiently large acoustic bandwidth, depends not only on the acoustic aperture L_1 but also on g_1^2 and, thus, the diffraction efficiency. This is because the penetration depth of the SAW and, thus, $\Gamma_{m1n1}{}^2$ varies with the acoustic frequency. In the following analysis the -3db interaction bandwidth, $2\Delta f_1$, for the case with center frequency f_{01} is calculated. Since at the exact Bragg condition ($\Delta\theta_1 = 0$) and at $f_1 = f_{01}$, the diffraction efficiency is given by $\{\sin g_1(f_{01})\}^2$, the half bandwidth Δf_1 can be determined from the following equality:

$$\frac{1}{\sqrt{2}} \frac{\sin f_1(f_{01})}{g_1(f_{01}\pm\Delta f_1)} \simeq \frac{\sin\left[g_1^2(f_{01}\pm\Delta f_1)+\{\pi(f_{01}\pm\Delta f_1)\Delta\theta_1 L_1/v_{R1}\}^2\right]^{1/2}}{\left[g_1^2(f_{01}\pm\Delta f_1)+\{\pi(f_{01}\pm\Delta f_1)\Delta\theta_1 L_1/v_{R1}\}^2\right]^{1/2}} \qquad (4a)$$

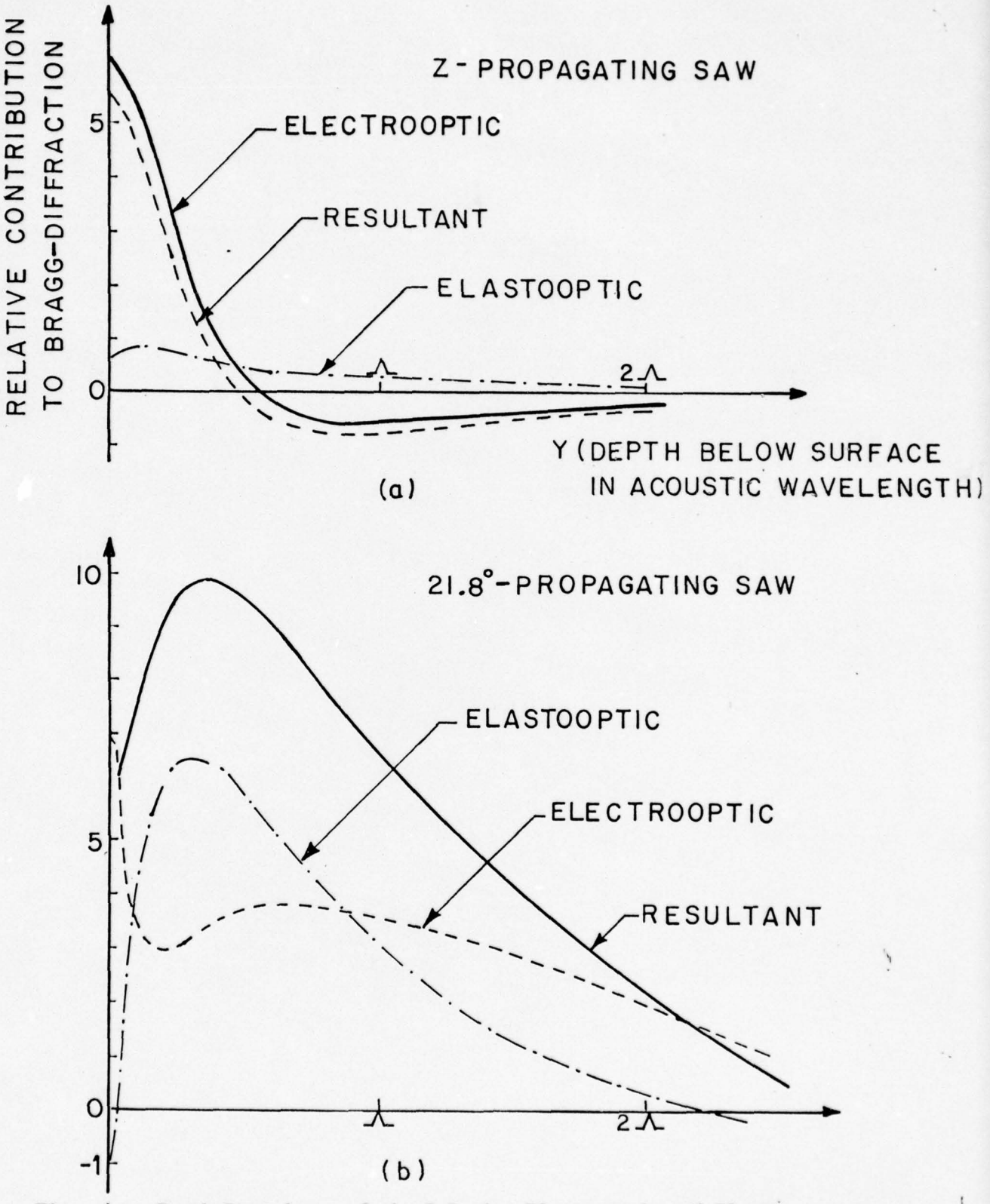

Fig. 4 Depth Dependence of the Relative Elasto-optic and Electro-optic Contributions to Bragg Diffraction: (a) For Z-Propagating SAW, (b) For 21.8° - Propagating SAW.

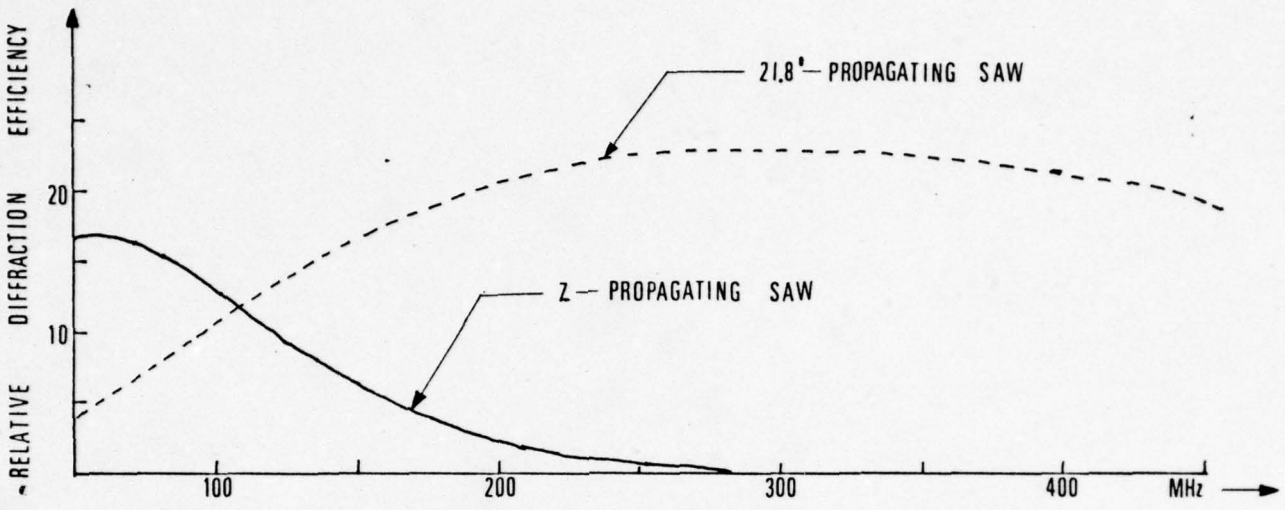

(a)

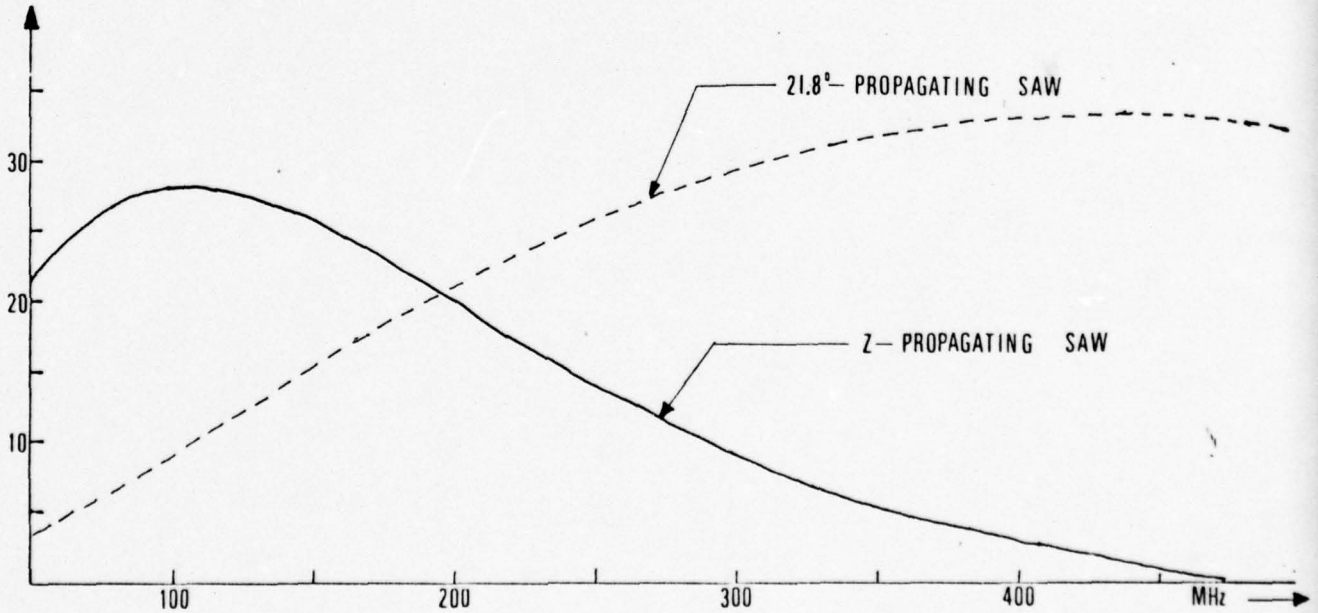

(b)

Fig. 5 Relative Bragg Diffraction Efficiency vs the Acoustic Frequency in Y-cut $LiNbO_3$ Out-Diffused Waveguides: (a) Penetration Depth of the TE_o Mode = 13.5μm, (b) Penetration Depth of the TE_o Mode = 7.0μm.

where

$$\Delta\theta_1 = \frac{\lambda_0}{2n_{m1}v_{R1}\cos\theta_{m1}} \left[1 - \{(n_{m1}^2 - n_{n1}^2)v_{R1}^2/f_{01}^2\lambda_0^2\} \right] \Delta f_1 \qquad (4b)$$

or

$$\Delta\theta_1 = \frac{\lambda_0}{2n_{m1}v_{R1}\cos\theta_{m1}} \Delta f_1 \qquad (\text{for } n_{m1} = n_{n1}) \qquad (4c)$$

and v_{R1} designates the velocity of the SAW.

Again, using the acoustic and optical field distributions and the elasto-optic and electro-optic parameters described previously a set of frequency response curves for the lowest order TE mode (TE_o), having g_1 as a parameter, have been obtained and are shown in Fig. 6. In these plots the acoustic waves are assumed to have center frequencies of 170,255 and 382 MHz, each with a 30% fractional acoustic bandwidth Δf_a. Fig. 6(a) is plotted for the acoustic apertures L_1 = 2.5mm, L_2 = 1.66mm and L_3 = 1.11mm while Fig. 6(b) is plotted for acoustic apertures 100% larger. It is seen that the interaction bandwidth decreases as the acoustic aperture increases and may become smaller than the acoustic bandwidth at large acoustic aperture. For example, a Bragg bandwidth of only 45 MHz is possible for a device using a Y-cut $LiNbO_3$ out-diffused waveguide of 7 μm penetration depth in which the acoustic aperture is .5 cm and the acoustic center frequency is 380 MHz.

From the analytical and numerical results presented above, we may conclude that the bandwidth of the guided-wave acousto-optic Bragg-devices using a single SAW is not only limited by the acoustic center frequency, the acoustic bandwidth and the aperture of the SAW but also depends on the diffraction efficiency and the optical modes involved. For the devices which employ the TE_0 and/or TE_1 modes the device bandwidth increases slightly as the diffraction efficiency increases. For other optical modes the device bandwidth may decrease as the diffraction efficiency increases. It is observed that for a device which utilizes a single SAW of low acoustic center frequency the absolute device bandwidth is mainly limited by the acoustic bandwidth. On the other hand, for a device which employs a single SAW of high acoustic center frequency, the absolute device bandwidth is mainly limited by the Bragg bandwidth. Thus, the diffraction efficiency-bandwidth product of a device using a single SAW is rather limited. However, it is clear that by employing a number of SAWs which are of staggered center frequency and tilted propagation direction, efficient Bragg diffraction in each frequency band will make it possible to achieve a large composite bandwidth and, thus, a large diffraction efficiency-bandwidth product.

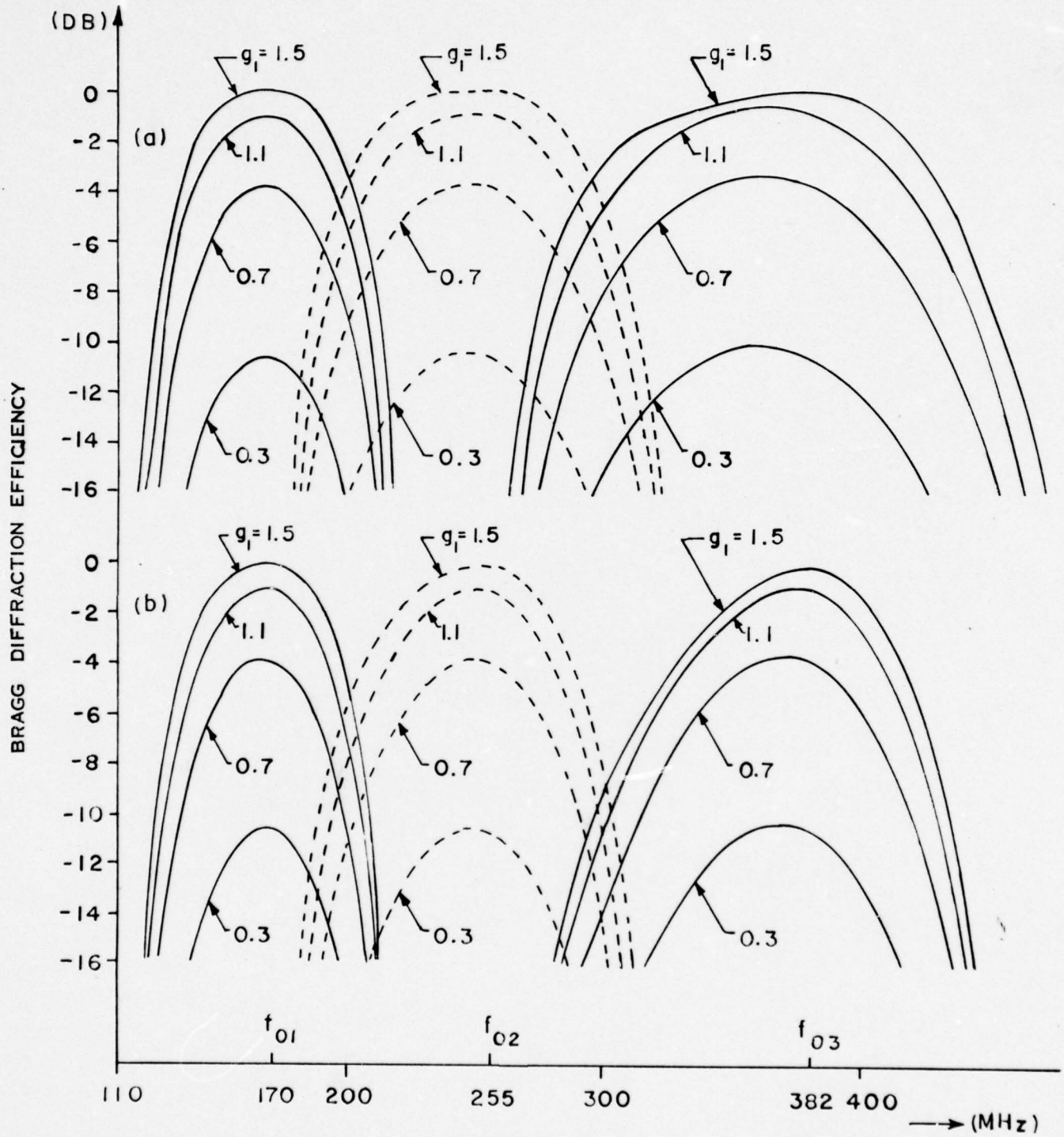

Fig. 6 Frequency Response of the Guided-Wave Acousto-optic Bragg-Diffraction From A Single SAW:

(a) L_1 = 2.5 mm, L_2 = 1.66 mm and L_3 = 1.11 mm

(b) L_1 = 5.0 mm, L_2 = 3.32 mm and L_3 = 2.22 mm

V. GUIDED-WAVE ACOUSTO-OPTIC BRAGG-DIFFRACTION FROM TWO TILTED SURFACE ACOUSTIC WAVES

A. Theory

As mentioned in the beginning of Section IV, the input boundary values (the diffracted and undiffracted light fields) for the interaction region of the second SAW are obtained by adding a phase factor, which accounts for the propagation delay between the two adjacent SAWs, to Equations (2c) and (2d). Thus, the methodology for numerical computation which has been developed for the case involving a single SAW can be conveniently extended to the case involving multiple tilted SAWs. For simplicity, only the case with two tilted SAWs (Figure 7) is treated in this section. Note that in Figure 7 the tilt angle, θ_t, between the two SAWs is set equal to the difference in the Bragg angles at the two acoustic center frequencies. We shall first calculate the resultant diffraction efficiency for this case.

For convenience we shall express the boundary values at the input edge of the second SAW as follows:

$$E_{m2}\,(L_1+\Delta x_{12}) = \alpha \tag{5a}$$

$$E_{n2}\,(L_1+\Delta x_{12}) = \beta \exp\,(j\varphi) \tag{5b}$$

where from Equations (2) and (3) we have,

$$\alpha = (1 - \zeta_1)^{1/2} \tag{5c}$$

$$\beta = (\zeta_1)^{1/2}$$

$$\varphi = \pi/2+(K_1\Delta\theta_1\Delta x_{12}/2)+ \tan^{-1} \{(K_1\Delta\theta_1/2q_1)\sin(q_1L_1)/\cos(q_1L_1) \} +\phi_1 \tag{5e}$$

where φ designates the relative phase between the undiffracted and diffracted light waves and includes the phase shift, ϕ_1, of the first SAW. Substituting Equation (5) into the general solutions for $E_{m2}(x)$ and $E_{n2}(x)$, which take the same form as $E_{m1}(x)$ and $E_{n1}(x)$, we obtain the electric fields of the diffracted light wave at the output of the interaction region:

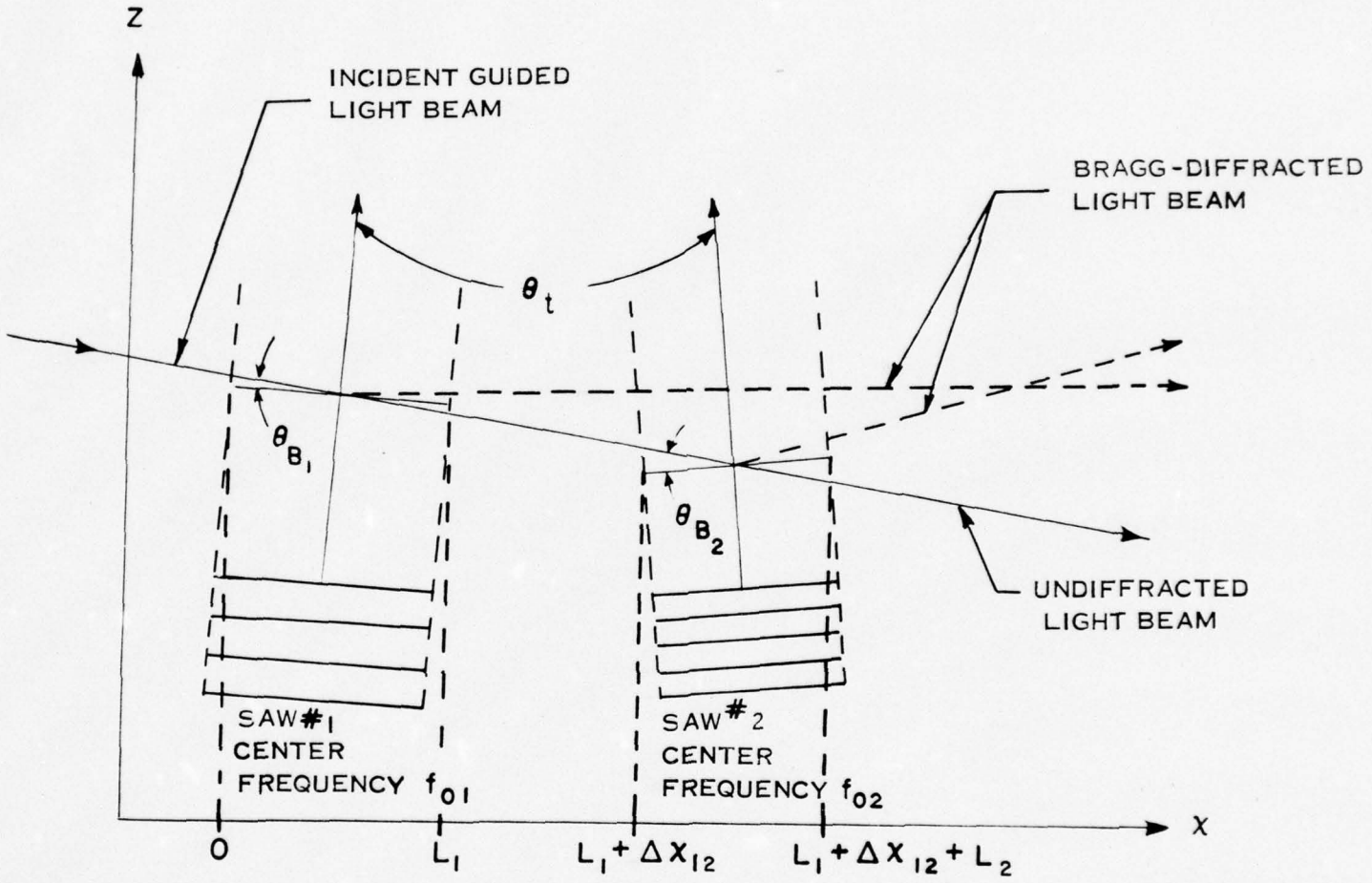

Fig. 7 Guided-Wave Acousto-optic Bragg-Diffraction From Two Tilted Surface Acoustic Waves.

$$E_{n2}(L_1+\Delta x_{12}+L_2) = \beta\cos(q_2L_2)+j(1/q_2)\{(K_2\Delta\theta_2/2)\beta+\alpha\ B_2\exp j(\phi_2-\varphi)\}\ \sin(q_2L_2)$$
$$\times\ \exp j\ \{-(K_2\Delta\theta_2L_2/2)\ +\ \varphi\ \} \qquad (6)$$

where K_2, ϕ_2, $\Delta\theta_2$, L_2, q_2 and B_2 are defined in the same manner as those in the first SAW.

In order to calculate the resultant diffraction efficiency ζ_T we first note that the diffraction efficiency ζ_1 due to the first SAW is simply $|\beta\ \exp(j\varphi)|^2$ which is given by Equation (3a). We also note that the diffraction efficiency ζ_2 due to the second SAW alone is given by $(B_2^2\ /\ q_2^2)\times \sin^2 q_2L_2$ because $A_2 = B_2$. Thus, the resultant diffraction efficiency which is simply $|E_{n2}(L_1+\Delta x_{12}+L_2)|^2$ is

$$\zeta_T=\zeta_1(1-\zeta_2)\ +\ \zeta_2(1-\zeta_1)+2\ \{\zeta_1(1-\zeta_1)\zeta_2\}^{1/2}\{(K_2\Delta\theta_2/2q_2)\sin(q_2L_2)\cos\ (\phi_2-\varphi)$$
$$-\ \cos(q_2L_2)\sin\ (\phi_2-\ \varphi\ )\} \qquad (7)$$

From Eq. (7), it is seen that $\zeta_T \simeq \zeta_1$ for the frequency range $f_a \leq f_{01}$ and $\zeta_T \simeq \zeta_2$ for the frequency range $f_a \geq f_{02}$. On the contrary, for the frequency range $f_{01} \leq f_a \leq f_{02}$ both acoustic waves contribute to the diffraction and the resultant diffraction efficiency is given by the sum of the three terms. The effect of the interference between the two acoustic waves on the resultant diffraction efficiency is represented by the cross term. It is clear that enhancement as well as reduction in the diffraction efficiency occurs as the phase shift $(\phi_2 - \varphi)$ varies.

Using Equation (7), a family of plots for the diffraction efficiency versus the acoustic frequency, with the phase shift between the two SAWs, $\Delta\phi_{12}$, as a parameter, have been generated. Some sample plots for a He-Ne laser light are shown in Figure 8. In order to compare these calculated plots with the measured ones to be shown in Section VII, the acoustic and the acousto-optic parameters for these plots are chosen to be identical to those used in Section VII, namely, f_{01} = 170 MHz, f_{02} = 255 MHz, L_1 = 2.5 mm and L_2 = 1.66 mm, and the tilt angle set equal to the difference in the corresponding Bragg angles at the center frequency for the individual SAWs, namely, 3.4 mrad. From the plots it is seen that the phase shift may cause destructive as well as constructive interference in the resultant diffracted light power. Consequently, the resultant (composite) bandwidth can be larger than the sum of the two individual bandwidths. Therefore, the phase shift as well as the tilt angle between adjacent SAWs are the important parameters,

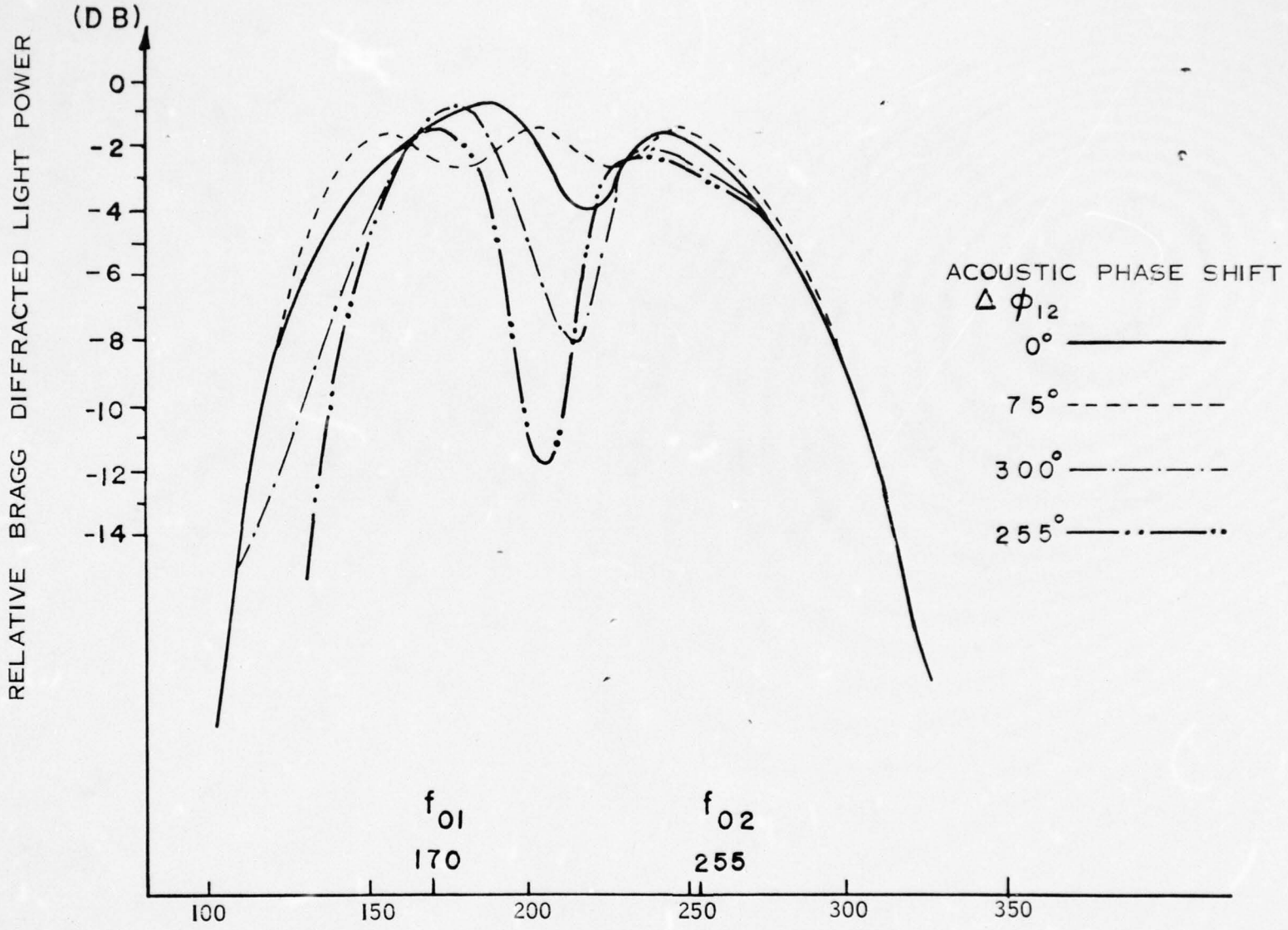

Fig. 8 Effect of the Phase Shift Between Two Tilted SAWs on the Resultant Frequency Response (Theoretical).

in addition to the center frequency and the acoustic aperture of the individual SAWs for the design of wideband high-diffraction efficiency Bragg devices.

In summary, the analysis and the methodology for the numerical calculation described above for the case involving two tilted SAWs may be extended to the case involving more than two tilted SAWs, and it can be concluded that by using multiple SAWs which are staggered in their center frequency and tilted in their propagation direction guided-wave acousto-optic Bragg devices with large diffraction efficiency-bandwidth product can be realized.

B. Experimental Results

A Y-cut $LiNbO_3$ substrate possesses an attractive combination of acoustic, piezoelectric, optical, acousto-optic and electro-optic properties (28, 29). In addition, an optical waveguiding layer may be easily created on the top of the substrate using a number of fabrication techniques. Thus, a number of multiple-tilted transducers (the transducer axes approximately along the z(c) axis) have been fabricated on such substrates to study the wideband technique discussed above. The waveguiding layers were grown using the out-diffusion technique (22) and the interdigital transducers were fabricated using the well established photolithographic method (30).

The configuration of an earlier device being studied is shown in Fig. 9. Detailed measurements for the device include the diffraction efficiency as well as the deflection angle of the light beam versus the frequency of the driving signal using a 6328 Å He-Ne laser light. The optical waveguiding layer could support one or two TE modes. Two interdigital SAW transducers having the designed center frequencies of 255 MHz and 382 MHz, respectively, and a tilt angle of approximately 0.3 degrees were fabricated on the top of the waveguide to generate two tilting acoustic waves propagating approximately along the z-axis of the $LiNbO_3$ crystal. Since it is desirable for the transducers to provide an acoustic bandwidth which is as wide as possible and since the fractional acoustic bandwidth of an interdigital transducer is inversely proportional to the number of interdigital finger electrode pairs, two and a half finger pairs was chosen for each of the two transducers.

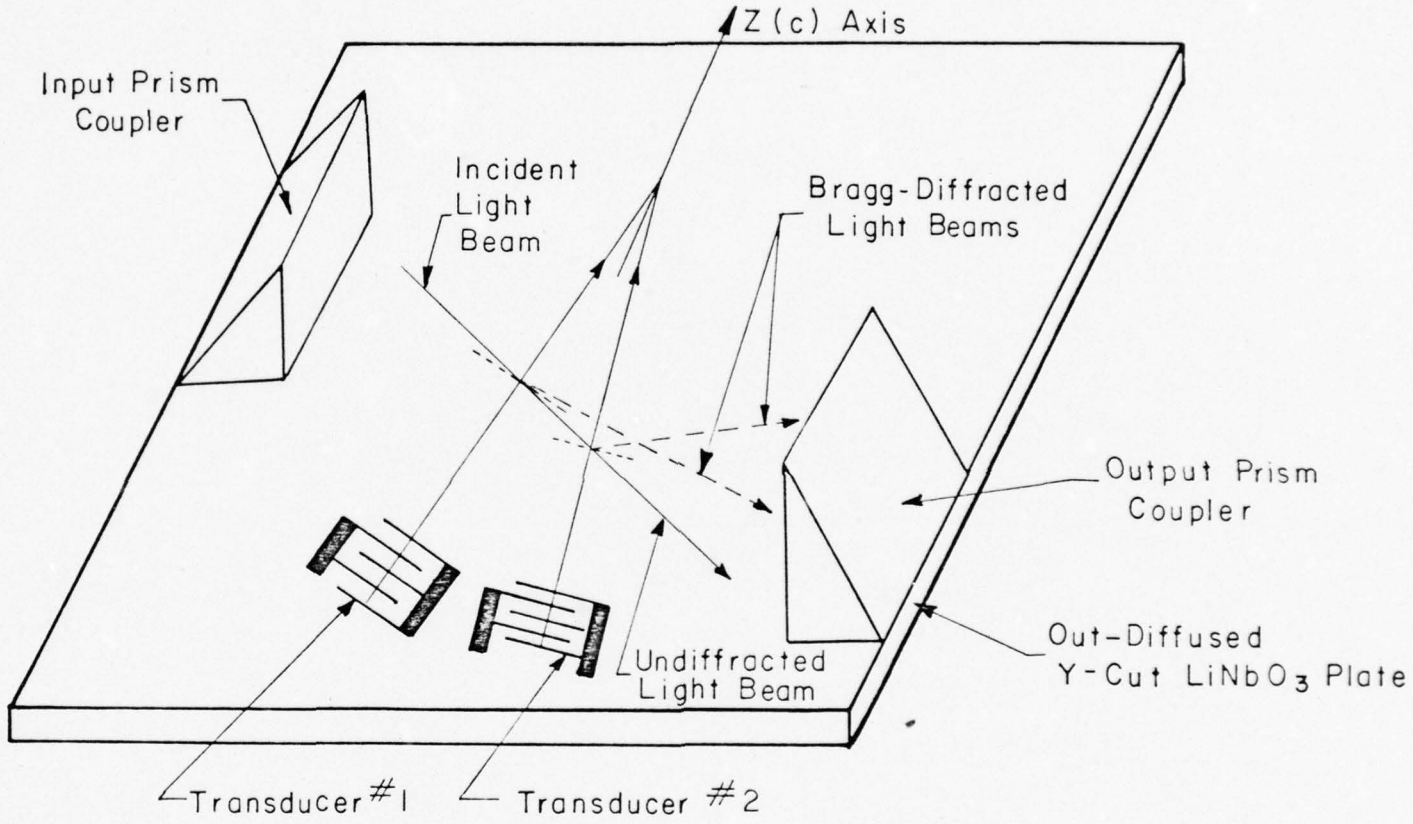

Fig. 9 Guided-Wave Acousto-optic Bragg-Diffraction From Two Tilting Surface Acoustic Waves.

The apertures of the two transducers are 1.66 and 1.11 mm, respectively, each being large enough to insure the individual diffraction to be in the Bragg regime. The two transducers were connected in parallel and their combined electrical capacitance was tuned out with an inductance. The measured frequency responses of the Bragg diffraction with the two transducers excited separately are shown in Figure 10(a) and that with the two transducers excited simultaneously is shown in Figure 10(b). From Figures 10(a) and 10(b) it is seen that the resultant device bandwidth (~190 MHz) is larger than the sum of the device bandwidth using acoustic wave #1 alone (85 MHz) and the device bandwidth using acoustic wave #2 alone (75 MHz). It is also seen that the Bragg diffraction peaks in a neighborhood of the transducer center frequencies, namely, 255 MHz and 382 MHz as expected. A flat response, instead of a dip, between the two peaks would be expected if the center frequencies of the two transducers were separated by a smaller amount than the one implemented. As a matter of fact an additional peak, located between the two peaks, was observed in an earlier design in which the separation of the two center frequencies, 170 MHz and 200 MHz, was considerably smaller (12). In this earlier version a resultant device bandwidth of 60 MHz was obtained. Similar frequency responses with the resultant device bandwidth varying from 155 MHz to 195 MHz was also obtained as the incident angle of the light beam was varied by approximately $\pm$ 25' from the optimum Bragg condition. Thus, a resultant device bandwidth close to 200 MHz has been achieved. Measurement of the strengths of the two surface acoustic waves, using a laser beam probe at normal incidence to the substrate, as a function of frequency indicates that the resultant device bandwidth is mainly limited by the acoustic bandwidths of the two transducers. Thus, a resultant device bandwidth larger than 200 MHz may be expected by inserting a wideband electric matching network between the signal generator and the two transducers. A further increase in the resultant device bandwidth should be possible by adding more transducers at the appropriate center frequency and tilt angle.

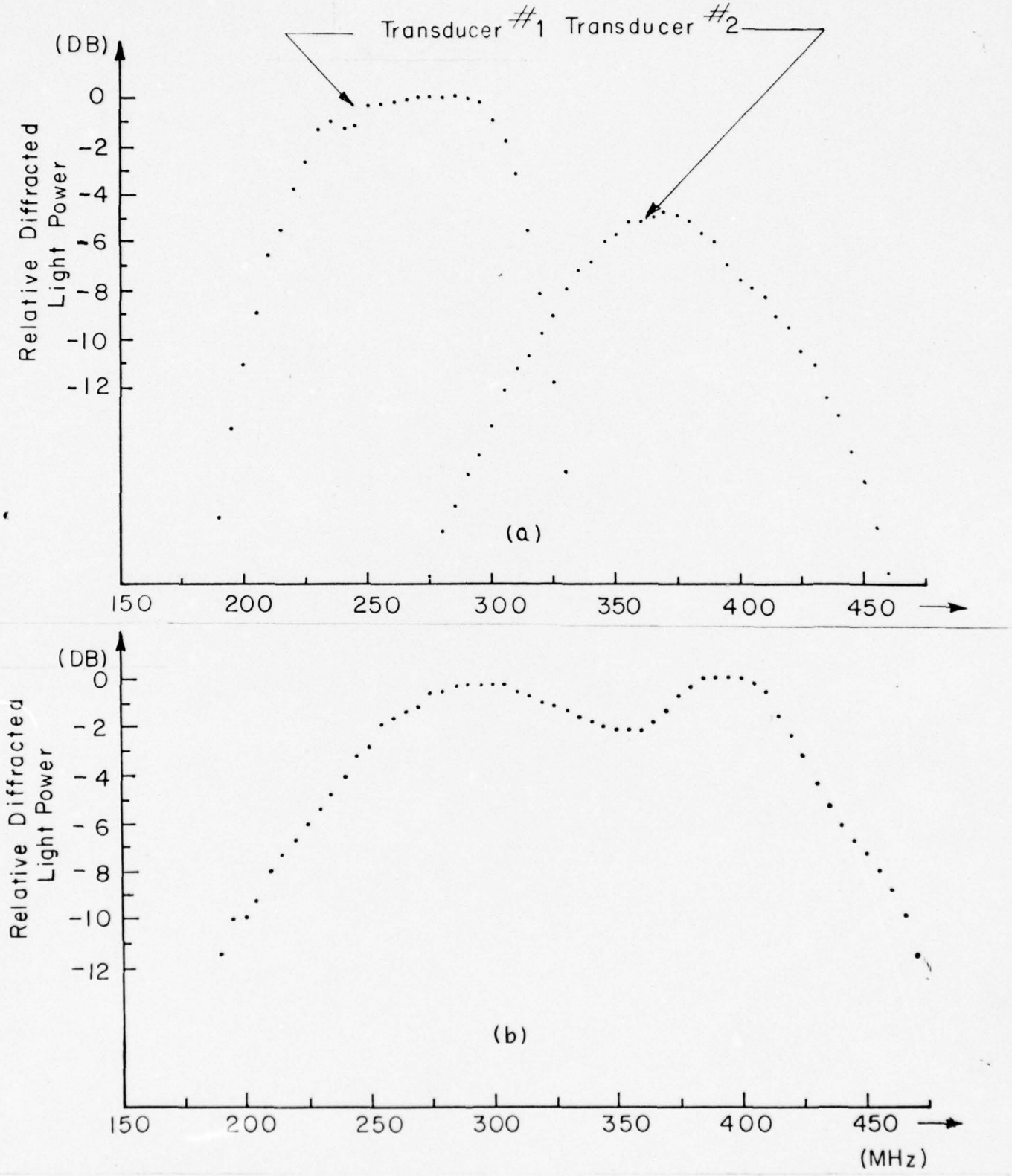

Fig. 10 (a) Frequency Responses of the Bragg-Diffracted Light Power for the Individual Acoustic Waves,
(b) Frequency Response of the Bragg-Diffracted Light Power for the Combined Acoustic Waves.

In beam deflection and switching applications the relation $N = (D/V_R)\Delta f$ prevails, where N designates the number of resolvable beam diameters, D the aperture of the light beam, V_R, the velocity of the surface acoustic wave and Δf the device bandwidth. Figure 11(a) shows the photograph of the diffracted light spots at the far-field as the frequency of the driving signal was varied from 240 MHz to 420 MHz for a light beam aperture of about 0.1 cm. Figure 11(b) shows the corresponding undiffracted and diffracted light spots at the far-field. With such a relatively small light beam aperture no degradation of either the undiffracted or the diffracted light beam was observed. From Figure 11(a) the number of resolvable spot diameters as defined by the Rayleigh criterion is estimated to be 48 which agrees well with the calculated value of 51. In the device being studied a light beam aperture of 0.4 cm with slight non-uniformity in light intensity was achievable after the light beam has propagated through the input and output prism couplers. Improvement of the surface condition of the prism couplers and the $LiNbO_3$ plate and the contact between them should result in a larger light beam aperture. Thus, the device should be able to deflect a light beam of 1 cm aperture into 575 resolvable spot diameters with a transit time of 2.8 microseconds. (The relevant surface acoustic wave velocity is 3.5×10^5 cm/sec.). The throughput coupling efficiency, after propagating through the input and output prism couplers, is approximately 20%. From Figure 11(b) it is also seen that the mode structure of the diffracted beam is the same as that of the undiffracted beam. We, therefore, conclude that no observable mode conversion was generated during the acousto-optic interaction with the device being studied.

The rf driving power of the device for a 50% diffraction efficiency was measured to be 200 mw, corresponding to an estimated acoustic power of at most 50 mw. This estimation is based on the assumption of a -3db electric acoustic conversion loss and an additional -3db insertion loss as a result of the bidirectional property of the interdigital transducer. Exact determination of the acoustic power was not possible because no receiving transducer was fabricated in the device being studied. For the earlier version of the device, referred to in Reference 12, the corresponding rf driving power and the estimated acoustic power are 140 mw and 35 mw, respectively, with a device bandwidth of 60 MHz. This driving power requirement is slightly lower than that of a comparable device (at $\lambda = 1.15\ \mu$) described in Reference 3.

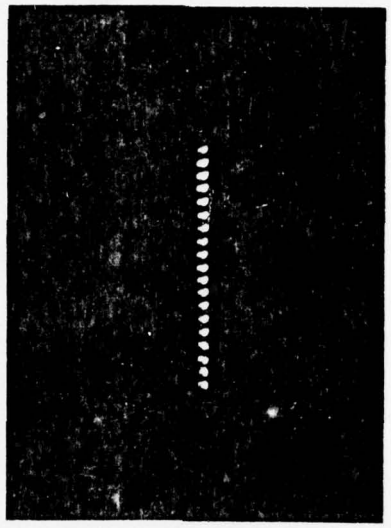

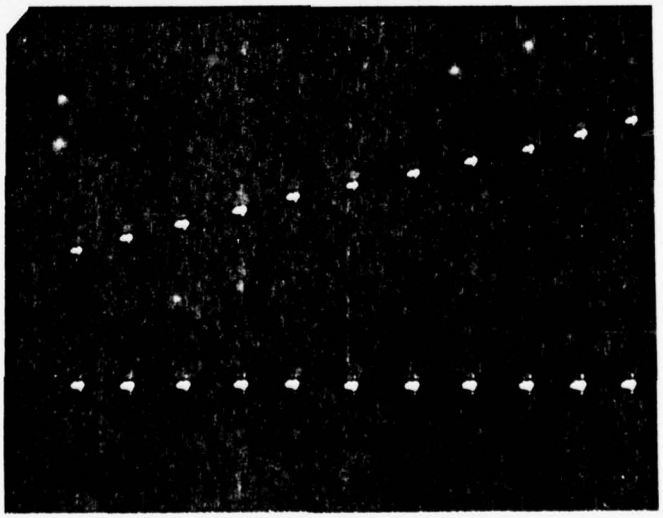

Fig. 11 (a) Diffracted Light Spot Positions at the Far-Field as the Frequency of the Driving Signal is Varied,
(b) Diffracted and Undiffracted Light Spot Positions at the Near-Field as the Frequency of the Driving Signal is Varied.

The very efficient diffraction achieved with our device is attributed to a close match of the penetration depths, estimated to be about 7 μ (22), between the lowest-order mode guided-light waves and the surface acoustic waves. Optimization of both electrical and acoustical parameters of the device should further improve its performance.

In conclusion, we have experimentally demonstrated, for the first time, that a substantial increase in the bandwidth of an acousto-optic guided-light beam deflector or switch, can be achieved by employing multiple tilted surface acoustic waves which are staggered in their operating frequency and tilted in their propagation direction. The measured performance figure of the device being studied, which employs two tilted surface acoustic waves, is among the best of those having been achieved in recent years. It has been demonstrated that such a device configuration is relatively easy to design and easy to fabricate. The new technique introduced here should be very useful for applications involving very wide bandwidths such as a guided-wave acousto-optic rf spectrum analyzer which requires a bandwidth of approximately 500 MHz (7) and high-speed multiport switches for integrated/fiber optics terminals.

VI. GUIDED-WAVE ACOUSTO-OPTIC BRAGG DIFFRACTION BY AN N-SAW ARRAY - GENERAL CASE

A. General Theory

We shall now extend the analysis of Section V to the general case in which an array of N-SAWs is involved (Figure 12). The advantage of using a separate coordinate system for each transducer (i.e., $x_i = 0$ at the input of each transducer) will become clear later. It is to be noted that tilt angles between adjacent transducers are all assumed small in the transducer array so that the separation between adjacent SAWs in the interaction region may be approximated by the corresponding transducer separation.

Consider the interaction in the region with surface acoustic wave aperture L and write the input boundary conditions in the normalized form: $E_m(0) \equiv \alpha$ and $E_n(0) \equiv \beta \exp(j\varphi)$, where $\alpha^2 + \beta^2 \equiv 1$ and φ is the relative phase difference between the diffracted and undiffracted light at the input. By matching these boundary conditions to the general solutions, the electric fields of the undiffracted and diffracted light at the output of the interaction region ($x = L$) are given as follows (14):

$$E_m(L) = \left[\alpha\cos(qL) + (j/q)\{\beta A \exp -j(\phi - \varphi) - \alpha(K\Delta\theta/2)\}\sin(qL)\right]\exp j(K\Delta\theta L/2) \quad (8a)$$

$$E_n(L) = \left[\beta\cos(qL)\exp j\varphi + (j/q)\{\alpha B \exp j\phi + \beta(K\Delta\theta/2) \exp j\varphi\}\right] \times \exp j(-K\Delta\theta L/2) \quad (8b)$$

where

$$q^2 = (K\Delta\theta/2)^2 + AB \quad (8c)$$

$$A = \frac{\omega_n^2 n_m^2 n_n^2}{4C^2 k_m \cos\theta_m}\left\{pS\int U_m U_n U_a dy + rE_p\int U_m U_n U_p dy\right\}\Big/\int U_m^2 dy \quad (8d)$$

$$B = \frac{\omega_m^2 n_m^2 n_n^2}{4C^2 k_n \cos\theta_n}\left\{pS\int U_m U_n U_a dy + rE_p\int U_m U_n U_p dy\right\}\Big/\int U_n^2 dy \quad (8e)$$

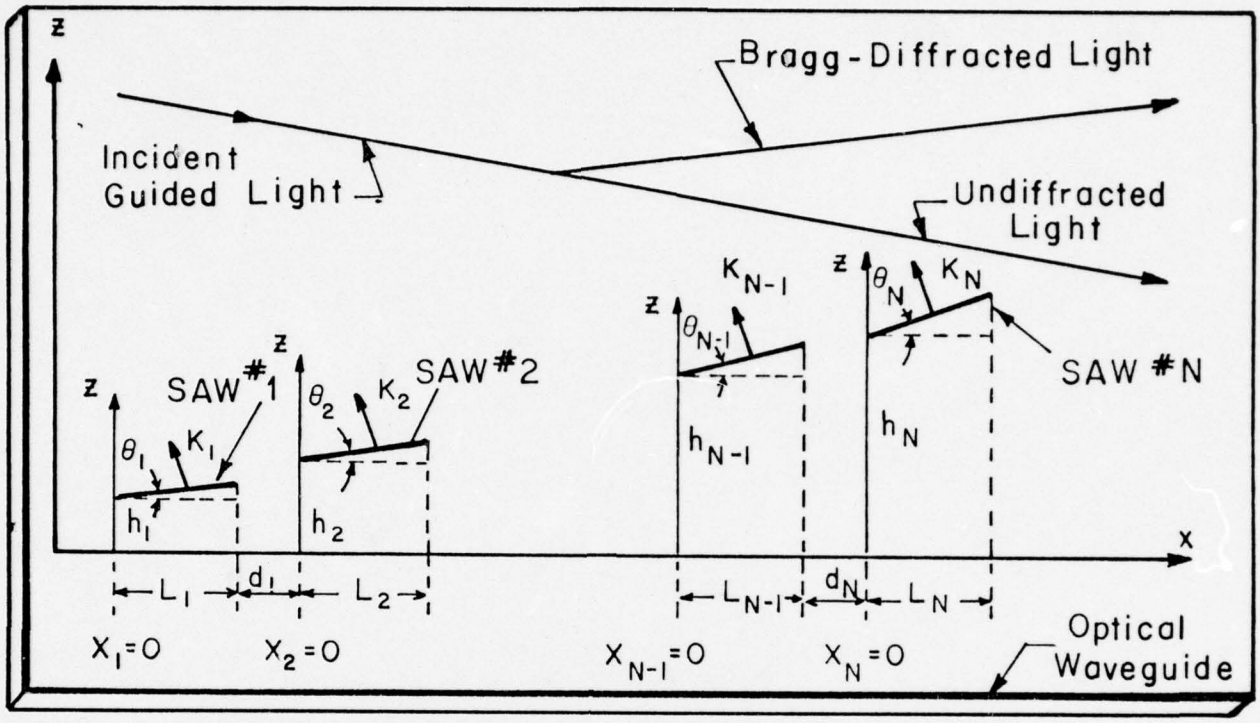

Fig. 12 General Interaction Configuration for Bragg-Diffraction from Multiple Surface Acoustic Waves.

in which p and r are, respectively, the relevant photo-elastic and electro-optic constants; c is velocity of light in free space; $\Delta\theta$ is deviation of the incident angle from the Bragg angle; θ_m, θ_n are angles of incidence and diffraction measured from the normal to the acoustic wave vector K, and n_m, n_n are the indicies of refraction of the undiffracted and diffracted lights. Other symbols are the same as that in Section V. It should be noted that the input boundary values for the next SAW are obtained by adding the phase factor exp j $(K\Delta\theta\ell)$, which accounts for the propagation delay between the two SAWs of separation ℓ, to Equations (8a) and (8b).

Using Equations (8a) and (8b), the electric fields of the undiffracted and diffracted light being output from the (i-1)-th SAW at $(L_{i-1} + d_{i-1})$ can be obtained. These output fields are the input to the i-th SAW, and so may be used, in turn, to determine the output electric fields from the i-th SAW. Thus, using the special coordinate system of Figure 12, Equations (8a) and (8b) can be applied successively to any number of SAWs. As previously, the input boundary conditions for the i-th SAW are written in the following form:

$$E_m(x_i = 0) = \alpha_i \tag{9a}$$

$$E_n(x_i = 0) = \beta_i \exp(j\varphi_i) \tag{9b}$$

where φ_i is the relative phase between $E_m(0)$ and $E_n(0)$. By generalizing Equations (8a) and (8b) and after some algebraic manipulation, α_i, β_i and φ_i are obtained as follows:

$$\alpha_i = (1 - \zeta_{T,\, i-1})^{1/2} \tag{9c}$$

$$\beta_i = (\zeta_{T,\, i-1})^{1/2} \tag{9d}$$

$$\varphi_i = K_{i-1}\Delta\theta_{i-1}d_{i-1} + \psi_{n,i-1} - \psi_{m,i-1} \tag{9e}$$

where $\zeta_{T,i-1}$ = the resultant diffraction efficiency due to the first (i-1) SAWs

$$\psi_{m,i-1} = \tan^{-1}\left(\frac{\beta_{i-1}\cos(\phi_{i-1} - \varphi_{i-1})\sqrt{\zeta}_{i-1} - \alpha_{i-1}(K_{i-1}\Delta\theta_{i-1}/2q_{i-1})\sin(q_{i-1}L_{i-1})}{\alpha_{i-1}\cos(q_{i-1}L_{i-1}) + \beta_{i-1}\sin(\phi_{i-1} - \varphi_{i-1})\sqrt{\zeta}_{i-1}}\right) \tag{9f}$$

$$\psi_{n,i-1} = \varphi_{i-1} + \tan^{-1}\left(\frac{\beta_{i-1}(K_{i-1}\Delta\theta_{i-1}/2q_{i-1})\sin(q_{i-1}L_{i-1}) + \alpha_{i-1}\cos(\phi_{i-1}-\varphi_{i-1}\sqrt{\zeta}_{i-1}}{\beta_{i-1}\cos(q_{i-1}L_{i-1}) - \alpha_{i-1}\sin(\phi_{i-1}-\varphi_{i-1})\sqrt{\zeta}_{i-1}}\right) \tag{9g}$$

ζ_{i-1} = the diffraction efficiency due to the (i-1)-th SAW with input electric fields

$$E_m(0) = 1 \text{ and } E_n(0) = 0,$$

ϕ_{i-1} = total phase (including the transducer electric phase and the acoustic phase due to the step height) of the (i-1)-th SAW.

The electric fields of output light from the N-th SAW are:

$$E_{m,N}(x_N = L_N) = \left[\alpha_N\cos(q_N L_N) + (j/q_N)\{\beta_N A_N \exp -j(\phi_N - \varphi_N) - (K_N\Delta\theta_N/2)\sin(q_N L_N)\}\right] \times \exp j(K_N\Delta\theta_N L_N/2) \tag{10a}$$

$$E_{n,N}(x_N = L_N) = \left[\beta_N\cos(q_N L_N)\exp j\varphi_N + (j/q_N)\{\alpha_N B_N \exp j\phi_N + (K_N\Delta\theta_N/2)\beta_N \exp j\varphi_N\}^{1/2}\right] \times \exp j(-K_N\Delta\theta_N L_N/2) \tag{10b}$$

Finally, the resultant diffraction efficiency is

$$\zeta_{T,N} \equiv \left|E_{n,N}(L_N)\right|^2 = \zeta_N(1-\zeta_{T,N-1}) + (1-\zeta_N)(\zeta_{T,N-1}) + 2\{\zeta_{T,N-1}(1-\zeta_{T,N-1})\zeta_N\}^{1/2} \times (K_N\Delta\theta_N/2q_N)\sin(q_N L_N)\cos\Phi_N - \cos(q_N L_N)\sin\Phi_N \tag{10c}$$

$$\text{where } \Phi_N = \phi_N - \varphi_N = \phi_N - K_{N-1}\Delta\theta_{N-1}d_{N-1} - \psi_{n,N-1} + \psi_{m,N-1} \tag{10d}$$

Equations (10c) and (10d) clearly show the manner in which the resultant diffraction efficiency depends upon that of the first (N-1) SAWs and the last (N-th)-SAW as well as the phase shifts of the light and acoustic waves. It is to be noted that for the first SAW, we have $\zeta_{T,0} = 0$, $\alpha_1 = 1$, $\beta_1 = 0$ and $\varphi_1 = \phi_1$. Thus, by utilizing these input boundary values for the first SAW and successively employing the general expressions given by Eq. (10a) and (10b) the resultant diffraction efficiency for any number of SAWs may be calculated numerically. The methodology for this numerical calculation has been established for the analysis and design of devices using either of the two wideband configurations.

B. Bragg-Diffraction From Multiple Tilted and Phased SAWs

1. Tilted SAW Configuration

It is clear that the configuration involving N tilted SAWs can be deduced from the general configuration of Figure12 by letting all step heights h_i equal zero and each tilt angle θ_i equal the difference between the Bragg angle of the i-th SAW and that of the first SAW, both at their respective center frequencies. Consequently, the resultant frequency response for the diffraction efficiency can be obtained from Equations (9) and (10) by imposing the above mentioned conditions. Previous study has established that the phase shift as well as the tilt angle between adjacent SAWs, in addition to the center frequency and the acoustic aperture of the individual SAWs, are the important parameters for the design of Bragg devices with large composite bandwidth (14).

2. Phased SAW Configuration

Similarly, the configuration of phased-arrays of N identical SAW element transducers can be deduced from the general configuration by letting $L_1=L_2=\ldots L_N$, $d_1=d_2=\ldots d_N$, all tilt angles θ_i equal zero, and center frequencies of all element transducers and all step heights between adjacent element transducers be identical. In addition, the separation and the step height between adjacent element transducers, d_i and (h_i-h_{i-1}), and the phase difference $\Delta\theta$ between adjacent SAWs are given by Equations (11a) to (11d). These results are similar to those of bulk acoustic phased-array transducers (31):

$$d = P(n_m \Lambda_o^2/\lambda_o) \tag{11a}$$

$$h_i - h_{i-1} = P(\Lambda_o/2) \tag{11b}$$

$$\Delta\theta = \{\pi + P(f/f_o)\pi\} \text{ for } P = \text{odd} \tag{11c}$$

$$= P(f/f_o)\pi \qquad P = \text{even} \tag{11d}$$

where Λ_o is the acoustic wavelength at the center frequency f_o and P designates the step height between adjacent element transducers in terms of the number of half acoustic wavelengths at the center frequency. Neglecting the overlap integral, it can be shown that as a result of first-order acoustic beam steering, the Bragg bandwidth Δf_B is approximately equal to $(2/P)f_o$ and is approximately N times larger than that of a single SAW possessing an aperture identical to that of the phased-array (32). Note that P imposes conflicting requirements on the performance figures; that is, a high diffraction efficiency requires a large P while a large bandwidth requires a small P.

VII. GUIDED-WAVE ACOUSTO-OPTIC BRAGG-DIFFRACTION FROM MULTIPLE TILTED SAWs—— EXPERIMENTAL RESULTS

As indicated earlier, a Y-cut $LiNbO_3$ substrate possesses an attractive combination of acoustic, piezoelectric, optical, acousto-optic and electro-optic properties (28, 29). In addition, an optical waveguiding layer may be easily created on the top of the substrate using a number of fabrication techniques. Thus, a number of multiple-tilted transducers (the transducer axes approximately along the z(c) axis) have been fabricated on such substrates to study the wideband technique discussed above. The waveguiding layers were grown using the out-diffusion technique (22) and the interdigital transducers were fabricated using the well established photolithographic method (30).

A. Design of the Tilted SAW Transducers

Two versions of the tilted SAW transducers, namely, three- and four-element transducers, were fabricated and employed in the experimental study. The center frequencies of the three-element transducers are 170, 255, and 382 MHz, with the corresponding acoustic apertures of 2.5, 1.66 and 1.11 mm, respectively, and the tilt angles between adjacent transducers are 3.4 and 3.2 mrad, corresponding to the difference in the Bragg angles at the center frequency of the adjacent transducers. In order to obtain as wide an acoustic bandwidth as possible the number of finger electrode pairs for each transducer was chosen to be as small as two and a half. The measured acoustic bandwidths of approximately 30 percent of the center frequencies, namely 50, 68 and 115 MHz were obtained by inserting a single inductance of proper value to each transducer. The acoustic wavelengths at the center frequency are, respectively, 20.5, 13.7 and 9.3 μm. This version of tilted transducers was used to study the frequency response as well as the effect of phase shift on the frequency response, and the electric drive power requirement.

The center frequencies of the four-element transducers are 140, 220, 290 and 400 MHz, with the corresponding apertures of 2.2, 2.2, 1.6 and 1.1 mm, respectively, and the tilt angles between the adjacent transducers are, respectively 2.5, 3.5 and 5.0 mrad. The number of finger electrode pairs for each transducer was chosen to be two, with the measured acoustic bandwidths of approximately 35 percent of the center frequencies, namely 45, 69, 90 and 150 MHz. Finally, the acoustic wavelengths at the center frequencies are, respectively 23.5, 16.4, 11.6 and 8.1 μm.

B. Optical Waveguide, Optical Beam and Acousto-optic Parameters

A He-Ne laser light at 0.6328 μm was utilized in the experiments. A rutile prism was used to couple an ungrided light beam into a guided light beam with the polarization approximately along the c-axis of the $LiNbO_3$ and a second rutile prism was used to couple out both the diffracted and the undiffracted light beams (Figure 13(a)). A photograph of one of the units used in this study is shown in Figure 13(b). Note that the prism couplers and the $LiNbO_3$ crystal are located in the middle of the brass plate. The out-diffused waveguide supports a single TE mode, namely TE_0, with a penetration depth of approximately 7 μm. The corresponding maximum change of refractive index at the surface is estimated to be approximately 5×10^{-4}. The best through-put coupling efficiency is as high as 25 percent. The aperture of the guided-light beam can be varied from 1 to 6 mm, with a slight degradation in the uniformity of the light beam for the widest aperture. The variation of the through-put coupling efficiency as a function of the diffraction spread of the incident light beam, which ranges from 1 to 16 mrad, was measured to be only two to one.

The Q parameters (defined as $2\pi\lambda_0 L/n\Lambda^2$) are, respectively, 11, 16 and 24 for the three-element version. Thus, Bragg-diffraction prevails in all frequency bands. Since the Q parameters for the four-element version are, respectively, 6.5, 13.1, 19.2 and 27, Bragg-diffraction also prevails in all frequency bands.

C. Frequency Responses and Electric Drive Power Requirement

The individual transducers were excited in parallel using power dividers and the phase shifts between adjacent SAWs were implemented by using sections of coaxial cables. The incident angle of the guided-light beam was adjusted by using a precision holder for the device to optimize for both the diffraction efficiency and the resultant bandwidth. Figure 14 shows the recorder plots of the resultant frequency response due to the three-element tilted SAW array and those due to the individual SAWs, together with plots calculated using Equations (9) and (10) of Section VI. The calculated plots are obtained using the SAW propagation parameters as given in Reference 25 and the normalized guided light field distribution for out-diffused waveguides as described in Reference 26. The penetration depth of the TE_0 mode employed in the experimental study is approximately 7 μ. It is seen that the device has a -3db resultant bandwidth of approximately 245 MHz while the bandwidths using the individual SAWs are, respectively 45, 65, and 83 MHz. Clearly, the resultant bandwidth is larger than the sum of the three individual bandwidths.

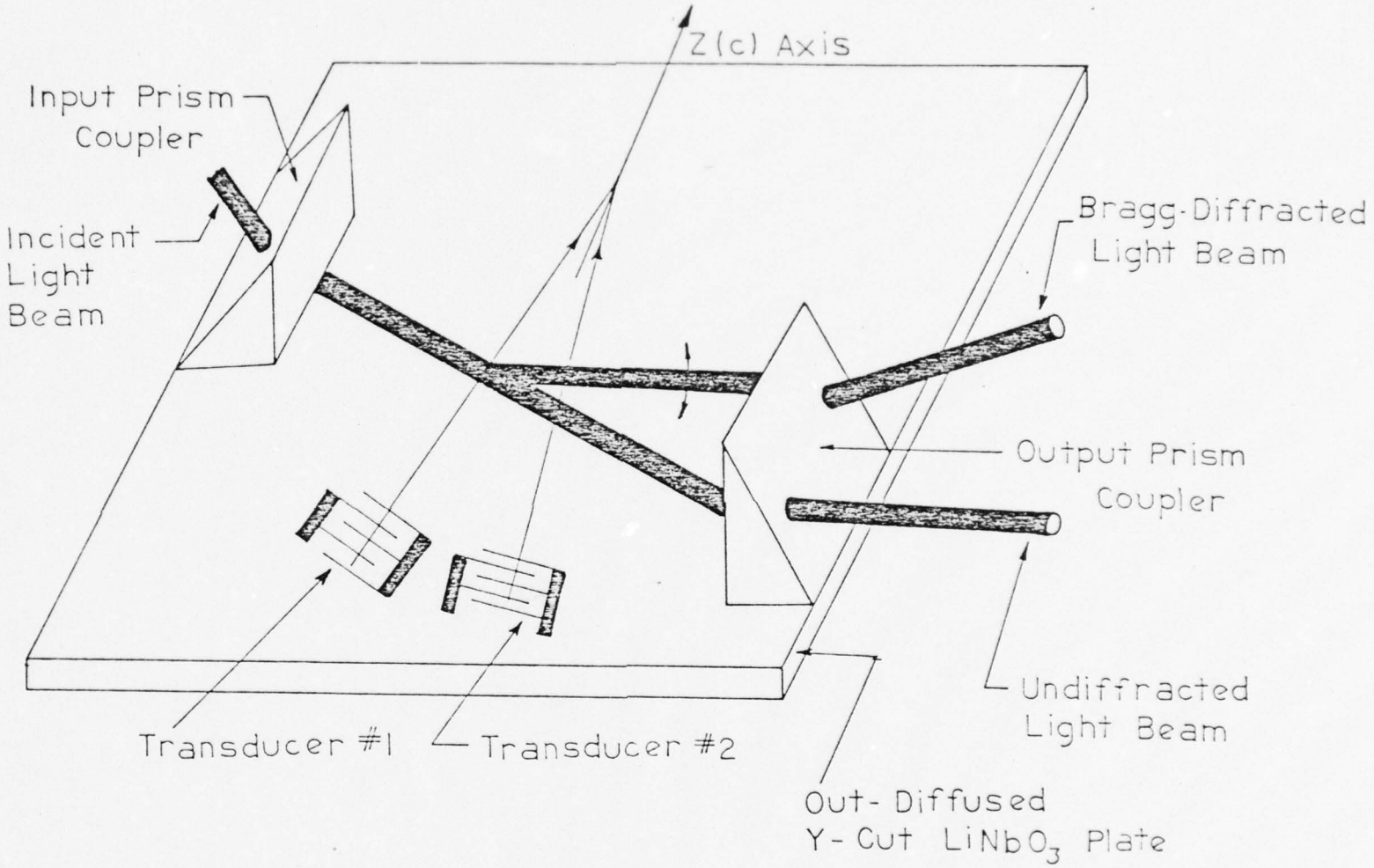

Fig. 13 a) Experimental Configuration for Guided-Wave Acousto-optic Bragg-Diffraction,

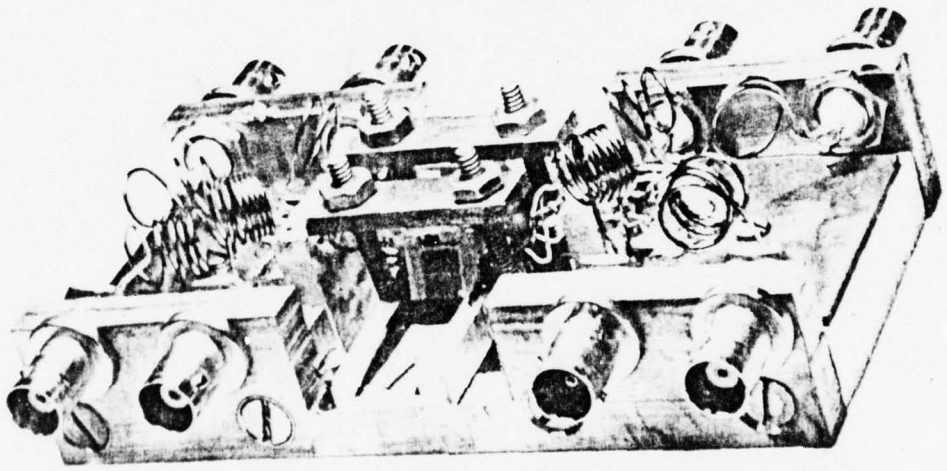

Fig. 13 b) Photograph of A Guided-Wave A-O Deflector Using Multiple Tilted SAWs.

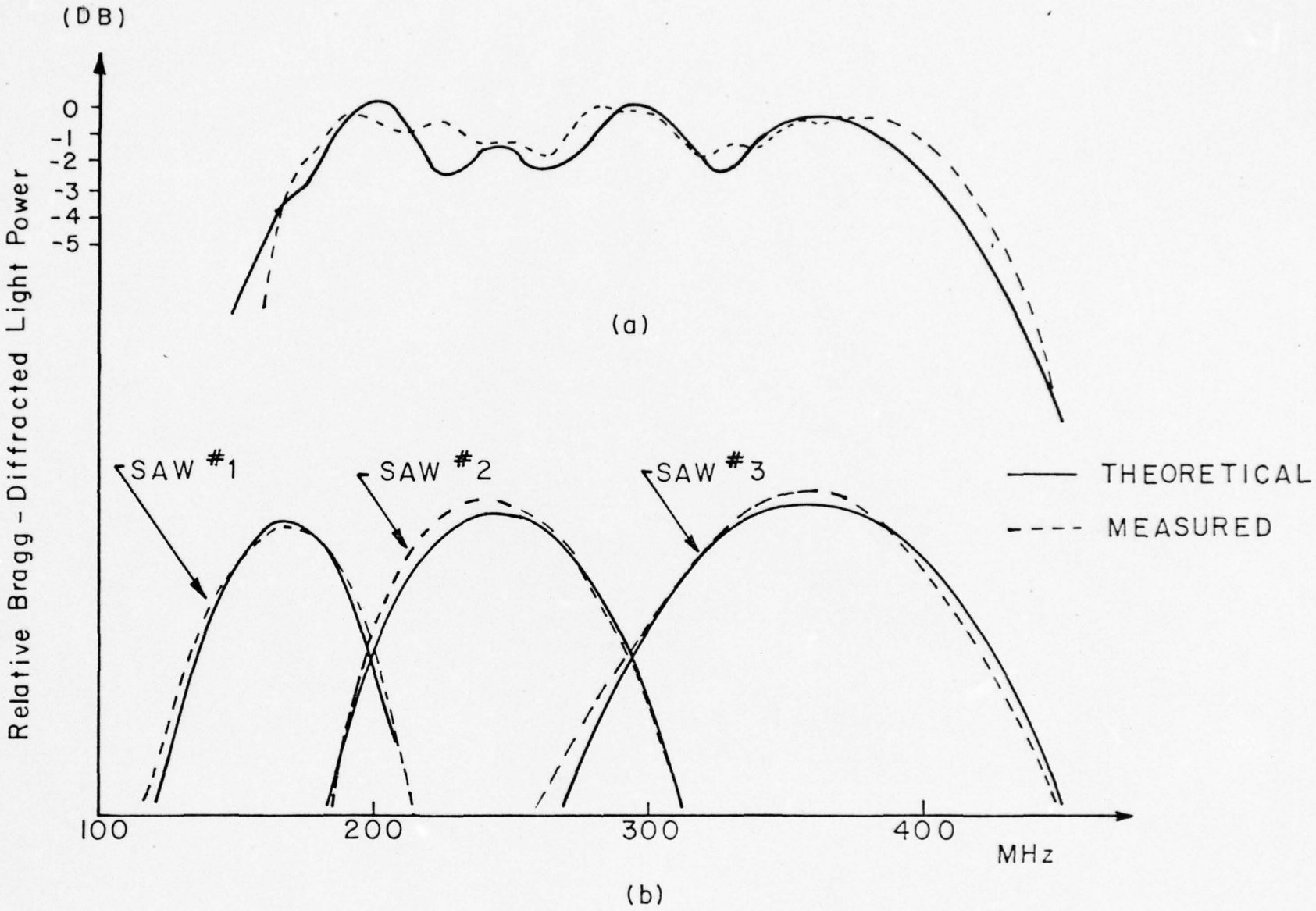

Fig. 14 Frequency Responses of the Bragg-Diffracted Light Power:
(a) For Three Combined SAWs,
(b) For Individual SAWs.

The allowable variation of the incident angle of the light beam (outside the crystal) to maintain the same bandwidth is approximately 0.5 degrees. Typical diffraction efficiency versus the total electric drive power at the center frequency is shown in Figure 15. It is seen that a total electric drive power of 220 mw is required to diffract 50 percent of the incident light. The corresponding total acoustic power is estimated to be at most 15 mw because the best conversion efficiency of the transducers was measured to be -13 db. Based on the above performance figures the bandwidth-diffraction efficiency product of this particular device is substantially larger than previous devices.

The frequency response for the four-element tilted SAWs device is shown in Figure 16. Clearly, a -3db resultant bandwidth of 358 MHz has been realized in this unit. Measurements of the device bandwidth and the diffraction efficiency as a function of the diffraction spread of the incident light beam indicate that they do not vary more than a factor of two for the range of diffraction spread mentioned previously. Although a detailed measurement of the diffraction efficiency versus the electric drive power had not been made for this unit before it was damaged an earlier measurement had indicated that the electric drive power required was two to three times larger than that of the unit with three-element tilted SAWs.

D. Effect of the Phase Shift Between Adjacent Transducers on the Resultant Frequency Response

As mentioned previously, interference between adjacent SAWs becomes important in the range of frequencies at which both adjacent transducers excite SAWs efficiently. This interference will in turn affect the diffraction efficiency and, thus, the resultant frequency response. Figure 17 illustrates this interference effect in the frequency band around 210 MHz and 310 MHz for the unit with three-element transducers. It is apparent that as the electric phase shift $\Delta\phi_{12}$ was varied from -22 degrees (Figure 17(a)) to +177 degrees (Figure 17(b)) the diffraction efficiency varied by a factor of -11db. Similarly, when the electric phase shift $\Delta\phi_{23}$ was varied from +84 degrees (Figure 17(a)) to -121 degrees (Figure 17(d)) the diffraction efficiency varied by a factor of -14db. It is to be noted that although it is difficult to compare the theoretical results with the experimental results based on the absolute phase shift (since in the experiments the phase shift was

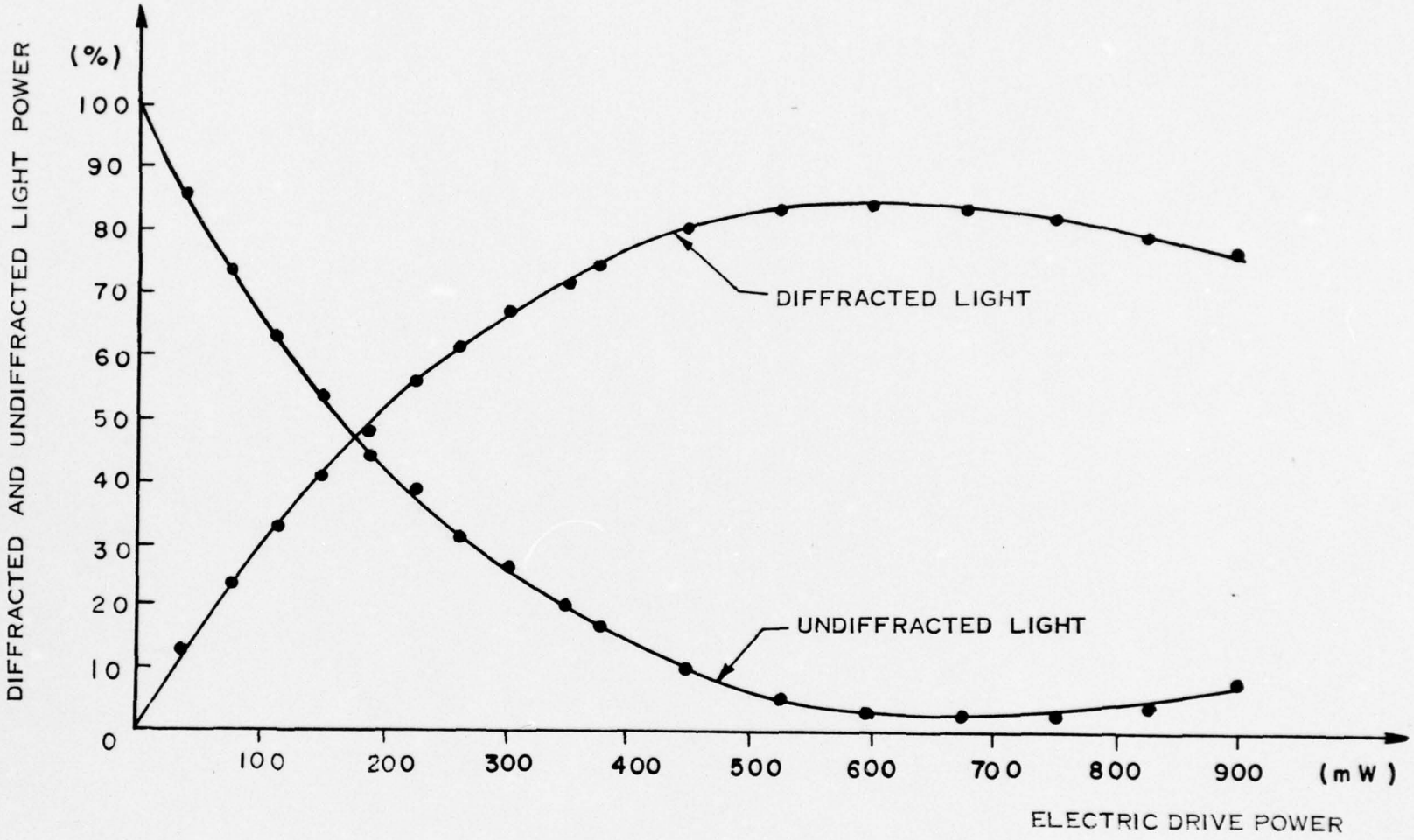

Fig. 15 Percentage Diffracted and Undiffracted Light Power vs the Total Electric Drive Power.

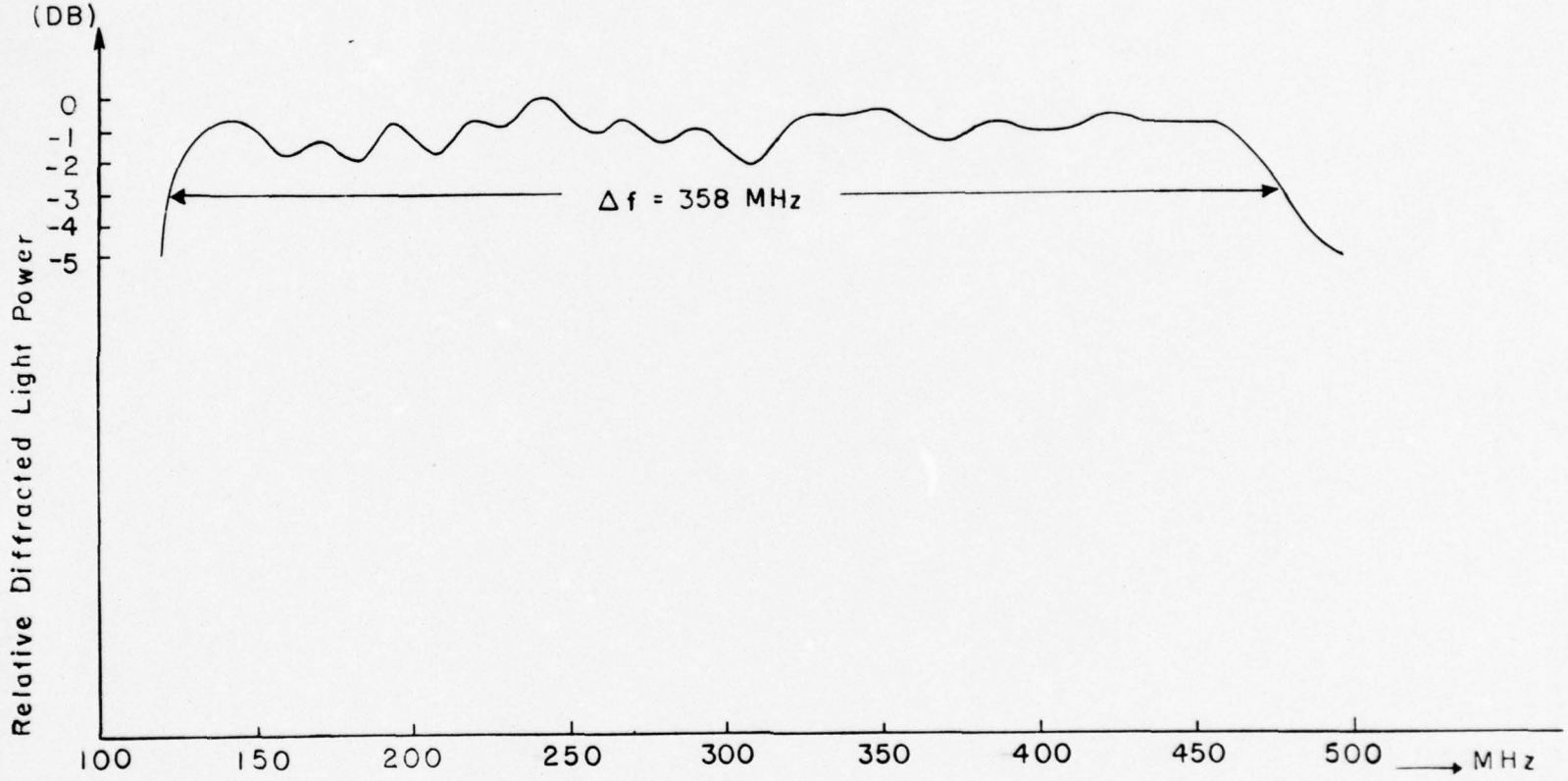

Fig. 16 Resultant Frequency Response of the Bragg-Diffracted Light Power from Four Tilted SAWs.

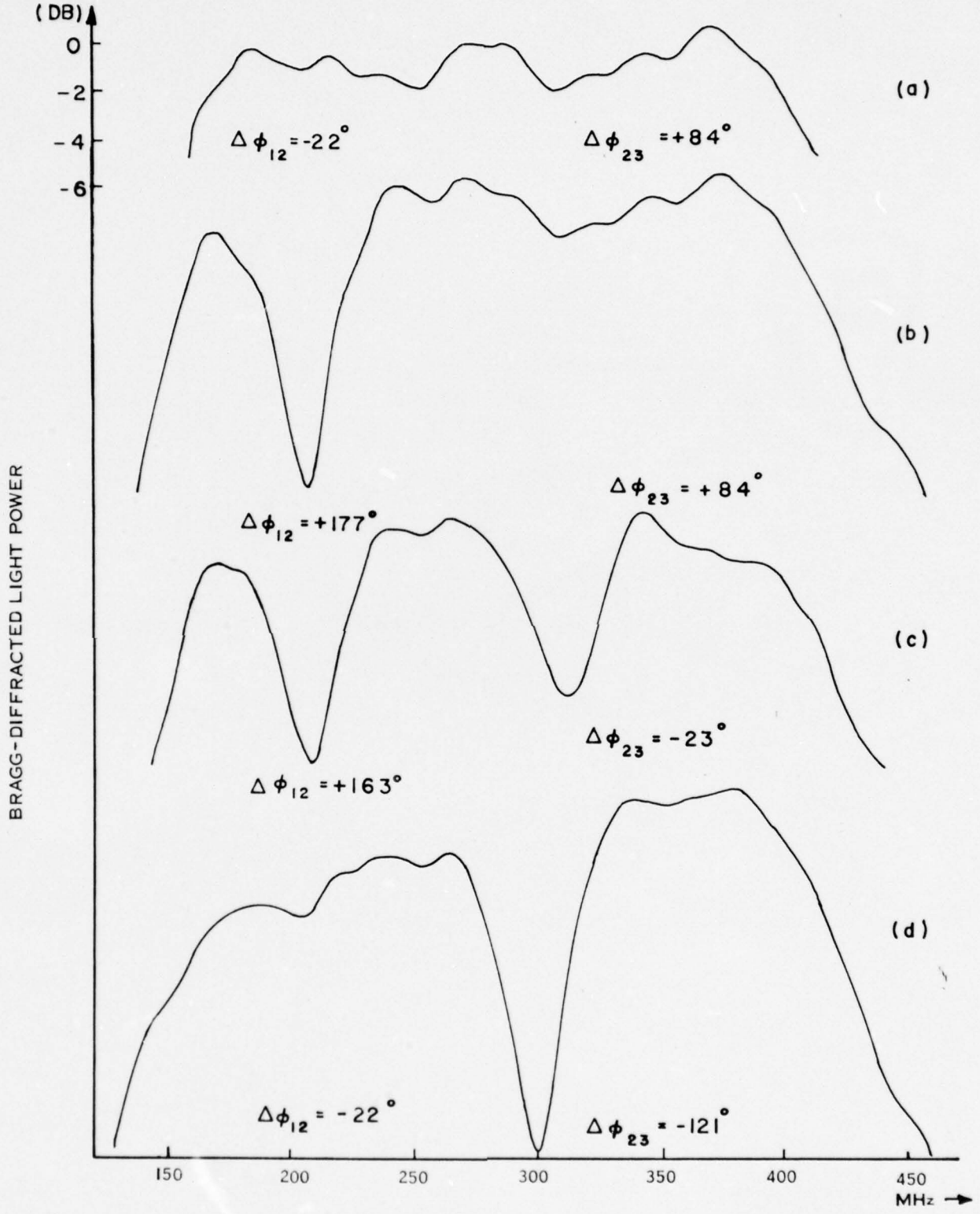

Fig. 17 Effect of the Electric Phase Shift Between Adjacent Transducers on the Resultant Frequency Response (Experimental).

implemented electrically while in the analysis the phase shift is assumed to be that between the adjacent SAWs), effect of the phase shift as predicted in the analysis (Figure 8) has been clearly demonstrated in the experiments (Figure 17). Figure 17 has clearly demonstrated that the resultant frequency response of the devices which employ multiple-tilted SAWs can be made flat by inserting appropriate phase shifters between adjacent transducers. Also, in doing so, the resultant device bandwidth may be made larger than the sum of the individual bandwidths.

E. Beam Profile and Number of Resolvable Spot Diameters

The optical waveguiding layers utilized in the devices being studies support the lowest order TE mode. No mode conversion between the diffracted and undiffracted light beams was observed. Figure 18(a) shows the undeflected light spot (when no rf power was applied to the device) and Figure 18(b) shows the deflected light spots, both at the far-field, for the unit with three-element transducers as the frequency of the driving signal was varied from 155 to 410 MHz. The aperture of the incident light beam employed is approximately 0.1 cm. It is observed that the quality of the undeflected light beam (rf power off) is preserved in the deflected light beam and that deflected light beams of satisfactory quality are achievable.

In beam deflection and switching applications the number of resolvable beam diameters, N, is given by the following relation:

$$N = \left(\frac{D}{V_R}\right) \Delta f = \tau \Delta f \qquad (12)$$

where D designates the aperture of the light beam, V_R the velocity of the SAW, Δf the device bandwidth, and τ the transit time of the SAW across the incident light beam aperture. (The transit time may be practically defined as the switching time of the device if the time response of the transducer and the electric drive circuit is sufficiently faster than the transit time.) Clearly, for a fixed device configuration a large N can be achieved by having a large D and/or a large Δf. However, a large D necessarily implies a large transit time and, therefore, a slower switching speed. In addition, as a result of the acoustic attenuation and/or the waveguide imperfection, a large D will cause some degradation in the beam quality of the deflected light and thus, some reduction in N. Therefore, it is more desirable to achieve a large N through a large Δf than a large D.

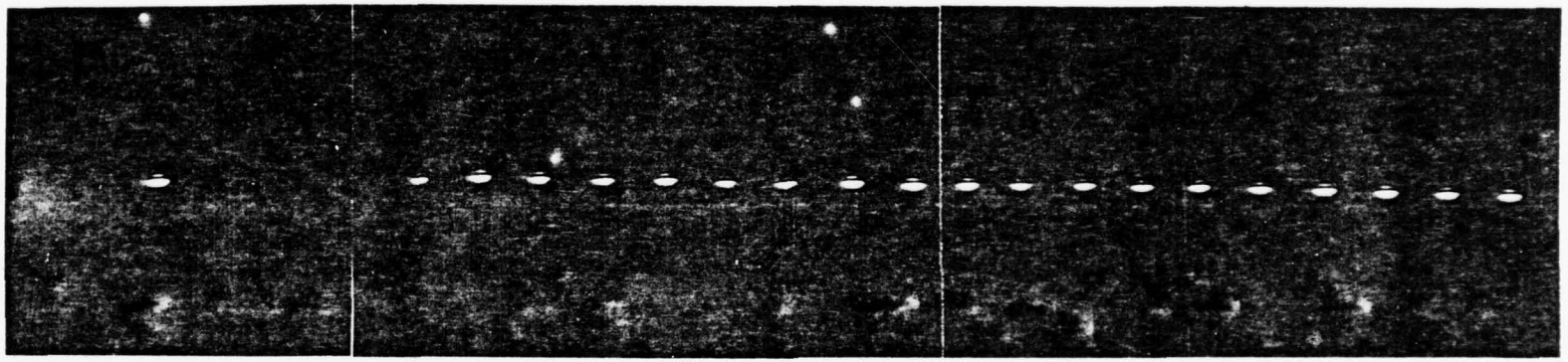

(a) (b)

Fig. 18 Far-Field Undeflected and Deflected Light Beams:
(a) Undeflected Light Beam With rf Power Off,
(b) Deflected Light Beam Positions as the Frequency of the Drive Signal was Varied From 155 to 410 MHz at 15 MHz Per Step.

In the various units that have been studied the maximum D obtainable was approximately 0.6 cm with some breakage into filaments in the middle of the light beam. However, a uniform beam of approximately 0.45 cm is achievable with the unit which has a 358 MHz bandwidth. Using 3.5×10^5 cm/sec for V_R we predicted from Equation (12) that the incremental frequency change required for deflection of one Rayleigh spot diameter (N= 1) is $\delta f \simeq 0.78$ MHz. The measured value as determined from the plots of the deflected light beam profiles (Figure 19) along the direction of deflection, as recorded by a fiber optic probe, is approximately 0.8 MHz. This close match between calculated and measured values indicates that the quality of the deflected light beam is not degraded appreciably by the diffraction process, in agreement with the beam quality illustrated in Figure 18. Since the total bandwidth of this device, Δf, is 358 MHz, the device can deflect a light beam of 0.45 cm aperture into 400 Rayleigh spot diameters at a random-access switching time of 1.28 μs.

If the aperture of the light beam is enlarged to 1 cm the light beam can be deflected by the same device into 1000 Rayleigh spot diameters at a random-access switching time of 2.8 μs. Equivalently, the same device is capable of switching a guided-light beam of 95 μm aperture into 10 beam positions (channels) at a switching time of 27ns. A 1-cm aperture should be achievable by either improving the surface condition of both the prism couplers and the $LiNbO_3$ plate and/or the contact between them or by using grating couplers (32). Indeed, a 1 cm aperture of very good beam quality was obtained by us by carefully adjusting the input and output prisms (see Figure 20).

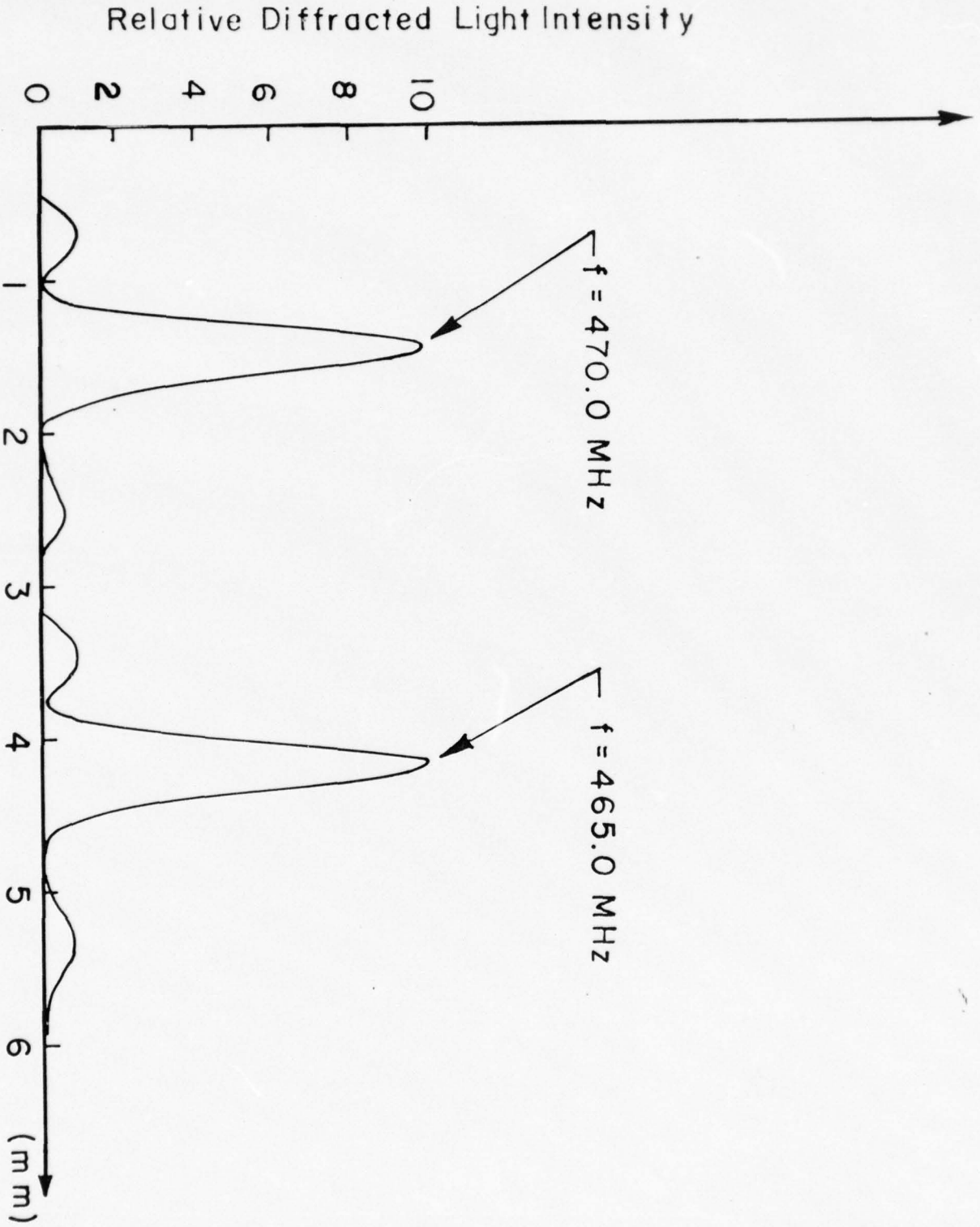

Fig. 19 Beam Profile of the Deflected Light at Two Acoustic Frequencies.

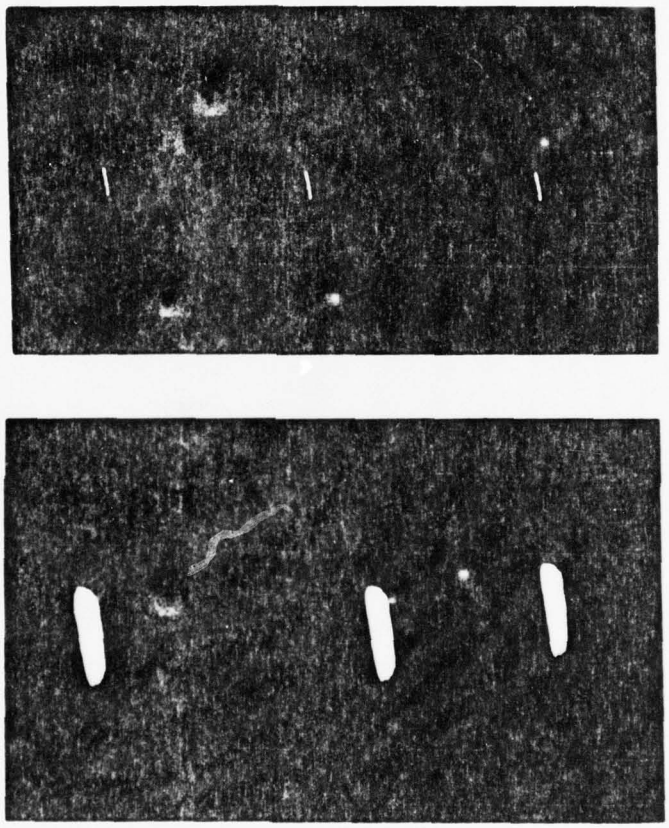

Fig. 20 An Output Light Beam of 1 cm Aperture After Transmission Through Input Prism Coupler, $LiNbO_3$ Waveguide and Output Prism Coupler.

VIII. GUIDED-WAVE ACOUSTO OPTIC BRAGG-DIFFRACTION FROM PHASED SURFACE ACOUSTIC WAVES

A. Introduction

As indicated earlier results of recent experiments involving surface acoustic wave (SAW) and guided optical waves in Y-cut $LiNbO_3$ waveguides have shown that very efficient interaction can be obtained by matching the acoustic wavelength with the optical waveguide penetration depth. However, the simultaneous achievement of both very high diffraction efficiency and very wide device bandwidth using a single aperture SAW transducer is impossible. A device configuration involving transducer of multiple apertures which are staggered in their center frequencies and tilted in their propagation directions, has been shown capable of providing very wide band-width with moderate diffraction efficiency. This moderate diffraction efficiency results from the fact that the effective acoustic beam aperture available for interaction is relatively small because not all of the element transducers in the tilted array transducer are excited at the same frequency range.

A higher diffraction efficiency (using the same electric drive power) together with a relatively wide device bandwidth should be achievable by using a device configuration which utilizes phased SAW's. This higher efficiency is obtained because in this configuration all element transducers are excited simultaneously and the resultant acoustic wavefront is scanned to track the Bragg condition for a wide frequency band. Although this device configuration has been suggested (6, 10, 11), little progress had been reported until most recently (21, 34). In this section we report the design considerations and the fabrication and evaluation of the guidedwave acousto-optic Bragg deflectors based on this device configuration. Experimental results using six-element phased SAW's of relatively small acoustic aperture ($P = 1$) and first-order acoustic beam steering, at the center frequency of 325 MHz, in Y-cut $LiNbO_3$ out-diffused waveguides have shown that accurate tracking of the Bragg condition is indeed achievable for a frequency band of more than 250 MHz. A frequency band of approximately 160 MHz was shown to be achievable for accurate tracking of the Bragg condition even though the acoustic aperture was increased by five times ($P = 5$). A device bandwidth of 112 MHz was obtained with the resulting deflector. This device bandwidth represents a six-fold increase over that of the deflector using a single SAW of identical aperture with no reduction in diffraction efficiency. Only 68 mW of electric drive power or 3.5 mW of acoustic power was required to diffract 50% of the light over this frequency band. Deflected light beam of very good quality was also demonstrated.

B. Design Considerations

Guided-wave acousto-optic Bragg diffraction from phased SAW array can be treated as a special case of the unified theory which concerns interactions between guided optical waves and multiple SAW's (35). However, for simplicity, we have adopted an approximate method similar to that adopted for acousto-optic Bragg-diffraction from a bulk phased acoustic array (36-39) to determine the design parameters of the relating phased (stepped) array transducer and also to analyze steering of its resultant acoustic beam. Note that only the approximate bandwidth of the related A-O Bragg devices can be derived using this simpler method. The exact dependence of the diffracted light intensity as a function of waveguide modes of the light waves, frequency and propagation direction of the acoustic waves can only be calculated numerically using a methodology which was developed in connection with the aforementioned unified theory (see Section VI).

We shall first note that although acousto-optic interactions took place in the near-field of the resultant acoustic beam in the experiments to be described in Section C, the analysis is being carried out in terms of the far-field of the resultant acoustic beam. This combined treatment is valid because the angular dependence of Bragg diffraction is independent of the location at which the light beam intersects the acoustic beam (along the direction of propagation) (37, 40) and also the far-field analysis is more convenient.

The relative phase difference Ψ between the wavefronts of adjacent elementary SAWs (at the far-field) which are generated by a stepped array transducer as shown in Figure 21 is

$$\Psi = \phi + 2\pi\left(\frac{h}{\Lambda}\right) + 2\pi\left(\frac{d}{\Lambda}\right)\sin\theta_A \qquad (13)$$

where ϕ = electrical phase shift between adjacent element transducers

h = step height between adjacent element transducers = $P(\Lambda_o/2)$

Λ, Λ_o = acoustic wavelengths at frequency f and center frequency f_o, respectively

P = integers

d = separation between adjacent element transducers

θ_A = angular position of the far-field point from the forward direction.

Note that in Equation (13) the small angular dependence of the phase velocity of the SAW is ignored.

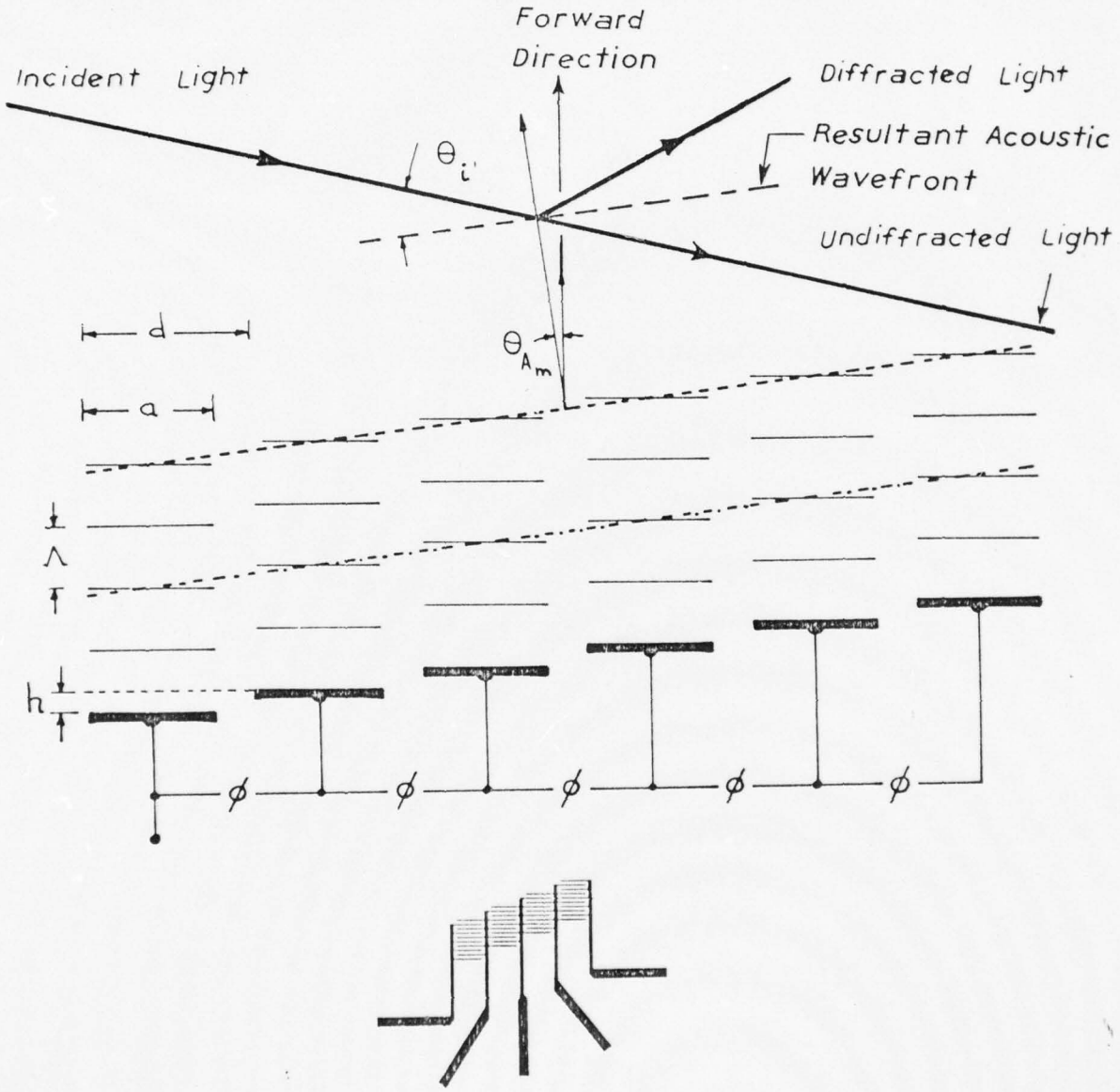

FIG. 21 ACOUSTOOPTIC BRAGG-DIFFRACTION FROM PHASED ACOUSTIC WAVE ARRAY

Constructive interference among all elementary acoustic waves occurs whenever $\Psi = 2\pi n$ with $n = 0, 1, 2, \ldots$. The n-th maximum of the intensity of the resultant acoustic wave, or the so-called n-th grating lobe, is located at the following angular position:

$$\theta_{Am}(f) = \frac{v}{2d}\left\{(2n - \frac{\phi}{\pi})\frac{1}{f} - \frac{P}{f_o}\right\} \quad , n = 0, 1, 2, \ldots \tag{14}$$

where v is the phase velocity of the acoustic wave. For optimal performance the particular grating lobe which is utilized to diffract the light beam should be located at the forward direction at the center acoustic frequency f_o. Thus, we must set $\theta_{Am}(f_o) = 0$. As a result, the relationship between ϕ and P is given as follows:

$$P = 2n - \frac{\phi}{\pi} \tag{15}$$

For P even ϕ must be 0 and for P odd ϕ must be π. This fixed electrical phase shift between adjacent elementary transducers is the characteristic of the so-called first-order acoustic beam steering (36-39). By substituting Equation (15) into Equation (14) we obtain the following relation:

$$\theta_{Am}(f) = P\left(\frac{v}{2d}\right)\left(\frac{1}{f} - \frac{1}{f_o}\right) \tag{16}$$

Note that Equation (16) differs from that given in References 10 and 11 because the former concerns the scanning of the acoustic wavefront while the latter concerns the scanning of the acoustic power flow. As is shown in the experimental results of Section C the related acousto-optic Bragg bandwidth is determined by the scanning angle of the acoustic wavefront. We also note from Equation (16) that the peak of the resultant acoustic beam is at the forward direction at the center frequency, namely, $\theta_{Am}(f_o) = 0$. (See Figure 22(a)) However, as the acoustic frequency is varied from f_o by $\pm \Delta f/2$, this peak is steered from 0 to $\pm \left(\frac{\Lambda_o}{2d}\right) P \left(\frac{\Delta f}{2f}\right)$. The intensity of this peak is reduced as the resultant acoustic beam is steered and the rate of reduction is determined by the aperture of the elementary acoustic beam a. Since the maximum acoustic scan angle possible (defined at -3dd points of the intensity is $(0.9\ \frac{\Lambda}{a})$, its corresponding range of frequency variation, Δf_{Am}, is given as follows:

$$\frac{\Delta f_{Am}}{f_o} \approx \frac{1.8}{P}\left(\frac{d}{a}\right) \text{ or } \Delta f_{Am} \approx \left(\frac{1.8}{P}\right)\left(\frac{d}{a}\right) f_o \tag{17}$$

Note that $\Delta f_{Am}/f_o$ is inversely proportional to P.

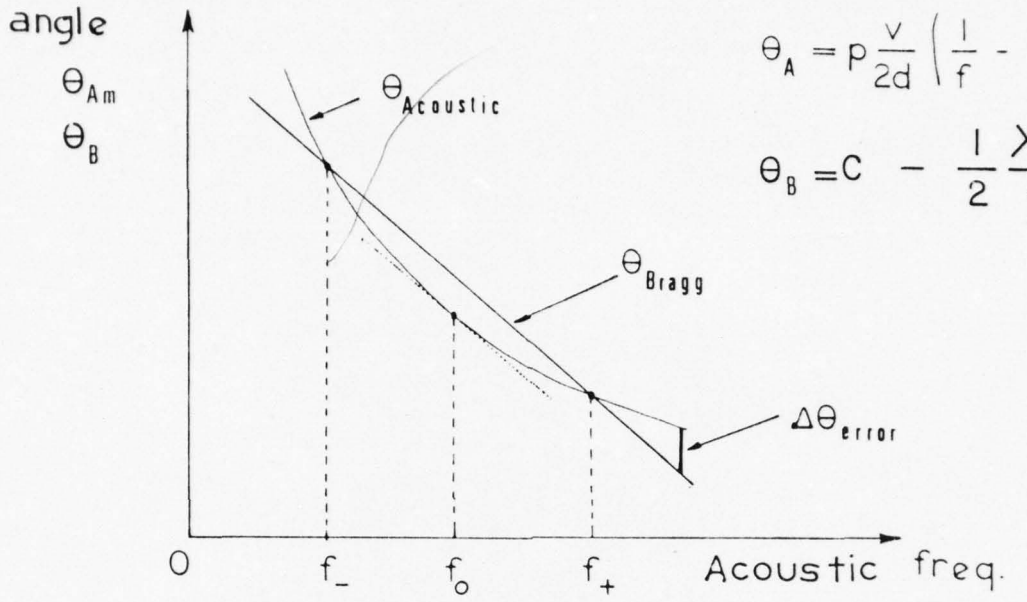

(B)

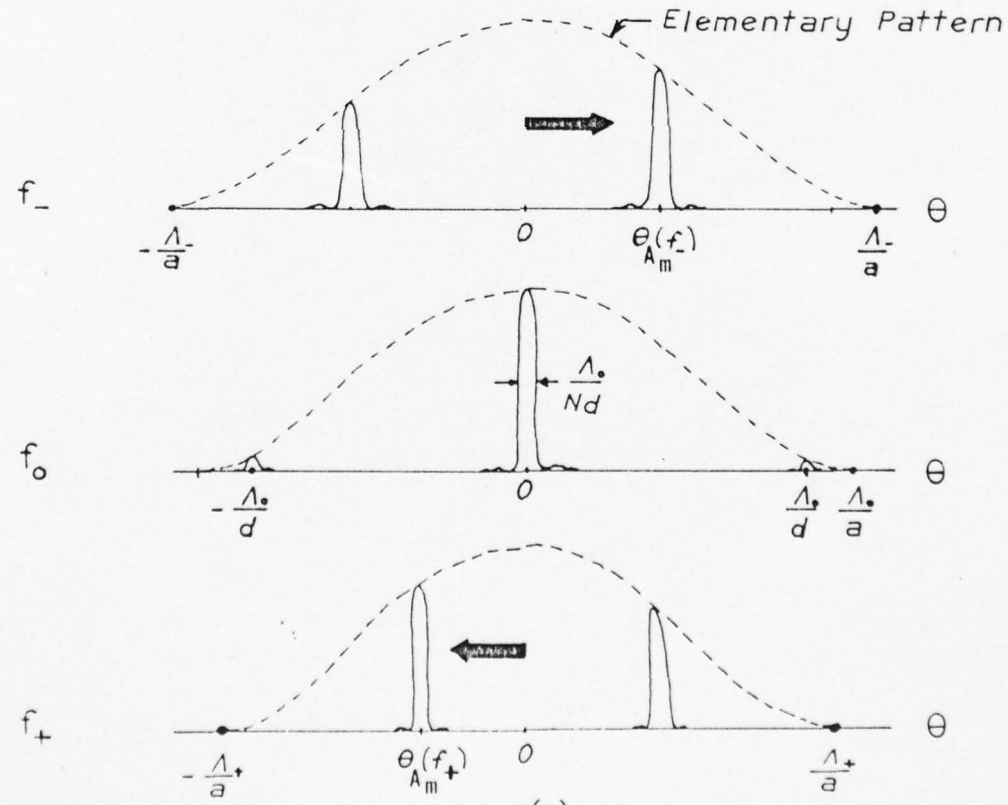

(A)

FIG. 22(A)(B) *TRACKING OF THE BRAGG ANGLE USING THE FIRST-ORDER ACOUSTIC BEAM STEERING WITH STEPPED (PHASED) ARRAY*

Figure 22(b) shows the inverse dependence of θ_{Am} on the acoustic frequency together with the linear dependence of the incident Bragg angle $\theta_B(f)$ on the acoustic frequency required for maximum diffraction (39). This Bragg angle is:

$$\theta_B(f) = C - \frac{1}{2} \frac{\lambda f}{v} \tag{18a}$$

$$C \equiv 2\theta_{Bo} - \theta_i \tag{18b}$$

where λ is the wavelength of the light wave in the medium; θ_i and θ_{Bo} are, respectively, the incident angle of the light beam and the Bragg angle (both with respect to the acoustic wavefront) at the center frequency. For best tracking over a wide range of frequency $\theta_B(f)$ and $\theta_{Am}(f)$ must intersect at one or two frequencies and their slopes must be approximately equal, as illustrated in Figure 22(b). The second requirement results in the following relation for the elementary transducer separation, d, for wideband first-order beam steering:

$$d = P \left(\frac{\Lambda_o}{\lambda}\right)^2 \tag{19}$$

With regard to the first requirement, by adjusting the constant C (i.e., the incident light angle) the intersection frequencies f_+ and f_- are varied. The acousto-optic Bragg bandwidth Δf_B is limited by the tracking error, $\Delta\theta_{error}$, which is in turn a function of f_+ and f_-. Calculation of Δf_B versus f_+ and f_- can be easily made using the numerical methodology previously referred to (35). Accurate tracking of the Bragg angle will prevail so long as this error is smaller than the beamwidth of the acoustic array (14) of N elements:

$$\left|\theta_B(f) - \theta_{Am}(f)\right| \leq 0.90 \left(\frac{\Lambda}{Nd}\right) \tag{20a}$$

By substituting Equations (16), (18a), and (18b) into Equation (20a) and noting that the constant C is just the Bragg angle at the center frequency ($\theta_{Bo} \approx \lambda f_o/2v$) the -3db Bragg tracking bandwidth Δf_B may be determined:

$$\Delta f_B = 2\sqrt{\frac{1.8}{NP}}\, f_o \tag{20b}$$

In the experiments to be described in Section C accurate tracking of the Bragg condition was found to hold over a frequency band of greater than 250 MHz and equal to 160 MHz, respectively, for the two deflector designs with P = 1 and P = 5.

Clearly, while the acoustic scan angle and thus Δf_{Am} is limited by the step height P alone, the Bragg tracking bandwidth Δf_B is limited by the step height, P, as well as the number of elementary transducers in the array, N. The overall A-O Bragg bandwidth as a function of $\sqrt{\frac{N}{P}}$ for two limiting cases are given as follows:

$$\Delta f_B \text{ overall} \simeq \left(\frac{1.8}{P}\right)\left(\frac{d}{a}\right) f_o \quad \text{for } \sqrt{\frac{N}{P}} \ll 1.5\left(\frac{a}{d}\right) \tag{20c}$$

$$\Delta f_B \text{ overall} \simeq 2\sqrt{\frac{1.8}{NP}}\, f_o \quad \text{for } \sqrt{\frac{N}{P}} \gg 1.5\left(\frac{a}{d}\right) \tag{20d}$$

Numerical calculation is required for the cases in between.

Our earlier study (14) has shown that the acousto-optic Bragg bandwidth of guided-wave deflectors which utilize optical waves of lowest order mode is practically identical to that of a bulk-type deflector (37). Thus, the acousto-optic Bragg bandwidth for a device which employs a single SAW of equivalent aperture Nd is

$$\frac{\Delta f_B}{f_o} = \frac{1.8\, v^2}{\lambda f_o Nd} = \frac{1.8}{NP} \tag{21}$$

From Equations (20c) and (21), we see that the overall A-O Bragg bandwidth of a guided-wave deflector which employs a light beam of lowest-order mode and a phased SAW array incorporating first-order beam steering can be nearly N times larger than that of a deflector employing a single SAW of identical aperture, provided that $(N/P)^{1/2} \ll 1.5\,(a/d)$.

Finally, the ultimate deflector bandwidth is determined by both the acoustic bandwidth and the overall A-O Bragg bandwidth and is, in general, smaller than the lesser of the two (14). The fractional acoustic bandwidth of the interdigital finger electrode transducer is equal to $1/N_e$ where N_e designates the number of finger electrode pairs. Thus, from Equation (17) it is clear that the deflector can be made acoustic bandwidth-limited by employing the phased SAW array of small P together with first-order beam steering. However, since the fractional transducer bandwidth of the interdigital finger electrodes SAW transducer employing a simple electrical matching network is in general smaller than its acoustic bandwidth, the bandwidth of guided-wave A-O Bragg deflectors can be further limited by the transducer bandwidth. This limitation appears to hold in the deflectors described in the next section.

C. Experimental Results

Design of several six-element stepped array transducers with the center frequency of 325 MHz and the finger electrode arrangement as shown in Figure 23(b) was made using the guidelines established in the last section. The array transducers were fabricated on Y-cut $LiNbO_3$ out-diffused waveguides using the standard photolithographic technique. The detailed design parameters of the array transducer as well as the relating acoustic, acousto-optic and electrical parameters are listed in Table 1. Each transducer pair (consisting of two adjacent elementary transducers with a common bonding pad) was tuned with a single inductor and the three pairs were electrically driven in parallel using a power divider (Figure 23(c)). The power divider split equally the rf drive power from the signal generator and drove the three transducer pairs. The electrical isolation between any two output ports was measured to be 32 db for the frequency range of 200 to 500 MHz. Total insertion loss of the power divider was measured to be -0.5 db. The optical wave-guide supported a single TE_o mode with a penetration depth of approximately 7 μm. Two directions of SAW propagation, Z-axis and $\pm$ 21.8° from Z-axis, were utilized in this study. Our earlier study (14) has shown that for the combination of this acoustic center frequency and this optical wave-guide penetration depth the 21.8° propagation SAW provides more efficient Bragg diffraction than the Z-propagation SAW. Consequently, most of the results to be described in this section are for the devices which employ 21.8°-propagation SAW. A rutile prism was used to couple in an unguided light beam from a He-Ne laser at 0.6328 μm and a second rutile prism was used to couple out both the Bragg diffracted and the undiffracted light beams (see Figure 24).

The incident light beam intersected the resultant SAW at a distance of approximately 2 mm from the tip of the transducer array. Thus acousto-optic interactions took place in the near-field of the resultant acoustic beam because the Fresnel distance of the elementary transducer and that of the array transducer are both considerably larger than 2 mm (see Table 1).

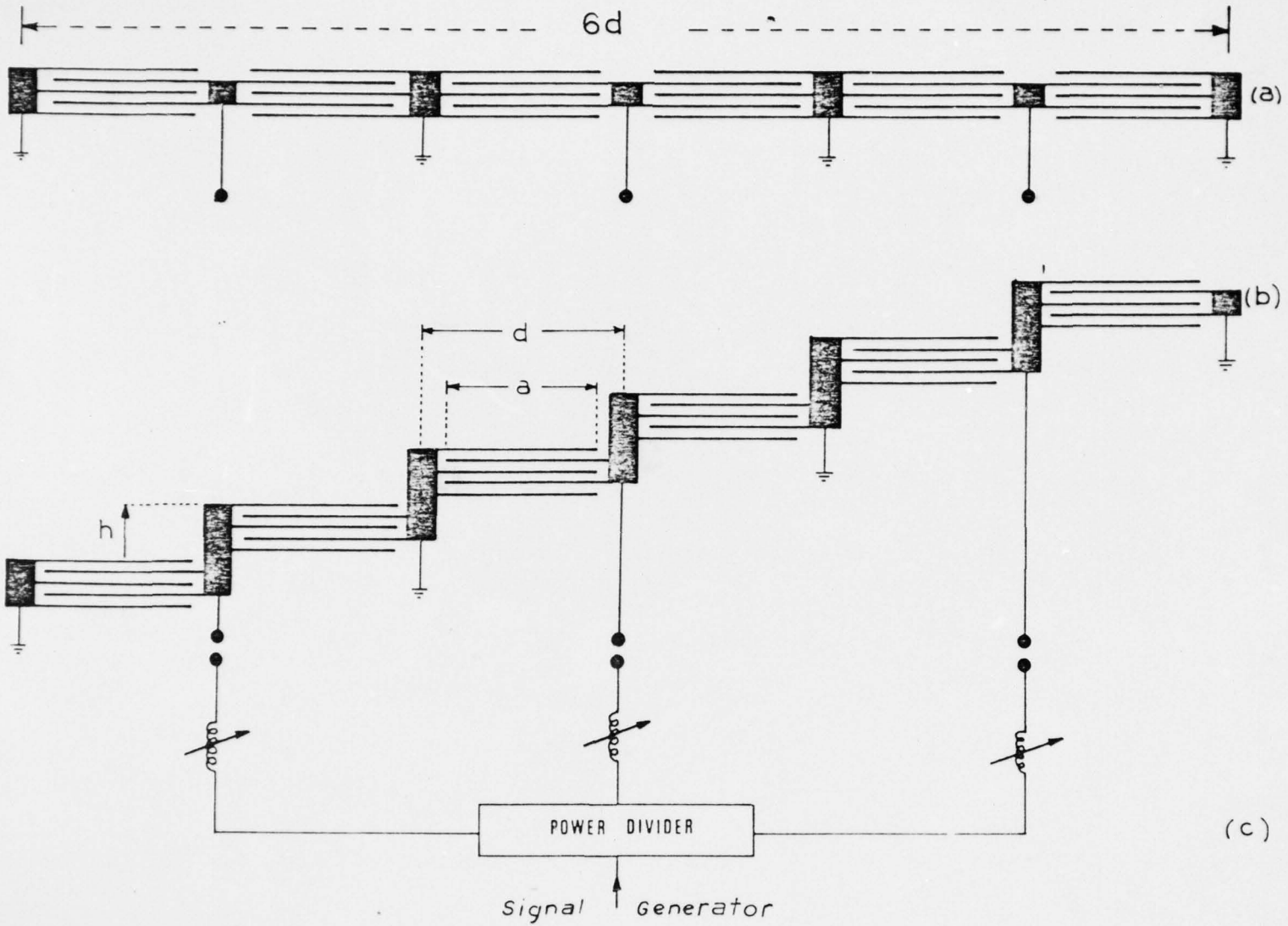

FIG. 23 (a) PLANE (UNSTEPPED) ARRAY TRANSDUCER

(b) PHASED (STEPPED) ARRAY TRANSDUCER

(c) ELECTRIC TUNING AND DRIVING CIRCUIT

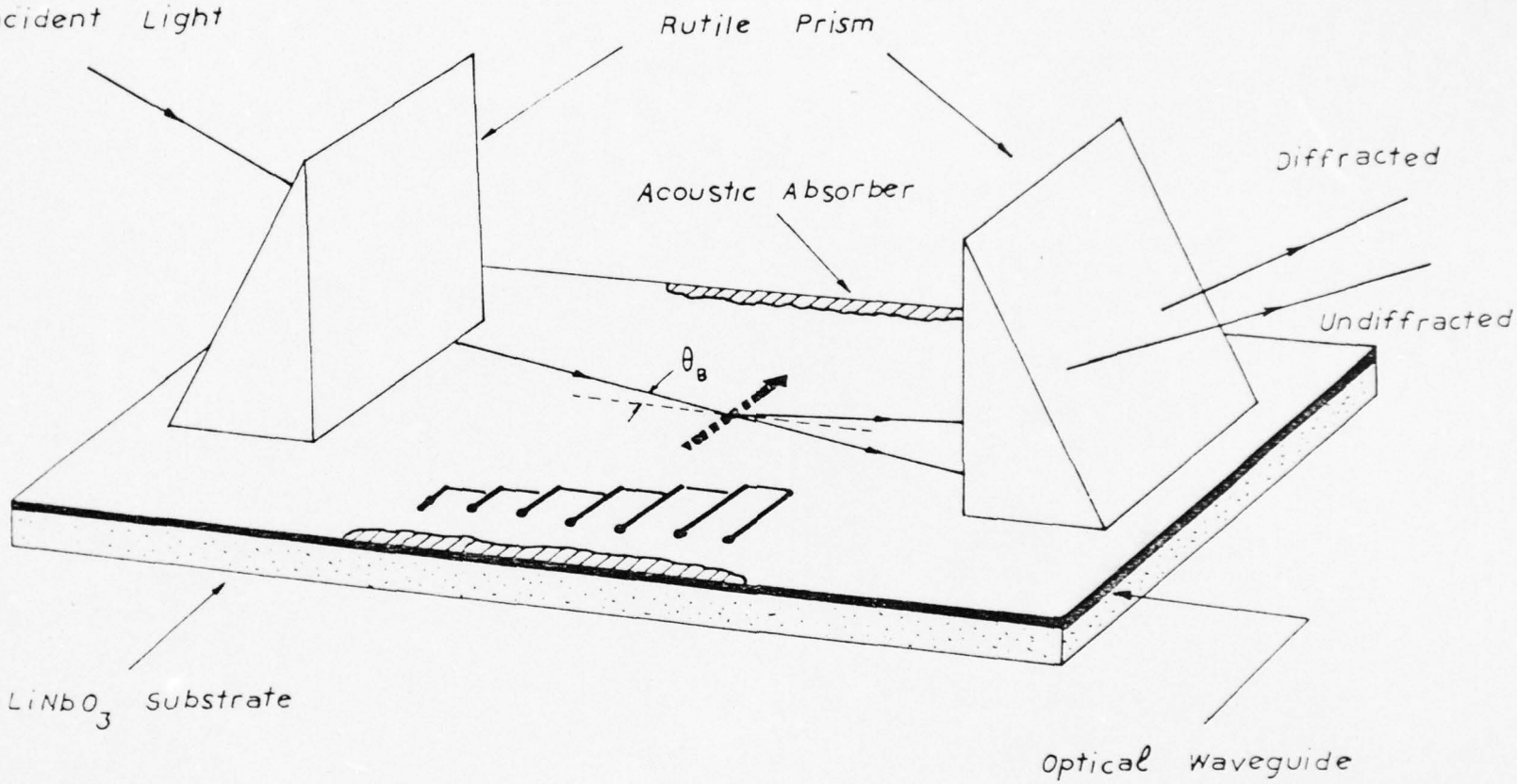

FIG. 24 GUIDED-WAVE ACOUSTOOPTIC BRAGG-DIFFRACTION FROM PHASED (STEPPED) SAW ARRAY

Table I. DESIGN AND MEASURED PARAMETERS OF THE A-O BRAGG DEFLECTORS USING PHASED SAW ARRAY

		P = 1	P = 5
Center frequency	f_o	325 MHz	325 MHz
Aperture	a	0.373 mm	1.74 ,,
Separation	d	0.464 mm	1.93 mm
Step Height	$h = P(\Lambda_o/2)$	5.27 μm	26.3 μm
Fresnel Distance at Center Frequency			
Single Element $\approx a^2/\Lambda_o$		1.3 cm	28.7 cm
Six-Element Stepped Array $\approx (4d+2a)^2/\Lambda_o$		64 cm	1189 cm
Acousto-optic Q		37.7	188.4
Acoustic Scanning Bandwidth $\Delta f_{\Lambda m}$			
Single Element Aperture		606 MHz	130 MHz
Six-Element Plane Array Aperture		82 MHz	19 MHz
Six-Element Stepped Array Aperture		728 MHz	130 MHz
Bragg Tracking Bandwidth Δf_B			
Six-Element Stepped Array Aperture		356 MHz	160 MHz
Number of Finger Electrode Pairs N_e		2.5	2.0
Capacitance of Each Transducer Pair		1.7 pf	6.4 pf
Tuning Inductance for Each Transducer Pair		0.139 μh	0.037 μh
Total Input Impedance of Each Transducer Pair at the Center Frequency		63 Ω	33 Ω
Acoustic Bandwidth $\Delta f_a \approx 1/N_e$		130 MHz	162 MHz
Electrical Bandwidth Based on the Input Impedance		200 MHz	150 MHz
Transducer Bandwidth		113 MHz	120 MHz

1. Beam Steering Using the First Grating Lobe

In the first design of a six-element stepped-array transducer, P was chosen to be 1, thus $h = \frac{\Lambda_o}{2} = 5.27$ μm. Since an electrical phase shift of π radians was implemented through the arrangement of the finger electrodes as shown in Figure 23(b) the first grating lobe (n = 1) was utilized to diffract the light beam. The acousto-optic angular spectrum of the device was measured using a method similar to that employed for bulk devices (40) and the calculated values were generated using the numerical methodology previously referred to (35). The angular spectrum was obtained by rocking the deflector around the Bragg angle to vary the incident light angle and recording the diffracted light intensity. Detailed experimental set-up is shown in Figure 25 and Figure 26(a) shows the measured and the calculated angular spectra. A good agreement between the calculated values and the measured results was obtained. Tracking of the Bragg condition which resulted from the first-order acoustic beam steering was then studied by measuring the rate of the acoustic scan angle as a function of the acoustic frequency. This measurement was accomplished by taking a set of acousto-optic angular spectra corresponding to a series of acoustic frequency and by determining, from these curves, the corresponding incident angle of the light beam at which the peak of the diffracted light occurred. A constant incident angle for a range of frequency variation Δf implies that a perfect tracking of the Bragg condition is maintained for the same frequency range. The rate of acoustic beam steering was deduced from this data and is plotted in Figure 26(b). From this figure, accurate tracking of the Bragg condition is seen to hold at least for a frequency range of from 200 MHz to 450 MHz as the acoustic beam exhibits the 1/f dependence on frequency in accordance with the prediction of Equation (16). Since both the calculated curves of Figure 26(a) and the relation given in Equation (16) are based on the phase velocity of the SAW, we conclude that both the angular spectrum of the SAW and the rate of acoustic beam steering relevant to the guided-wave acousto-optic Bragg diffraction are determined by the acoustic wavefront instead of the acoustic power flow. They are, therefore, not increased by a factor $(1 + \gamma)$ as is the case for acoustic power flow (41). Note that γ designates the anisotropy factor for the SAW on Y-cut $LiNbO_3$ substrate and is 0.393 and -0.901 for the 21.8°-propagation and the Z-propagation SAWs, respectively.

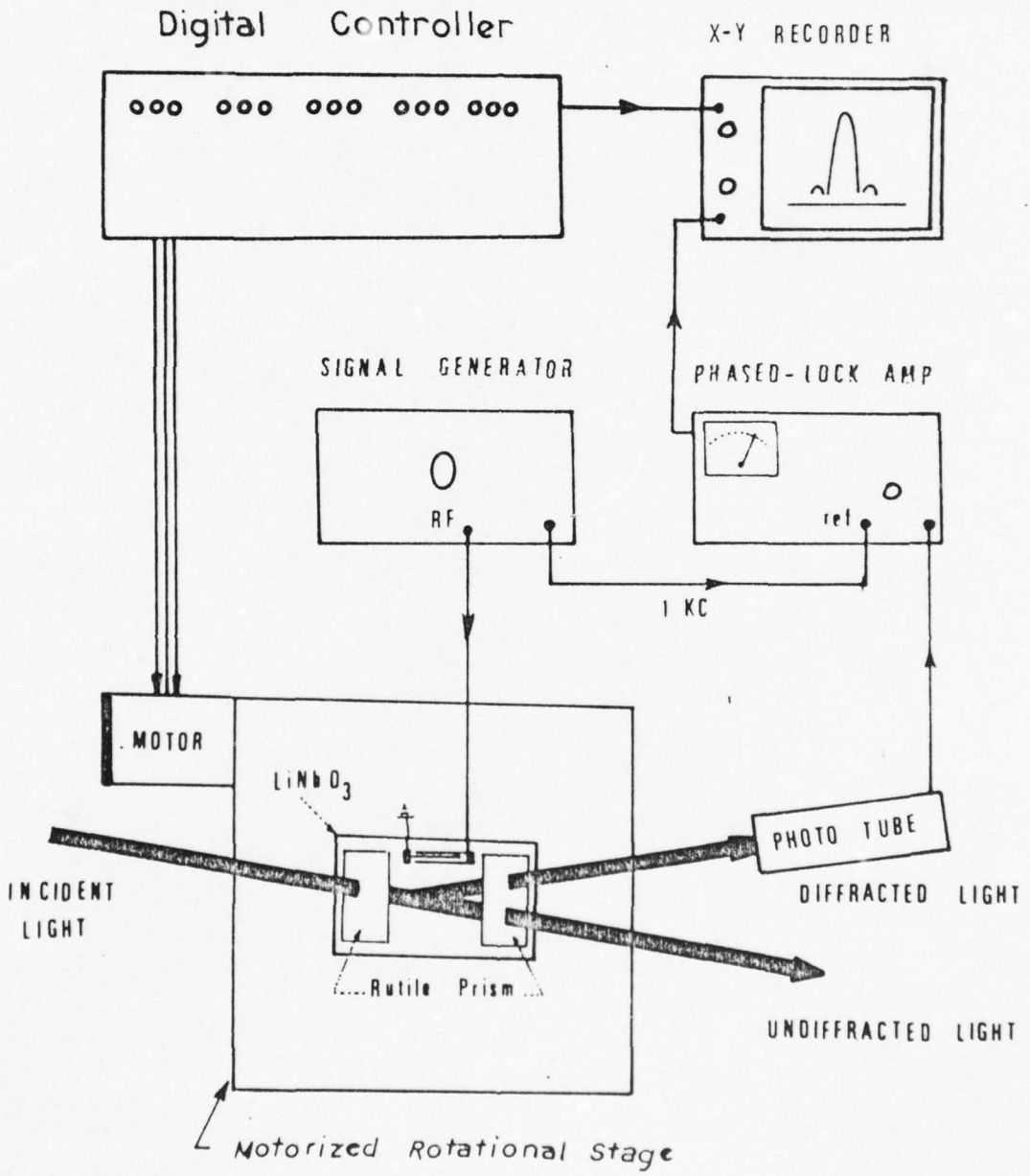

FIG. 25 BLOCK DIAGRAM FOR THE MEASUREMENT OF THE BRAGG-DIFFRACTED LIGHT POWER AS A FUNCTION OF THE INCIDENT LIGHT ANGLE

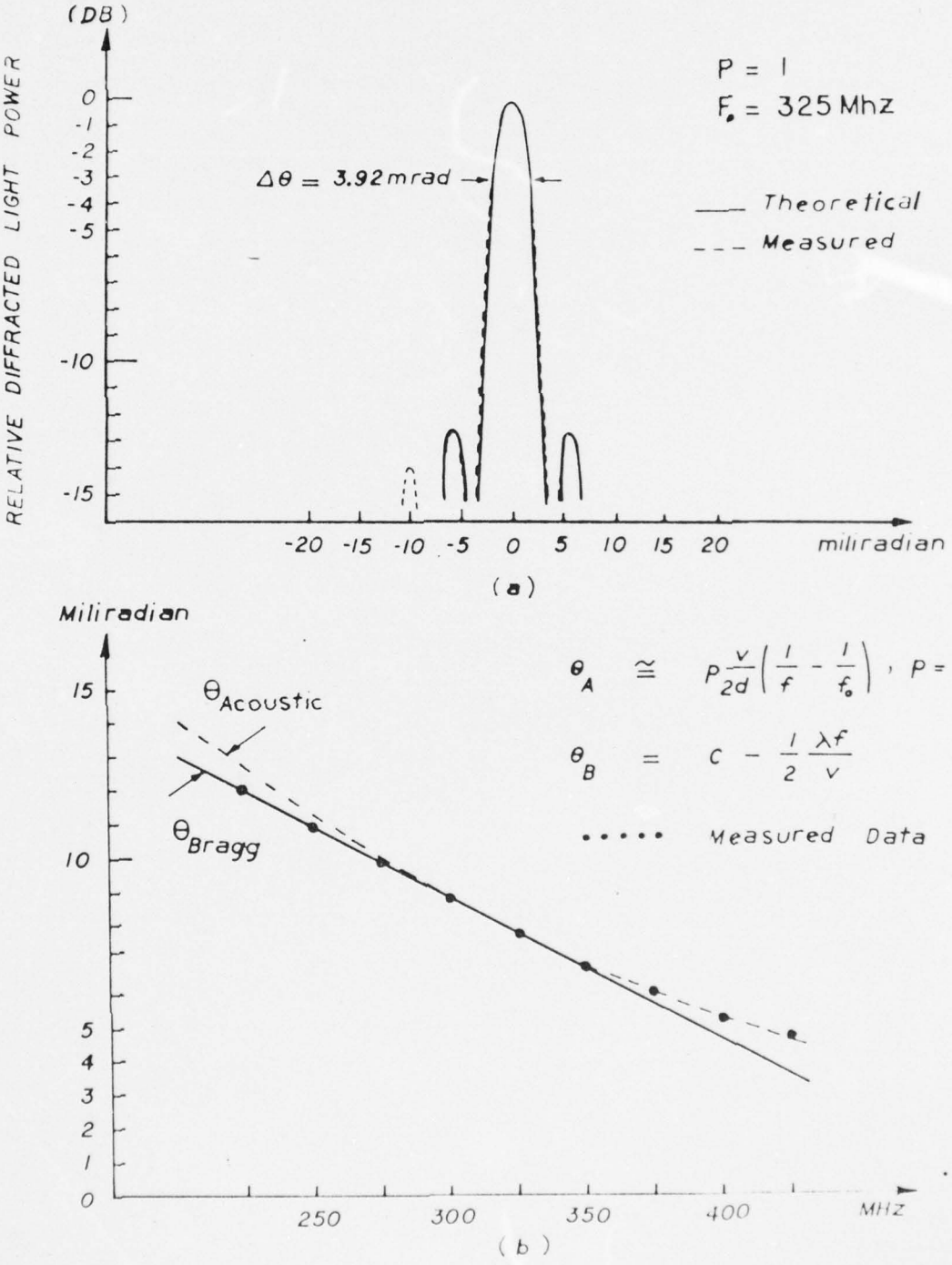

FIG. 26 (a) BRAGG-DIFFRACTED LIGHT POWER AS A FUNCTION OF THE INCIDENT ANGLE OF THE GUIDED-LIGHT BEAM

(b) TRACKING OF THE BRAGG ANGLE USING FIRST-ORDER ACOUSTIC BEAM STEERING FROM A STEPPED SAW ARRAY ($P = 1$)

Measurements with the devices which employ the Z-propagation SAW also result in the same conclusion. Although accurate Bragg tracking was shown to hold for a frequency range of more than 250 MHz, the device bandwidth was measured to be only 110 MHz. This measured device bandwidth is considerably smaller than the calculated Bragg bandwidth of 356 MHz. It was limited by both the acoustic and the electrical bandwidth of the transducer. This limitation is in agreement with the discussion given at the end of Section B because the theoretical acoustic bandwidth of the transducer (N_e = 2.5) was only approximately 130 MHz and was further reduced by the simple electrical matching network employed. A wider device bandwidth could be obtained by increasing both the acoustic bandwidth and the electrical bandwidth of the transducer. Finally, the total electric drive power for 50% diffraction efficiency was measured to be 315 mW at the acoustic center frequency (325 MHz).

2. Beam Steering Using the Third Grating Lobe

In order to utilize a wider acoustic beam aperture so that a higher diffraction efficiency per mW of electric drive power can be obtained, either a larger P and/or a larger N must be employed. We chose to employ a larger P but the same N, namely, six in the second design because of the associated simplicity in fabrication and rf excitation. P was chosen to be 5 and a ϕ of π radians was again implemented using the same electrode layout as in the first design. Accordingly, the third grating lobe (n = 3) of the acoustic beam was responsible for the light beam deflection. From the analysis of Section B, it should be clear that the third grating lobe points in the forward direction (θ_A = 0) at the center frequency providing the most intense acoustic beam (main lobe) for acousto-optic interactions. The detailed design parameters of the array transducer and the relating acoustic and acousto-optic parameters are listed in Table 1. Note that the aperture of the elementary transducer was enlarged by a factor of 4.7. In order to study the effect of acoustic beam steering upon the frequency response of the Bragg diffraction, a plane (unstepped) array transducer with the same aperture dimensions as the stepped array transducer was also fabricated on the same $LiNbO_3$ substrate (Figure 23(a)). No beam steering would be possible on the resultant acoustic beam generated by this plane array transducer.

AD-A039 659 CARNEGIE-MELLON UNIV PITTSBURGH PA DEPT OF ELECTRICA--ETC F/G 9/5
THIN-FILM ACOUSTO-OPTIC SURFACE WAVE INTERACTIONS AND DEVICES.(U)
AUG 76 C S TSAI N00014-75-C-0948

UNCLASSIFIED NL

2 OF 2
AD A039659

END

DATE FILMED
6-77

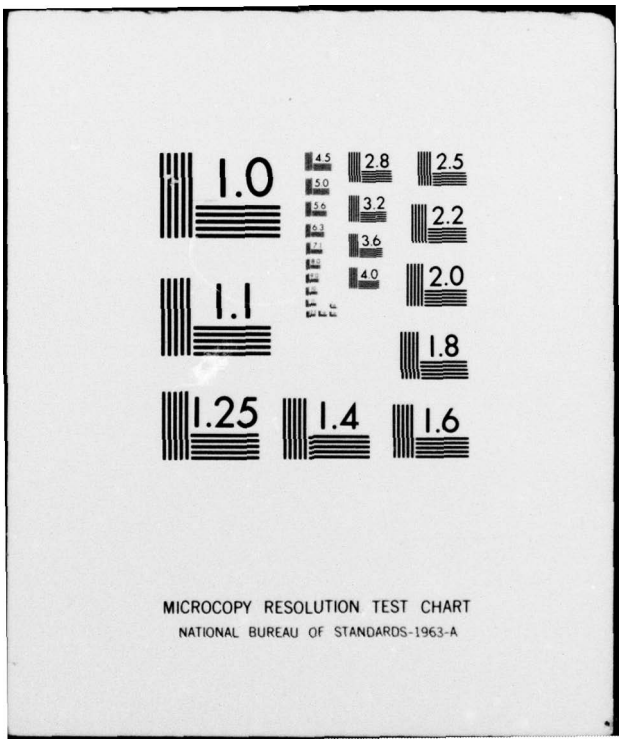
1.0
1.1
1.25
1.4
1.6
1.8
2.0
2.2
2.5
2.8
3.2
3.6
4.0
4.5
5.0
5.6
6.3
7.1
MICROCOPY RESOLUTION TEST CHART
NATIONAL BUREAU OF STANDARDS-1963-A

The acousto-optic angular spectrum was first measured to determine the optimal incident angle of the light beam for accurate beam steering. Figure 27(a) shows the measured and calculated angular spectra. The measured acoustic beamwidth is 1.0 milliradian as compared to a calculated value of 0.94 milliradian. From the plot on the rate of acoustic beam steering versus frequency shown in Figure 27 (b), accurate tracking of the Bragg condition is seen to extend from 265 MHz to 425 MHz, indicating a Bragg tracking bandwidth of 160 MHz. Figure 28 shows the frequency responses of the Bragg diffraction from an elementary SAW as well as those from the six-element phased and plane arrays. It should be noted that in the measurement of the Bragg tracking bandwidth, the finite acoustic scanning bandwidth of the elementary SAW was ignored. From Figure 28(b) the measured -3db bandwidth for the elementary SAW is 103 MHz, as compared to a calculated bandwidth of 95 MHz. It is to be noted that a 40% acoustic bandwidth was assumed for the calculated curve. From Figure 28(a) the bandwidths for the phased and the plane SAW arrays are, respectively, 112 MHz and 21 MHz which compare well with the calculated bandwidths of 110 MHz and 19 MHz. The nulls of the frequency response for the plane array were not well resolved because of the small light beam width used. Clearly, a nearly six-fold improvement in the device bandwidth with no sacrifice in the diffraction efficiency has been achieved by incorporating the first-order acoustic beam steering. As in the device employing the first grating lobe this measured device bandwidth is smaller than the acoustic scanning bandwidth (130 MHz) because of the limitations set by the acoustic and the electrical bandwidths of the transducer. Diffraction efficiency versus the total electric drive power at the center frequency (325 MHz) was also measured and is shown in Figure 29. A total electric drive power of only 68 mW was required to diffract 50% of the incident light. Since the one-way transducer conversion loss was measured to be -13db, only 3.5 mW acoustic power was required in achieving this diffraction efficiency. The average one-way transducer conversion loss was determined by measuring the through-put conversion loss of two transducers fabricated back to back at a separation of 1 cm on the same $LiNbO_3$ substrate. To further reduce the electric drive power an array transducer with better conversion efficiency would have to be employed. Figure 30(a) shows the undeflected light spot (when no rf power was applied to the device) and Figure 39(b) shows the undeflected light spot with rf power both at the far field. The deflected light spot at the far-field is shown in Figure 30(c).

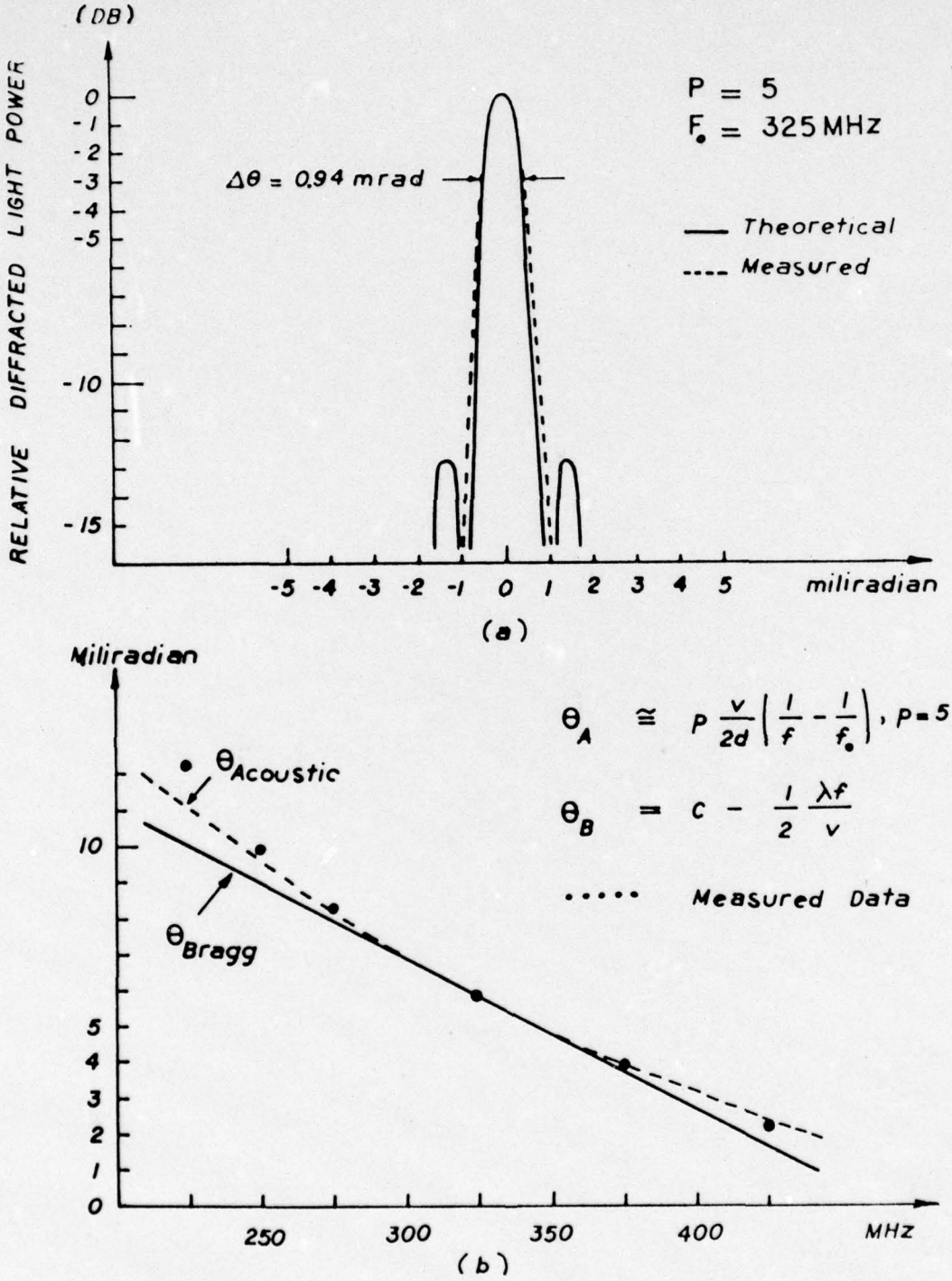

FIG. 27 (a) BRAGG-DIFFRACTED LIGHT POWER AS A FUNCTION OF THE INCIDENT ANGLE OF THE GUIDED-LIGHT BEAM

(b) TRACKING OE THE BRAGG ANGLE USING FIRST-ORDER ACOUSTIC BEAM STEERING FROM A STEPPED SAW ARRAY (P = 5)

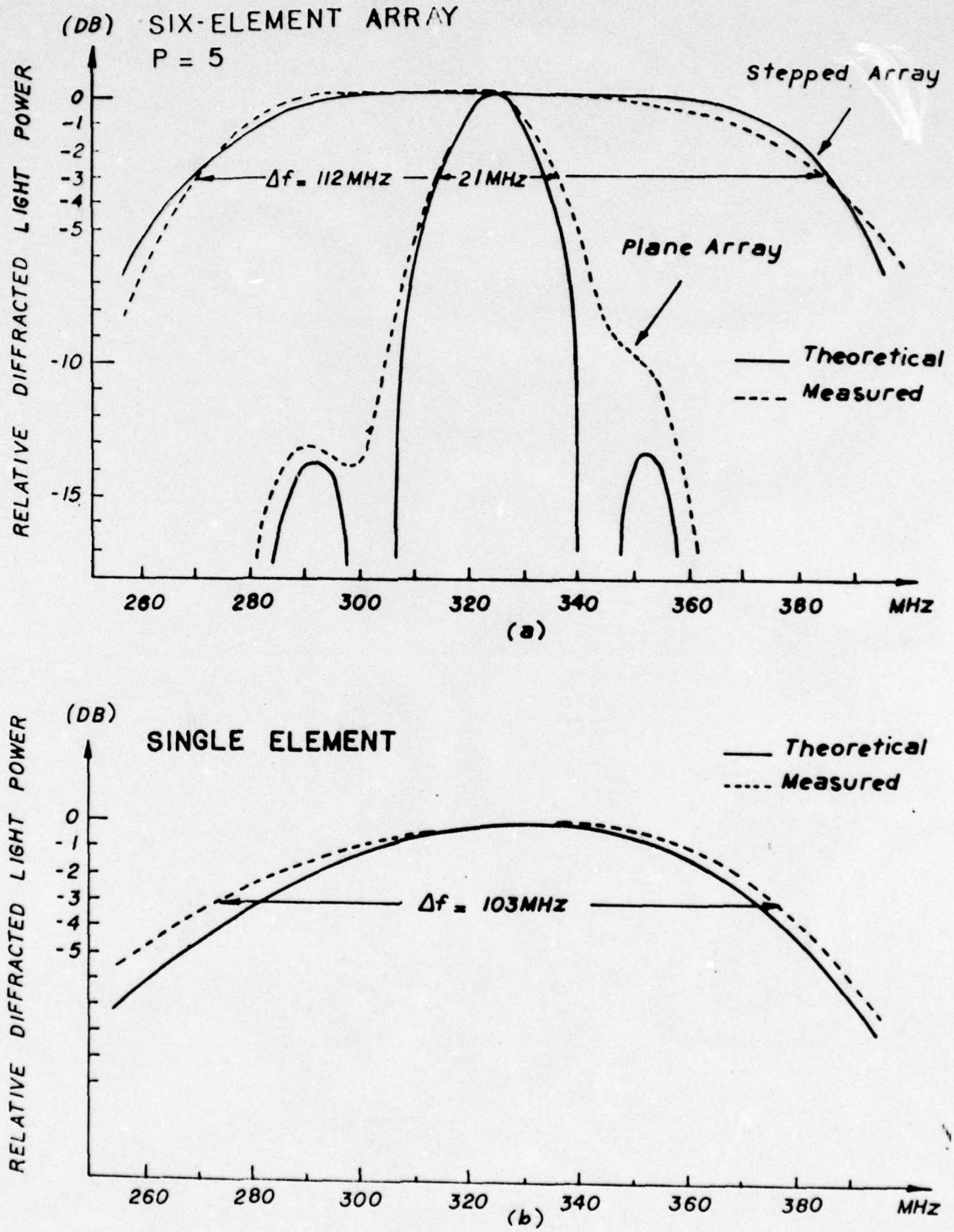

FIG. 28 (a) FREQUENCY RESPONSES OF THE BRAGG-DIFFRACTED LIGHT POWER FROM A STEPPED SAW ARRAY AND FROM ITS CORRESPONDING PLANE ARRAY (b) FREQUENCY RESPONSE OF THE BRAGG DIFFRACTED LIGHT POWER FROM A SINGLE ELEMENT SAW OF THE STEPPED ARRAY IN (a)

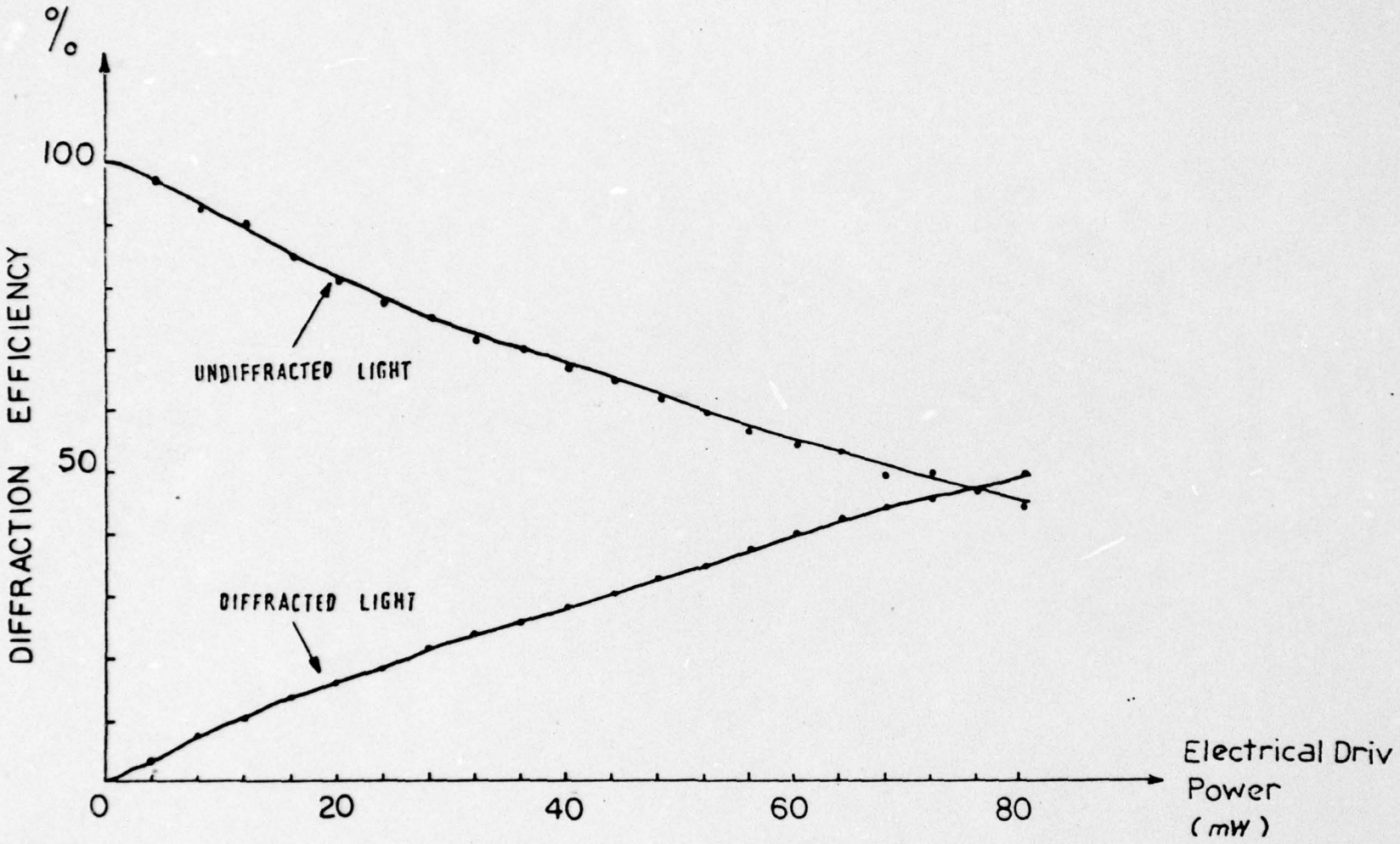

FIG. 29

DIFFRACTION EFFICIENCY vs THE TOTAL ELECTRIC DRIVE POWER (FOR THE STEPPED SAW ARRAY

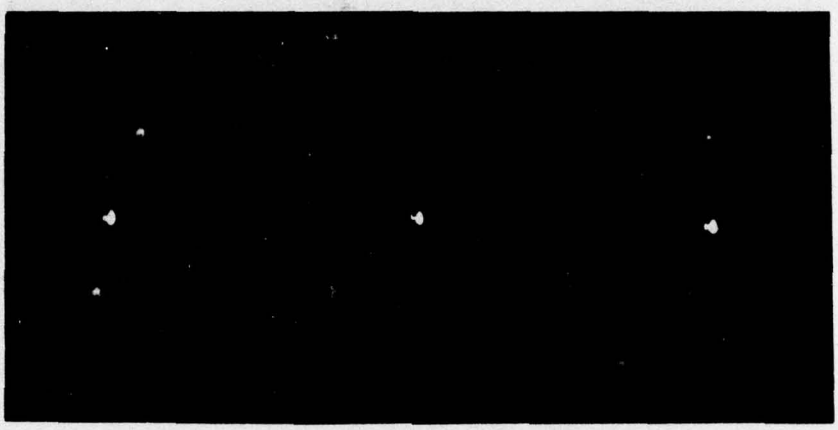

(a) (b) (c)

FIG. 30 *FAR-FIELD UNDEFLECTED AND DEFLECTED LIGHT SPOTS USING PHASED SAW ARRAY*

(a) *UNDEFLECTED LIGHT WITH NO RF POWER*

(b) *UNDEFLECTED LIGHT WITH RF POWER*

(c) *DEFLECTED LIGHT*

The quality of the undeflected light beam (rf power off) was preserved in the deflected light beam and deflected light beams of very good quality were achieved. Also, no mode conversion between the deflected and the undeflected light beams was observed.

D. Concluding Remarks

The results of theoretical and experimental studies have shown that guided-wave acousto-optic Bragg deflectors of very high diffraction efficiency and moderate bandwidth can be realized by employing phased SAW's of 325 MHz center frequency and first-order beam steering in Y-cut $LiNbO_3$ out-diffused waveguides. As indicated at the outset of Section C, the optical waveguide employed in the experimental study had a penetration depth of approximately 7 μm. However, our theoretical study (14) shows that even higher diffraction efficiency and wider Bragg bandwidth would result if the penetration depth of the $LiNbO_3$ optical waveguide is smaller than 7 μm. Thus, assuming that the bandwidth of the transducer is greatly increased by incorporating a suitable matching network further improvement in the performance figures should be achievable by employing an optical waveguide of smaller penetration depth. This type of waveguide can be fabricated by sputtering (42), epitaxy (43) and in-diffusion (44). In addition, as suggested in Reference (45) and partially demonstrated in Reference (34), very large bandwidth and very high diffraction efficiency can be realized by employing a combination of tilted- and phased-SAW's. Another approach to achieve the same purpose would be to employ the phased SAW's which incorporate second-order beam steering (38).

Due to the planar structure of such guided-wave deflectors, design and fabrication of the related stepped array transducer are much more flexible and simpler than their bulk-type counterparts. This fact is particularly true at the higher frequency range in which fabrication of the bulk type stepped array transducer becomes difficult (39). While means for wideband matching of interdigital transducer are available, a large fractional transducer bandwidth is in general more difficult to obtain with the SAW transducers than with the thin-film piezoelectric transducers employed in the bulk-type deflectors.

The high-performance guided-wave A-O Bragg deflectors described in this section may be used in a number of applications including processing (convolution, correlation, etc.) of wideband rf signals, high-speed optical pulse modulation, acousto-optical spectrum analysis of very wideband rf signals, high speed multiport beam switching and deflection for fiber/integrated optic systems. These applications have been demonstrated experimentally and some of the results are described in the following section.

VIV. WIDEBAND APPLICATIONS USING GUIDED-WAVE ACOUSTO-OPTIC BRAGG DEVICES

The results of theoretical and experimental studies have shown that guided-wave acousto-optic Bragg devices of large diffraction efficiency-bandwidth product can be realized by employing either tilted SAWs or phased SAWs. Specifically, a very wide device bandwidth (on the order of 360 MHz) and moderate diffraction efficiency is achievable for devices utilizing tilted SAWs. Also, a moderate device bandwidth (on the order of 110 MHz) and very high diffraction efficiency has been demonstrated in a device utilizing phased SAWs. The ultimate device bandwidth is limited by the acoustic bandwidth of the interdigital transducer. RF drive power requirements, device bandwidth, and random-access switching time of these two types of devices are superior to those of existing acousto-optic devices. It should be possible to achieve even better performance figures when a step-index waveguide of smaller optical confinement is used instead of a gradient-index waveguide such as the out-diffused waveguides employed in this study. A waveguide structure which consists of a thin step-index layer of As_2S_3 (or other acousto-optic material of larger figure of merit) deposited on a $LiNbO_3$ substrate can also provide better performance figures than those provided by $LiNbO_3$ out-diffused waveguides. In addition, it is clear that by employing a combination of tilted and phased-SAW devices, very large bandwidth and very high diffraction efficiency can be realized.

The development of the wideband technique presented in this report has made it possible to design and fabricate very wideband guided-wave acousto-optic Bragg-devices and has, thus, paved the way for a number of potential applications using such devices. Possible wideband applications, similar to those common to bulk-type acousto-optic devices, include processing (convolution, correlation, etc.) of wideband rf signals, high-speed optical pulse modulation, acousto-optic spectrum analysis of very wideband rf signals, high-speed multiport beam switching and deflection for fiber/integrated optic systems. Wideband applications which have been experimentally demonstrated include high-speed multiport beam deflection/switching for future integrated/fiber optic systems, acousto-optic spectrum analysis of very wideband rf signals, processing (convolution, correlation, etc.) of wideband rf signals, high-speed optical pulse modulation, and optical time-multiplexing/demultiplexing. Only the measured performance figures of the first four will be described here.

(1) High-Speed Multiport Beam Deflection/Switching:

The number of resolvable beam diameters actually obtained is 400 with the deflector which has 358 MHz bandwidth and using a light beam aperture of 4 mm. This measured value is in good agreement with the calculated value based on $N = \tau\Delta f$. The corresponding random-access switching time is 1.24 μs. Figure 18 shows the deflected light spots as the acoustic frequency was varied. Figure 20 shows an output light beam of 1 cm aperture. The quality of the light beam was very good. Thus, the deflector with 358 MHz bandwidth should be able to deflect this light beam aperture into 1000 resolvable beam diameters at a random-access switching time of 2.8 μs. Equivalently, this same device is capable of switching a guided light beam of 95 μ aperture into 10 beam positions (channels) at a switching time of 27 ns. Consequently, noncollinear coplanar guided-wave acousto-optic Bragg diffraction constitutes the most promising scheme for planar multiport beam switching/deflection for future fiber/integrated optic systems at medium speed. For ultrahigh speed deflection/switching applications, guided-wave electro-optic devices, in particular those utilizing simple tilted electrodes (28, 29), may be employed.

(2) Spectrum Analysis of Very Wideband rf Signals:

When a spectrum of electro-magnetic signals are applied to the transducer, each spectral component generates an acoustic wave which deflects the incident light beam in a corresponding direction. Thus, by measuring the positions and intensities of the deflected light spots the frequency and strength of each spectral component may be determined. Again, using the basic formula $N = \tau\Delta f$ and a Δf of 358 MHz, we see that a guided light beam of 0.45 cm aperture is capable of processing 400 channels at a frequency resolution, δf, of 0.78 MHz. Two rf signals of varying frequency separation were applied to the deflector referred to above and the beam profiles of the deflected light beams were measured with a fiber optic probe. The plots (Figure 19) clearly show that a frequency resolution of approximately 0.8 MHz was achieved experimentally. This frequency resolution can be reduced to 0.36 MHz to achieve 1000 channels when the light beam aperture is enlarged to 1.0 cm. Advantages of this guided-wave acousto-optic spectrum analyzer (7, 45) over its bulk counter part (46) are reduced drive power requirement, reduced device size, reduced weight, and less critical with isolation and alignment problem.

In spectrum analysis application, inter-modulation and cross-modulation between different frequency components (channels) are among the important parameters. We have recently carried out a preliminary measurement using two independent rf signals of various frequency separation and power level to determine the strengths of such undesirable modulations with the guided-wave A-O deflectors referred to above. The corresponding deflected light spots for two rf signals centering at 250 and 270 MHz are shown in Figure 31. Measurements have also shown that even for the worst case of 43% diffraction, the strongest inter-modulation was -38db down from the diffracted light power. For the practical cases the diffraction efficiency would be much lower than 43% and the corresponding inter- and cross-modulation would also be much lower than -38 db down.

(3) Processing of Wideband rf Signals:

Real-time convolution of pulse-modulated rf signals has been demonstrated. Two end-to-end identical tilted array transducers were deposited on the top of the $LiNbO_3$ waveguide (Figure 32). One pulse-modulated rf signal (say, the reference signal) was applied to one array transducer to generate a SAW propagating in one direction and the other pulse-modulated rf signal (the signal to be processed) was applied to the other array transducer to generate a second SAW propagating in the opposite direction. The two Bragg-diffracted light beams are frequency shifted and overlap, and thus can be collected by a lens and then mixed in a photodetector. It can be easily shown that the electrical output from the photodetector contains a component which is a convolution of the two rf pulses. This convolution signal has a carrier frequency equal to the sum of the two acoustic frequencies and can be further processed and then displaced on an oscilloscope. Typical waveforms of the convolution for single-pulse and double-pulse rf signals are shown in Figure 33. A time-bandwidth product of 305 with 107 MHz bandwidth and a dynamic range of 50 db have been demonstrated with the convolver described above. Since it is possible to achieve a very large bandwidth using the tilted SAWs it should be possible to achieve a time-bandwidth product much larger than 305.

(4) High Speed Optical Pulse Modulation:

A rise- and decay-time of approximately 10 ns (Figure 34) has been achieved with a device of 100 MHz bandwidth. The experimental set-up for this study is shown in Figure 35. A faster modulation speed should be achievable using the unit with larger bandwidth.

In summary, the very encouraging performance figures obtained with the preliminary devices indicate that the wideband guided-wave acousto-optic Bragg devices developed in this study may find many applications in future wideband multi-channel fiber and integrated optic systems.

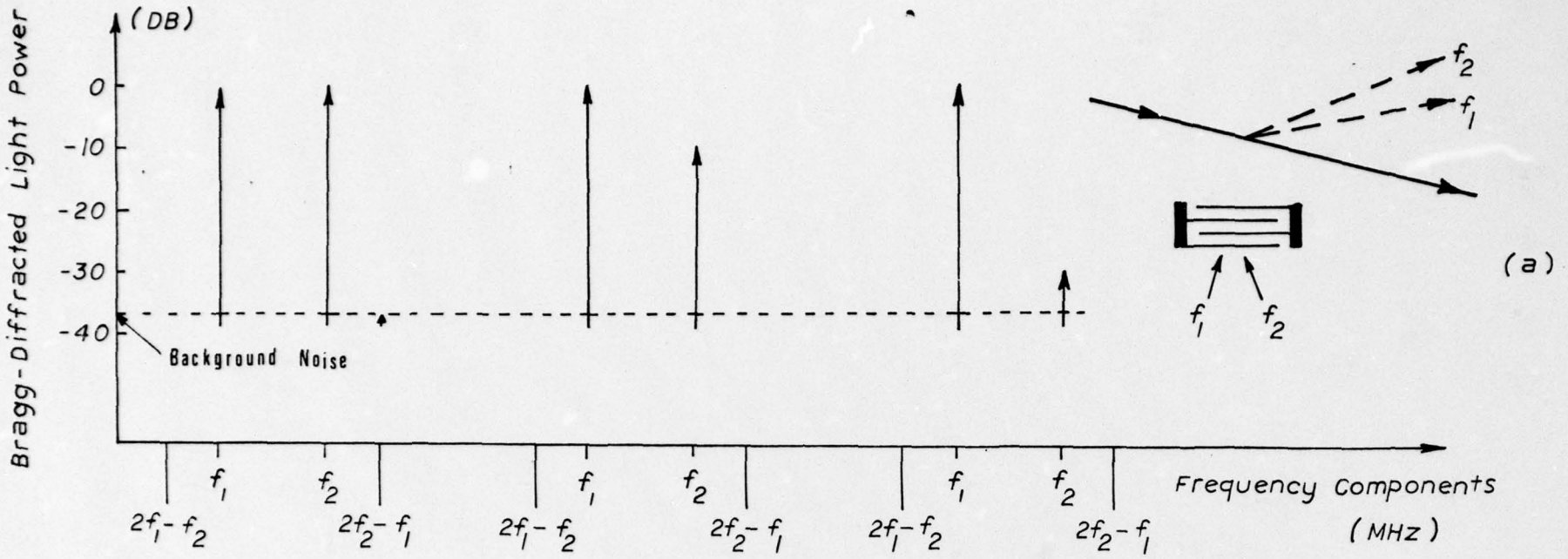

$f_1 = 250$, $f_2 = 270$, $2f_1 - f_2 = 230$, $2f_2 - f_1 = 290$

Total Diffraction Efficiency : 43% , Inter-Modulation < -37 db

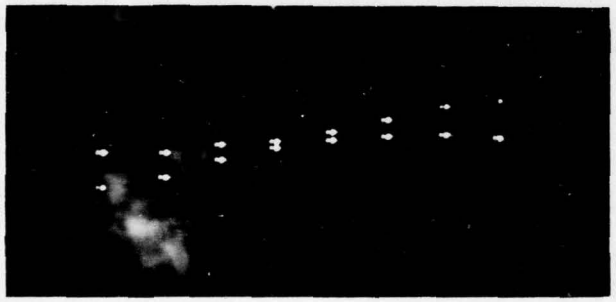

(b)

FIG. 31

Spectrum Analysis of RF Signals Using Guided-Wave Acousto-Optic Bragg-Diffraction :
(a) Measurement of Inter-Modulation between Two Frequency Components f_1 and f_2
(b) Deflected Light Spots from Two Frequency Components of Various Frequency Separation and Power Level

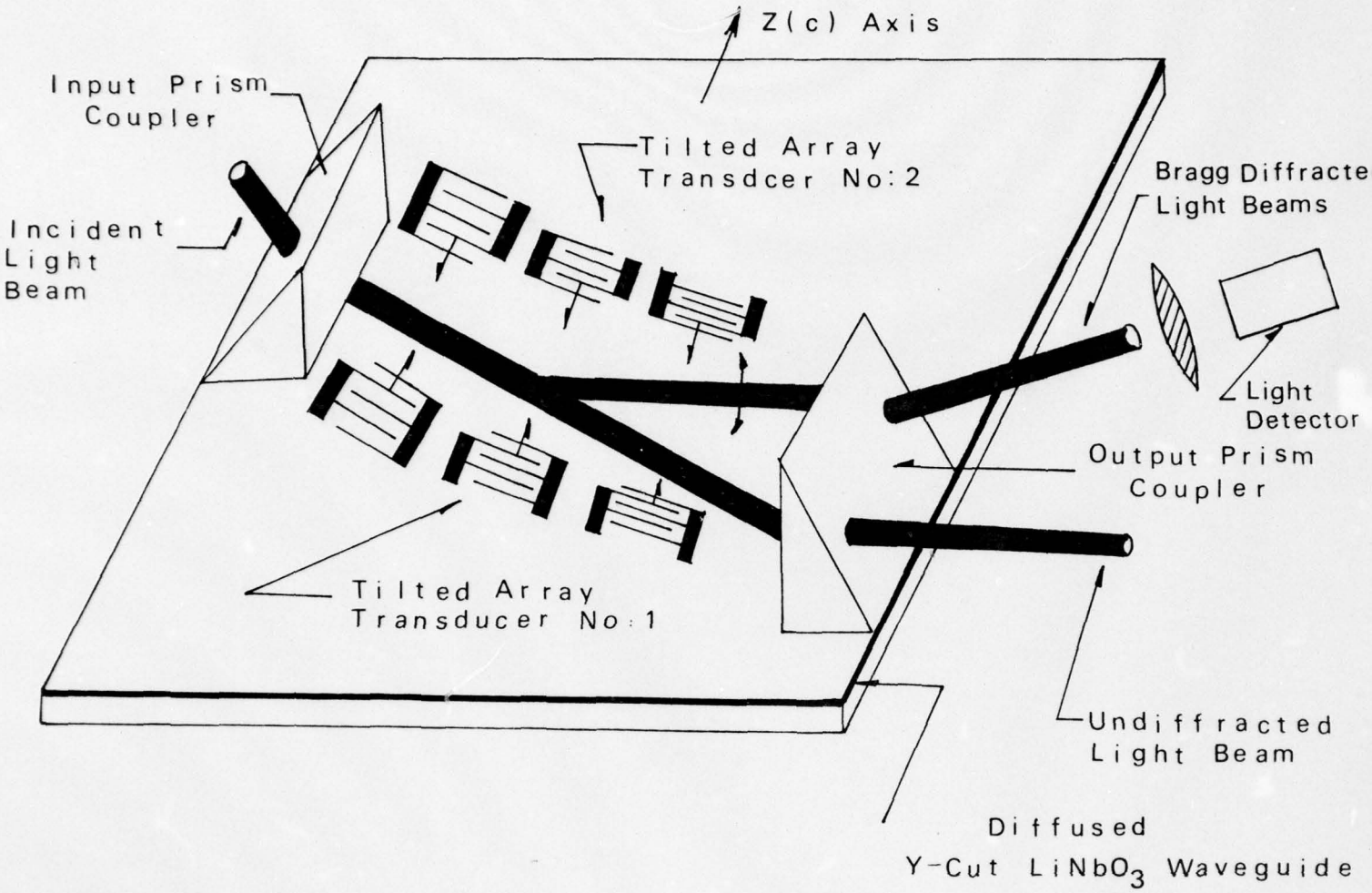

FIG. 32 Guided-Wave Acoutooptic Signal Processing Using Multiple Tilted Surface Acoutic Waves in $LiNbO_3$ Waveguide

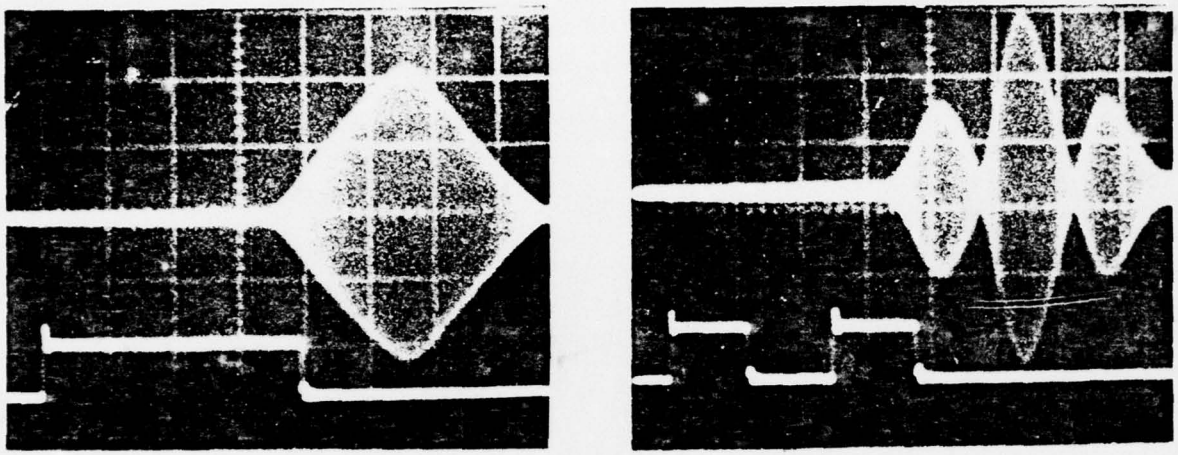

a b

FIG. 33 Pulse–Modulated RF Signals (Lower Traces) and Their Corresponding Autoconvolution Outputs:

(a) Single RF Pulse: Center Frequency (164 MH_z), Vertical Scale (20mV/Div), Horizotal Scale (0.5 us/Div.)

(b) Double RF Pulses: Center Frequency (164 MH_z), Vertical Scale (10 mV/Div.), Horizontal Scale (0.5 us/Div)

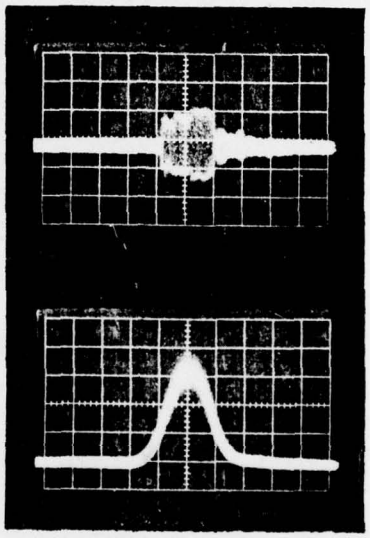

FIG. 34 TIME-RESPONSE OF A GUIDED-WAVE ACOUSTOOPTIC PULSE MODULATOR:

(A) PULSE-MODULATED RF WAVEFORM

(B) PULSE-MODULATED DIFFRACTED LIGHT WAVEFORM

(HORIZONTAL SCALE: 20 NS PER MAJOR DIVISION)

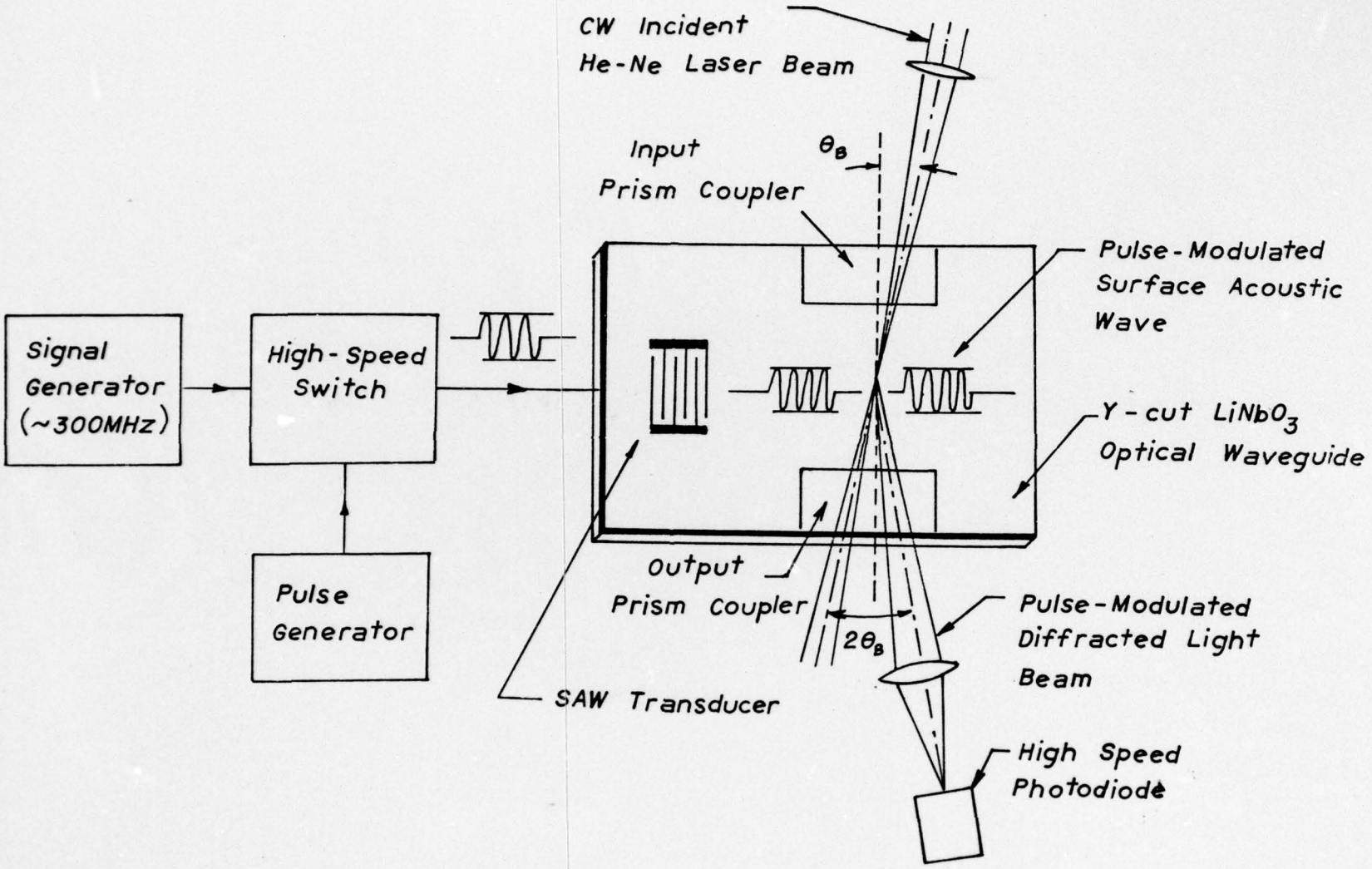

FIG. 35 Block Diagram For Guided-Wave Acoustooptic Pulse Modulation Experiment

X. CONCLUSIONS AND RECOMMENDATIONS

In conclusion, guided-wave A-O deflector of large bandwidth-diffraction efficiency product can be realized by employing either tilted SAWs or phased SAWs in Y-cut $LiNbO_3$ waveguides. Overall performance characteristics including rf drive power requirements, device bandwidth, and random-access switching time, etc., have exceeded those of existing A-O deflectors. Relevant parameters as well as important considerations for the design of such wideband devices have been established. It should be possible to achieve even better performance figures by employing a combination of tilted and phased SAWs and/or using an optical waveguide of smaller confinement and SAWs of higher center frequency. Other potentially useful materials are As_2S_3, GaAs, Si, Tl_3AsS_4 and TeO_2. Although opaque at visible wavelength, GaAs and Si possess the potential for integrating the A-O device with photodetectors and other electrical components for signal processing. To the best of our knowledge little work has been done on the last two materials in thin-film form. These two materials and As_2S_3 possess much larger acousto-optic figure of merit. The development of the wideband technique presented in this report has made it possible to design and fabricate very wideband guided-wave acousto-optic Bragg-devices and has, thus, paved the way for a number of potential applications using such devices. Thus a further study of the wideband technique with emphasis on operating frequency, waveguide-material combination and a more detailed investigation on the wideband applications are recommended.

REFERENCES FOR PART II

(1) L. Kuhn, M. L. Dakss, P. F. Heidrich, and B. A. Scott, "Deflection of an Optical Guided-Wave by a Surface Acoustic Wave", Appl. Phys. Lett., 17, 265 (1970); L. Kuhn, P. F. Heidrich, and E. G. Lean, "Optical Guided-Wave Mode Conversion by an Acoustic Surface Wave", Appl. Phys. Lett., 19, 428 (1971).

(2) T. G. Giallorenzi, "Acousto-optical Deflection in Thin-Film Wave-Guides", J. Appl. Phys., 44, 242 (1973).

(3) Y. Ohmachi, "Acousto-Optical Light Diffraction in Thin Films", J. Appl. Phys., 44, 3928 (1973).

(4) P. K. Cheo and T. M. Reeder, Optical Society of America Spring Meeting, 1973 (unpublished).

(5) R. V. Schmidt, I. P. Kaminow, and J. R. Carruthers, "Acousto-Optic Diffraction of Guided Optical Waves in $LiNbO_3$", Appl. Phys. Lett., 28, 417 (1973).

(6) C. S. Tsai, "Thin-Film Acousto-Optic Surface Wave Interactions", presented at the ONR-ARPA Electro-optic Program Review, Arlington, Virginia, Oct. 2-4, 1973.

(7) M. C. Hamilton and D. A. Wille, "Acousto-Optic Diffraction in Optical Waveguides", presented at the 1974 Topical Meeting on Integrated Optics, Tau. 21-24, New Orleans, Louisiana.

(8) J. F. Weller, T. G. Giallorenzi and A. F. Milton, "Light Deflection in Single and Multimode Waveguides Using Acousto-optic Interaction", Topical Meeting on Integrated Optics, Paper WA9-1, Jan. 21-24, 1974, New Orleans, Louisiana.

(9) N. Chubachi, J. Kushibiki and Y. Kikuchi, "Monolithically Integrated Bragg Deflector for an Optical Guided Wave Made of Zinc-Oxide Film", Elect. Lett., 9, 193-194, 1973. Also, J. Kushibiki, H. Sasaki, N. Chubachi, N. Mikoshiba, and K. Shibayama, "Thickness Dependence of the Diffraction Efficiency of Optical Guided Waves by Acoustic Surface Waves", in Proc. 1974 Ultrasonics Symposium IEEE Cat. 74, CH0896-ISU, pp. 85-89.

(10) R. M. De La Rue, C. Steward, C. D. W. Wilkinson, and I. R. Williamson, "Frequency-Controlled Beam Steering of Surface Acoustic Waves Using A Stepped Transducer Array", Electron. Lett., 8, 326 (July 1973).

(11) C. S. Tsai and Le T. Nguyen, "Surface Acoustic Wave Array Transducers and Their Applications", Proceedings of the Symposium on Optical and Acoustical Microelectronics, Polytechnic Press of the Polytechnic Institute of New York, Vol. XXIII, pp. 583-597, (April, 1974).

(12) C. S. Tsai, S. K. Yao and M. A. Alhaider, "High Performance Guided-Wave Acousto-optic Deflection Using Multiple Surface Acoustic Waves", presented at Integrated Optics and Fiber Optics Communication Conference, NELC, San Diego, Calif., May 15-17, 1974, Post-Deadline Paper D.12 (unpublished).

(13) C. S. Tsai, L. T. Nguyen and M. A. Alhaider, "A Wideband Acousto-optic Guided-Light Beam Deflector Using Intersecting Surface Acoustic Waves", Proceedings of the 1974 Ultrasonics Symposium, IEEE Cat. 74, CH0896-ISU, pp. 768-772. Also, C. S. Tsai, L. T. Nguyen, S. K. Yao and M. A. Alhaider, "High Performance Acousto-optic Guided-Light Beam Device Using Two Tilting Surface Acoustic Waves", Appl. Phys. Lett., 26, 140 (Feb. 1975).

(14) C. S. Tsai, M. S. Alhaider, L. T. Nguyen and B. Kim, "Wideband Guided-Wave Acousto-Optic Bragg Devices Using Multiple Tilting Surface Acoustic Waves", presented at the 1975 IEEE/OSA Conference on Laser Engineering and Application, May 28-30, Washington, D. C., Digest of Technical Papers, p. 10; C. S. Tsai, M. A. Alhaider, L. T. Nguyen, and B. Kim, "Wideband Guided-Wave Acousto-optic Bragg Diffraction and Devices Using Multiple Tilted Surface Acoustic Waves", Proc. IEEE, Vol. 64, pp. 318-328 (March, 1976).

(15) K. Loh and W. Chang, "Bragg Diffraction of Optical Guided Waves by Surface Acoustic Waves in GaAs and $LiNbO_3$ Waveguides", presented at the NSF Meeting on Optical Communication Systems, University of Illinois, Nov. 14-15, 1974.

(16) E. G. Lean, P. F. Heidrich and J. M. White, "Thin-Film Acousto-optic Devices - Review and Assessment", 1974 Ultrasonics Symposium Proceedings, IEEE Cat. 74, CH0896-ISU, pp. 81-84. Also, J. M. White, P. F. Heidrich, Electron. Lett., Vol. 10, pp. 510-511 (Nov. 1974). Also, E. C. Lean, J. M. White and C. D. W. Wilkinson, "Thin-Film Acousto-optic Devices", Proc. IEEE, Vol. 64, pp. 779-788 (May, 1976).

(17) R. V. Schmidt and I. P. Kaminow, "Acousto-optic Bragg Deflection in $LiNbO_3$ Ti-diffused Waveguides", IEEE Journal of Quantum Electronics, January 1975, pp. 57-59.

(18) The possibility of enhancement in diffraction efficiency due to the electro-optic effect was first suggested by the authors at the NSF Workshop on Acoustical Microelectronics, November 7, 1973, Stanford University. This enhancement was observed by people at IBM (Ref.16) and the authors a year later.

(19) W. R. Smith, H. M. Gerard, J. H. Collins, T. M. Reeder and H. J. Shaw, "Design of Surface Wave Delay Lines with Interdigital Transducers", IEEE Trans. Microwave Theory and Tech. MTT-17, 865 (Nov. 1969).

(20) C. F. Quate, C. D. W. Wilkinson, and D. K. Winslow, "Interaction Of Light and Microwave Sound", Proc. IEEE, Vol. 53, 1604 (Oct. 1965); E. I. Gordon, "A Review of Acousto-optical Deflection and Modulation Devices", Appl. Opt., Vol. 5, 1629 (Oct. 1966); N. Uchide and N. Niizeki, "Acousto-optic Deflection Materials and Techniques", Proc. IEEE, Vol. 61, 1073 (1973); N. Uchida and N. Niizeki, "Acousto-optical Deflection Materials and Techniques", Proc. IEEE, Vol.61, 1073, (Aug. 1973).

(21) C. S. Tsai, Le T. Nguyen, and B. Kim, "Wideband Guided-Wave Acousto-optic Bragg-Diffraction Using Phased-Surface Acoustic Wave Array in $LiNbO_3$ Waveguides", presented at the 1975 Ultrasonics Symposium, Symposium Digest, pp. 42-43, Los Angeles, Calif., Sept. 22-24.

(22) I. P. Kaminow and J. R. Carruthers, "Optical Waveguiding Layers in $LiNbO_3$ and $LiTaO_3$", Appl. Phys. Lett., 22, 326 (1973); N. F. Hartman, R. P. Kenan, P. R. Sievert, C. M. Verber and V. E. Wood, "Characteristics of Diffused Waveguiding Layers in $LiNbO_3$", presented at the Integrated Optics Meeting, New Orleans, January 21-24, 1974.

(23) R. W. Dixon, "Acoustic Diffraction of Light in Anisotropic Media", IEEE J. Quantum Electron., QE-3, 85 (Feb. 1967).

(24) Microwave Acoustics Handbook, Vol. 1A, Surface Wave Velocities, AFCRL-TR-73-0597, Oct. 1, 1973, Edited by A. J. Slobodnik, E. D. Conway and R. T. Delmonico.

(25) R. N. Spaight and G. G. Koerber, "Piezoelectric Surface Waves on $LiNbO_3$", IEEE Trans. Sonics and Ultrasonics, SU-18,237 (Oct. 1971).

(26) D. Marcuse, "TE Modes of Graded-Index Slab Waveguides", IEEE J. Quantum Electron., QE-9, 1000 (Oct. 1973).

(27) R. W. Dixon and M. G. Cohen, "A New Technique for Measuring Magnitudes of Photo-elastic Tensors and Its Application to Lithium Niobate", Appl. Phys. Lett., 8, 205, (Apr. 1966).

(28) C. S. Tsai, Le T. Nguyen and P. Saunier, "New Guided-Wave Acousto-optic and Electro-optic Devices Using $LiNbO_3$", presented at the 1975 IEEE Symposium on Applications of Ferroelectrics, June 9-11, Albuquerque, New Mexico, Symposium Digest, pp. 78-79.

(29) C. S. Tsai and P. Saunier, "Ultrafast Guided-Light Beam Deflection/Switching and Modulation Using Simulated Electro-optic Prism Structures in $LiNbO_3$ Waveguides", Appl. Phys. Lett., 27, 248 (Aug. 1975).

(30) H. I. Smith, F. J. Bachner and N. Efremow, "A High-Yield Photolithographic Technique for Surface Wave Devices", J. Electrochem. Soc. 118, 821 (May 1971).

(31) A. Korpel, R. Alder, P. Desmares, and W. Watson, "A Television Display Using Acoustic Deflection and Modulation of Coherent Light", Proc. Inst. Elec. Electron. Eng., 1966, 54, 1429; G. A. Coquin, J. P. Griffin, and L. K. Angerson, "Wideband Acousto-optic Deflectors Using Acoustic Beam Steering", IEEE Trans. 1970, SU-17, 34; D. A. Pinnow, "Acousto-optic Light Deflection: Design Considerations for First Order Beam-Steering Transducers", ibid., 1971, SU-18, 209.

(32) Le T. Nguyen and C. S. Tsai, "Efficient Wideband Guided-Wave Acousto-optic Bragg-Diffraction Using Phased-Surface Acoustic Wave Array in $LiNbO_3$ Waveguides", to be published in Appl. Opt., Feb., 1977.

(33) M. L. Dakss, L. Kuhn, P. F. Heidrich, and B. A. Scott, "Grating Coupler for Efficient Excitation of Optical Guided Waves in Thin Film", Appl. Phys. Lett., 16, 523 (June 15, 1970).

(34) C. D. W. Wilkinson, R. De La Rue and G. Trantor, "Light Beam Deflector Using SAW-Optical Interaction", presented at the 1975 International Electron. Devices Meeting, Dec. 1-3, Washington, D. C.

(35) C. S. Tsai, B. Kim, P. Saunier and L. T. Nguyen, "Acousto-optic Bragg-Diffraction Using Multiple Surface Acoustic Waves and Electro-optic Deflection/Modulation Using Tilted Electrodes", presented by the 1976 Topical Meeting on Integrated Optics, Jan. 12-14, Salt Lake City, Utah, Technical Digest, p. TuA2 Optical Society of America, 75CH1039-7 QEC; B. Kim and C. S. Tsai, "High-Performance Guided-Wave Acousto-optic Scanning Devices Using Multiple Surface Acoustic Waves", Invited Paper, Proc. IEEE, Vol. 64, pp. 788-793 (May, 1976).

(36) A. Korpel, R. Adler, P. Desmares, and W. Watson, "A Television Display Using Acoustic Deflection and Modulation of Coherent Light Proc. IEEE, Vol. 54, No. 10, Oct. 1966, pp. 1429-1437.

(37) E. I. Gordon, "A Review of Acousto-optic Deflection and Modulation Devices", Proc. IEEE, Vol. 54, pp. 1391-1401 (Oct. 1966).

(38) G. A. Coquin, J. P. Griffin and L. K.Anderson, "Wideband Acousto-optic Deflectors Using Acoustic Beam Steering", IEEE Trans. on Sonics and Ultrasonics, Vol. SU-17, No. 1, Jan. 1970, pp. 34-40.

(39) D. A. Pinnow, "Acousto-optic Light Deflection: Design Considerations for First Order Beam Steering Transducers", IEEE Trans. on Sonics and Ultrasonics, Vol. SU-18, No. 4, Oct. 1971, pp. 209-214.

(40) M. G. Cohen and E. I. Gordon, "Acoustic Beam Probing Using Optical Techniques", Bell System Technical Journal, Apr. 1975, pp. 693-721.

(41) See, for example, T. L. Szabo and A. J. Slobodnik, Jr., "The Effect of Diffraction on the Design of Acoustic Surface Wave Devices", IEEE Trans. on Sonics and Ultrasonics, Vol. SU-20, No. 3, July 1973, pp. 240-251.

(42) Y. Ohmachi, "Acousto-optical Light Diffraction in Thin Films", Journal of Applied Physics, 44, 3923 (Sept. 1973); J. Kushibiki, H. Sasaki, N. Chubachi, N. Mikoshiba, and K. Shibayama, "Thickness Dependence of the Diffraction Efficiency of Optical Guided-Waves by Acoustic Surface Waves", in Proc. 1974 Ultrasonics Symposium; N. Mikoshiba, "Optical Waveguides of Single-Crystal $LiNbO_3$ Film Deposited by rf Sputtering", Applied Physics Letter, Vol. 24, pp. 490-492, (May, 1974).

(43) S. Miyazawa, "Growth of $LiNbO_3$ Single-Crystal Film for Optical Wave-guides", Appl. Phys. Lett., 23, pp. 198-200 (Aug. 1973); P. K. Tien, S. Riva-Sanseverino, R. J. Martin, A. A. Ballman and H. Brown, "Optical Waveguide Modes in Single-Crystalling $LiNbO_3$ - $LiTaO_3$ Solid-Solution Films", Appl. Phys. Lett., Vol. 26, pp. 503-506 (May 1974).

(44) H. F. Taylor, W. E. Martin, D. B. Hall and V. N. Smiley, "Fabrication of Single-Crystal Semiconductor Optical Waveguides by Solid-State Diffusion", Appl. Phys. Lett., Vol. 21, pp. 95-98 (Aug. 1972); J. M. Hammer and W. Phillips, "Low-Loss Single-Mode Optical Waveguides and Efficient Speed Modulators of $LiNb_xTa_{1-x}$ on $LiTaO_3$, Appl. Phys. Lett., Vol. 24, pp. 545-547 (June 1974); R. V. Schmidt and I. P. Kaminow, "Metal-Diffused Optical Waveguides in $LiNbO_3$, Appl. Phys. Lett., Vol. 25, pp. 458-460 (Oct. 1974).

(45) C. S. Tsai, "Wideband Guided-Wave Acousto-optic Bragg Devices and Applications", in Proc. 1975 Ultrasonics Symposium, IEEE Cat. 75, CH0994-4SU, pp. 120-125.

(46) D. L. Hecht, "Broadband Acousto-optic Spectrum Analysis", Proc. of the 1973 Ultrasonics Symposium, p. 98.

XI. PUBLICATIONS

1. C. S. Tsai and Le T. Nguyen, "Scanning of Acoustic Surface Wave Phased-Array", Proc. IEEE, Vol. 62, 535-537, June, 1974.

2. C. S. Tsai and Le T. Nguyen, "Surface Acoustic Wave Transducer Arrays and Their Applications", Proceedings of the MRI Symposium on Optical and Acoustical Micro-Electronics, New York: Polytechnic Press, 1974, Vol. XXII, pp. 583-597.

3. C. S. Tsai, "Ultrahigh Data Rate Time-Multiplexed PCM Fiber/Integrated Optics Communication Systems", Invited Paper, Proceedings of the 1974 National Electronics Conference, Oct. 16-18, pp. 381-386.

4. C. S. Tsai, Le T. Nguyen, S. K. Yao and M. A. Alhaider, "A High Performance Acousto-optic Guided-Light Beam Device Using Two Tilting Surface Acoustic Waves", Appl. Phys. Lett., 26, 140-142 (Feb. 1975)

5. C. S. Tsai, M. A. Alhaider, Le T. Nguyen, and B. Kim, "Wideband Guided-Wave Acousto-optic Bragg Devices Using Multiple Tilting Surface Acoustic Waves", 1975 IEEE/OSA Conference on Laser Engineering and Applications, Washington, D. C., May 28-30, Technical Digest, p. 10.

6. C. S. Tsai, "Wideband Guided-Wave Acousto-optic Bragg Devices and Applications", Invited Paper, Proceedings of the 1975 Ultrasonic Symposium, IEEE Cat. 75 CHO-994-4SU, pp. 120-125.

7. C. S. Tsai, B. Kim, P. Saunier and Le T. Nguyen, "Acousto-optic Bragg Diffraction Using Multiple Surface Acoustic Waves and Electro-optic Deflection/Modulation Using Tilted Electrodes", Technical Digest, paper TuA^2, OSA/IEEE Topical Meeting on Integrated Optics, Jan. 12-14, 1976.

8. C. S. Tsai, M. A. Alhaider, Le T. Nguyen and B. Kim, "Wideband Guided-Wave Acousto-optic Bragg Diffraction and Devices Using Multiple Tilted Surface Acoustic Waves", Proceedings of IEEE Vol. 64, pp. 318-328, March, 1976.

9. B. Kim and C. S. Tsai, "High-Performance Guided-Wave Acousto-optic Scanning Devices Using Multiple Surface Acoustic Waves," Invited Paper, Special Issue on Surface Acoustic Waves, Proc. IEEE., Vol. 64, pp. 788-793, (May, 1976).

10. I. W. Yao and C. S. Tsai, "Signal Processing Using Guided-Wave Acousto-optic Bragg-Diffraction in $LiNbO_3$ Waveguides," Presented at the 1976 International Microwave Symposium, June 14-16, Cherry Hill, New Jersey; Digest of Technical Papers, pp. 21-23, IEEE Cat . No. 76CH1087-6MTT.

11. Le T. Nguyen and C. S. Tsai "Efficient Wideband Guided-Wave Acousto-optic Bragg Diffraction Using Phased-Surface Acoustic Wave Array in $LiNbO_3$ Waveguides", to be published in Applied Optics, Feb. issue, 1977.

12. C. S. Tsai, "Device Applications Using Guided-Wave Acousto-optic Deflectors", Invited Paper, Technical Symposium of the Society of Photo-Optical Instrumentation Engineers, Aug. 23-27, 1976, San Diego, Calif., to be published in Symposium Proceedings.

XII. INVENTION DISCLOSURES AND PATENT APPLICATIONS

1. Signal Processor for a Receiving Phased-Array Antenna Using Acoustic Surface Wave Transducer Arrays, Invention Disclosure (Oct. 1972). Also, Navy Technical Disclosure Bulletin vol. 1, No. 2, 47-52 (June 1976), Navy Case No. 59781.
2. Acoustooptic Guided Light Beam Device, ONR Patent Application No. 616338, 24 September, 1975 (ONR Boston Patent Office).

SECURITY CLASSIFICATION OF THIS PAGE (When Data Entered)

REPORT DOCUMENTATION PAGE

READ INSTRUCTIONS BEFORE COMPLETING FORM

1. REPORT NUMBER: FINAL REPORT
2. GOVT ACCESSION NO.:
3. RECIPIENT'S CATALOG NUMBER:

4. TITLE (and Subtitle): THIN-FILM ACOUSTO-OPTIC SURFACE WAVE INTERACTIONS AND DEVICES

5. TYPE OF REPORT & PERIOD COVERED: Final Report. 1 May 73-5/1/73 - 6/30/76 (30 Jun 76)

6. PERFORMING ORG. REPORT NUMBER: None

7. AUTHOR(s): Professor Chen S. Tsai

8. CONTRACT OR GRANT NUMBER(s): N00014-75-C-0948

9. PERFORMING ORGANIZATION NAME AND ADDRESS:
Professor Chen S. Tsai
Department of Electrical Engineering
Carnegie-Mellon University, Pittsburgh, PA 15213

10. PROGRAM ELEMENT, PROJECT, TASK AREA & WORK UNIT NUMBERS: NR384-411

11. CONTROLLING OFFICE NAME AND ADDRESS:
Office of Naval Research
Physics Program Office, Department of the Navy
Arlington, VA 22217

12. REPORT DATE: August 1976

13. NUMBER OF PAGES: 119 pages, 43 figures (122p.)

14. MONITORING AGENCY NAME & ADDRESS (if different from Controlling Office):

15. SECURITY CLASS. (of this report): Unclassified

15a. DECLASSIFICATION/DOWNGRADING SCHEDULE:

16. DISTRIBUTION STATEMENT (of this Report)

Approved for public release; distribution unlimited.

17. DISTRIBUTION STATEMENT (of the abstract entered in Block 20, if different from Report)

Reproduction in whole or in part is permitted for any purpose of the United States Government.

18. SUPPLEMENTARY NOTES

403 445

19. KEY WORDS (Continue on reverse side if necessary and identify by block number)

Thin-Film (Guided-Wave) Acoustooptic Interactions/Devices, plane/stepped Array Transducers, Diffraction of Multiple Surface Acoustic Waves (SAW), SAW Signal Processor, Acoustooptic Bragg Diffraction, Multiple Tilted SAWs Phased SAWs, Elastooptic Effect, Electrooptic Effect, Overlap Ingegral, Integrated/Fiber Optics, Bandwidth, Diffraction Efficiency, Switching/Deflection, Acoustooptic Spectrum Analyzer, Acoustooptic convolver

20. ABSTRACT (Continue on reverse side if necessary and identify by block number)

Part I. We have studied the diffraction pattern and its electronic scanning of the resultant acoustic beam from plane and stepped array transducers. The results show that for a limited angular scan the diffraction patterns and their phase and frequency scanning may be described, to a large degree, in terms of the phased-and frequency-scanning array antenna theory with

over

DD FORM 1 JAN 73 1473 EDITION OF 1 NOV 65 IS OBSOLETE
S/N 0102-014-6601 |

SECURITY CLASSIFICATION OF THIS PAGE (When Data Entered)

6pg

some modifications. Some applications with both types of array transducers are described. In particular, the stepped array transducer is shown to have several immediate applications in connection with wideband guided-light beam deflection.

Part II We have studied two device configurations involving multiple tilted and phased surface acoustic waves (SAW) for wideband guided-wave acoustooptic Bragg diffraction. First, the diffraction efficiency and the bandwidth of the acousto-optic Bragg diffraction using a single SAW in a Y-cut $LiNbO_3$ out-diffused optical guiding layer are analyzed in detail. The methodology for numerical computation has been established to calculate the diffraction efficiency and the bandwidth as a function of the optical and acoustic parameters such as the penetration depth of the guiding layer, waveguide modes, direction of propagation, center frequency and aperture of the SAW. The same analytical approach and numerical computation methodology are then applied to the case of two tilted SAWs and finally to the case of N-tilted and phased SAWs. The resultant diffraction efficiency and the bandwidth, as a function of various device parameters such as the center frequency and the beam aperture of the individual SAWs, the tilt angle and the step height as well as the phase shift between adjacent SAWs, and the optical wave-guide modes involved are calculated. Experiments using two to four tilted SAWs and two to six-element phased SAWs in single-mode Y-cut $LiNbO_3$ out-diffused wave-guides were carried out to verify the theoretical predictions. In one of the wideband units being studied, a device bandwidth of 358 MHz has been realized. A bandwidth of 358 MHz enables the device to deflect a light beam of 1-cm aperture into 1000 resolvable spot diameters at a random-access switching time of 2.8 μs.

The development of the two wideband techniques presented in this report has made it possible to design and fabricate very wideband guided-wave acousto-optic Bragg-devices and has, thus, paved the way for a number of potential applications using such devices. Possible wideband applications, similar to those common to bulk-type acousto-optic devices, include processing (convolution, correlation, etc.) of wideband rf signals, high-speed optical pulse modulation, acousto-optic spectrum analysis of very wideband rf signals, high-speed multiport beam switching and deflection for fiber/integrated optic systems. Wideband applications which have been experimentally demonstrated include high-speed multiport beam deflection/switching for future integrated/fiber optic systems, acousto-optic spectrum analysis of very wideband rf signals, processing (convolution, correlation, etc.) of wideband rf signals, high-speed optical pulse modulation, and optical time-multiplexing/demultiplexing.